Modeling the Process of Fabricating Cell-Encapsulated Tissue Scaffolds and the Process-Induced Cell Damage

A Thesis Submitted to the College of

Graduate Studies and Research

in Partial Fulfillment of the Requirements

for the Degree of Doctor of Philosophy

in the Department of Mechanical Engineering

University of Saskatchewan

Saskatoon

By

Xiaoyu Tian

PERMISSION TO USE

In presenting this thesis in partial fulfillment of the requirements for a Postgraduate degree from the University of Saskatchewan, I agree that the Libraries of this University may make it freely available for inspection. I further agree that permission for copying of this thesis in any manner, in whole or in part, for scholarly purposes may be granted by the professor or professors who supervised my thesis work or, in their absence, by the Head of the Department or the Dean of the College in which my thesis work was done. It is understood that any copying or publication or use of this thesis or parts thereof for financial gain shall not be allowed without my written permission. It is also understood that due recognition shall be given to me and to the University of Saskatchewan in any scholarly use which may be made of any material in my thesis.

Requests for permission to copy or to make other use of material in this thesis in whole or part should be addressed to:

Head of the Department of Mechanical Engineering

University of Saskatchewan

Saskatoon, Saskatchewan S7N 5A9

ABSTRACT

Tissue engineering is an emerging field aimed to combine biological, engineering and material methods to create a biomimetic three dimensional (3D) environment to control cells proliferation and functional tissue formation. In such an artificial structural environment, a scaffold, made from biomaterial(s), plays an essential role by providing a mechanical support and biological guidance platform. Hence, fabrication of tissue scaffolds is of a fundamental importance, yet a challenging task, in tissue engineering. This task becomes more challenging if living cells need to be encapsulated in the scaffolds so as to fabricate scaffolds with structures to mimic the native ones, mainly due to the issue of process-induced cell damage. This research aims to develop novel methods to model the process of fabricating cell-encapsulated scaffolds and process-induced cell damage. Particularly, this research focuses on the scaffold fabrication process based on the dispensing-based rapid prototyping technique - one of the most promising scaffold fabrication methods nowadays, by which a 3D scaffold is fabricated by laying down multiple, precisely formed layers in succession.

In the dispensing-based scaffold fabrication process, the flow behavior of biomaterials solution can significantly affect the flow rate of material dispensed, thus the structure of scaffold fabricated. In this research, characterization of flow behavior of materials was studied; and models to represent the flow behaviour and its influence on the scaffold structure were developed. The resultant models were shown able to greatly improve the scaffold fabrication in terms of process parameter determination.

If cells are encapsulated in hydrogel for scaffold fabrication, cell density can affect the mechanical properties of hydrogel scaffolds formed. In this research, the influence of cell density on mechanical properties of hydrogel scaffolds was investigated. Furthermore, finite element

analysis (FEA) of mechanical properties of scaffolds with varying cell densities was performed.The results show that the local stress and strain energy on cells varies at different cell densities. The method developed may greatly facilitate hydrogel scaffolds design to minimize cell damage in scaffold and promote tissue regeneration. .

In the cell-encapsulated scaffold fabrication process, cells inevitably suffer from mechanical forces and other process-induced hazards. In such a harsh environment, cells deform and may be injured, even damaged due to mechanical breakage of cell membrane. In this research, three primary physical variables: shear stress, exposure time, and temperature were examined and investigated with regard to their effects on cell damage. Cell damage laws through the development phenomenal models and computational fluidic dynamic (CFD) models were established; and their applications to the cell-encapsulated scaffold fabrication process were pursued. The results obtained show these models and modeling methods not only allow one to optimize process parameters to preserve cell viability but also provide a novel strategy to probe cell damage mechanism in microscopic view.

ACKNOWLEDGEMENTS

I am heartily grateful to my supervisor, Prof. Daniel Chen. His encouragement, guidance and support through my study program enabled me continuously achieve my research goals. His expertise and enthusiasm inspired me to face and explore every challenge in my research.

I also would like to appreciate my PhD advisory committee: Prof. Chris Zhang, Prof. Fangxiang Wu and Prof. Joel L. Lanovaz for their examination and valuable advices in my research program.

Several other professors and technician also enriched my research. I would like to thank Prof. David Schreyer and Mrs. Ruilin Zhai in the Department of Anatomy and Cell Biology. They provided me with a lot of useful advices and technical supports in my experiments at City Hospital. Also, my thanks go to Mr. Doug Bitner in our department for his technical assistance for my experiments.

Special thanks are due to my friends for their help and support during my research. They are Minggan Li, Nahshon Bawolin, Ning Zhu, Ning Cao, Jianwei Li, Yijing Guan, Xin Yan, Mindan Wang, Chenglin Liu, Ajay Rajaram, Zohreh Izadifar, Huishu Hou, and Rui Fang.

I gratefully acknowledge the financial support from the Department of Mechanical Engineering (through the Scholarship), Natural Science and Engineering Research Council (NSERC) and Saskatchewan Health Research Foundation (SHRF). I also acknowledge the copy right permission from the publisher of American Society of Mechanical Engineering (ASME), Institute of Physics (IOP) and Marry Ann Liebert to include the published papers in my thesis.

Finally, I wish to thank my families for their continuous support and valuable advices for my research.

CONTENTS

LIST OF TABLE

LIST OF FIGURE

CHAPTER 1

INTRODUCTION AND OBJECTIVES

1.1 Introduction

Tissue engineering is an important emerging field in biomedical engineering to create biological alternatives for restoration, replacement and regeneration of devastated and dysfunctional tissues and organs. The strategy of tissue engineering is generally to incorporate cells into an artificial and three dimensional (3D) scaffold and by cell culture, to form a new tissue for implanting it to defect area of host tissue. During the entire process, tissue scaffolds, made from biomaterials, acts as a biological and mechanical environment to support and guide cell attachment, migration, proliferation, differentiation and assembly into a new 3D tissue, while they degrades. Thus, tissue scaffolds are an indispensible and fundamental element in tissue engineering.

Tissue scaffolds are typically of a porous 3D structure of biomaterials with one or several ingredients of cells and proteins. They are fabricated with mechanical properties that provide structural support for cell and tissue regeneration as well as with appropriate pore size, porosity and interconnectivity that facilitate oxygen and nutrition supply and waste removal[1]. Also, sometimes they are fabricated with controllable growth factor and cells distributions to guide and promote the growth of functional tissue[2, 3]. To produce the desirable tissue scaffolds, various scaffold fabrication methods have been constantly evolved and developed.

Among many fabrication methods, the dispensing-based rapid prototyping method is one of the most promising bio-rapid prototyping(BioRP) techniques which has attracted a large amount of attentions due to its repeatability, controllability, easy-operation and maintenance[4, 5]. In this method, biomaterials or cell mixtures are extruded from a fine needle onto a substrate

or a crosslinking solution to form a 3D structure in a layer by layer. A schematic cell-encapsulated bio-dispensing process and a 3D structure are shown in Fig 1.1. Current bio-dispensing system is usually used to fabricate scaffolds in a trial and error fashion because of the lack of means to understand and describe the bio-dispensing process. In this process, the flow behavior of the biomaterials solution being dispensed and the system parameters (such as the needle size and the force applied for dispensing) have significant influence on the scaffold formed, including pore size, porosity and pore interconnection [6]. Therefore, the investigation into the bio-dispensing process and development of quantitative models for this process is of great importance to facilitate its control and optimization.

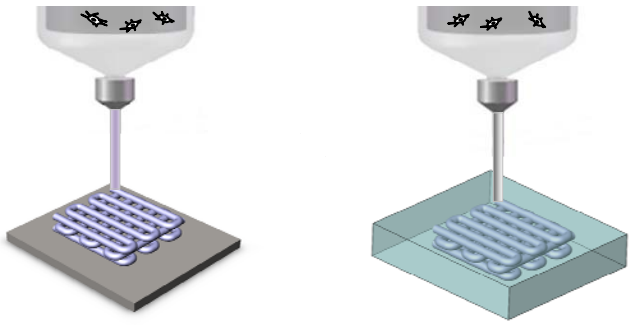

(a) (b)

Fig 1. 1 Cell–encapsulated bio-dispensing process: cell mixture is extruded onto a substrate(a) cell mixture is extruded into a solution for a crosslinking (b).

It is noted that, nowadays, scaffolds encapsulated with cells have emerged for use in tissue engineering applications, such as bone and cartilage regeneration, due to the excellent biocompatibility and biomimetic capacity. As aforementioned, the mechanical property is one of critical aspects for successful application of scaffolds in tissue engineering. Cells, whose

mechanical properties are different from biomaterials, are involved into the scaffold from the beginning of its fabrication process. The density of cells encapsulated is a non-ignorable factor that affects the mechanical properties of hydrogel scaffolds and thus affects cell differentiation and tissue growth. Although a few attempts are reported in the literature, no research presents a comprehensive and quantitative analysis on the effect of cell density on mechanical properties. Hence, in this research, the effect of cell density on scaffold under mechanical force and cell mechanical response for scaffold deformation with different cell densities were studied and modeled. This part of study is essential to design scaffolds with desired properties and gives a new means of controlling cell densities to fabricate desirable scaffolds.

In cell-encapsulated scaffold fabrication process, cells are naturally subjected to the pressure in the reservoir and/or the shear stress in the needle. Besides, in some cell-encapsulated biofabrication processes, operating temperatures may also be involved and affect the processes. In a physiological range, the forces elicit cell adaptive responses complicatedly and chronically. If the force exceeds certain thresholds, and/or cells suffer for a certain period, and/or operation temperature reaches at a certain value, biological and mechanical properties of cell membrane will change and even it will be not able to keep its integrity and finally decomposes irreversibly. From material failure perspective, cell membrane breakage is considered as cell damage[7]. Not all cells survive and maintain their phenotype during fabrication process, depending on the cell types and the process conditions. In order to improve the biofabrication process control, the knowledge with regard to the influence of force, exposure time and temperature on cell damage is essential.

1.2 Objectives

The aim of this research work is to perform a comprehensive study on the bio-dispensing-based tissue scaffolds fabrication process, with a focus on addressing the key issues identified in the previous section. Specifically, three main objectives are set to achieve in this research.

The first objective is to develop models to represent the flow behavior of scaffold biomaterials and its influence on the scaffold fabrication process, so as to providing means to better control the process for desirable scaffolds.

The second objective is to investigate the influence of cell density on mechanical properties of hydrogel scaffolds and develop models to represent the cell density effects on local strain energy and stress on cells. This would allow for determining appropriate cell density in scaffold fabrication process to better control mechanical properties of scaffolds and to preserve cell viability.

The third objective is to develop cell-damage models to investigate the force, exposure time and temperature effects on cell damage and on this basis, develop methods to predict the cell-damage rate or percentage in the dispensing-based biofabrication process. This research will facilitate the prediction of process-induced cell damage and then optimize the fabrication process parameters and strategies to preserve the cell-viability in scaffold biofabrication.

1.3 Organization of the Dissertation

This dissertation comprises of eight chapters. Besides this chapter, it includes six manuscripts (published or submitted for possible publication), followed by the conclusions drawn from this research.

Chapter 2 presents a literature review on current bio-rapid-prototyping techniques and cell damage modeling methods. Their technical features and pros and cons were examined, along with the discussion on their potential applications.

Chapter 3 presents the investigation into the flow behavior of alginate/hydroxyapaptite (HA) mixtures and its influence on the scaffold fabrication process. The flow behaviour concerned is examined and illustrated dependent on the concentration of both alginate and HA, and temperature. The relationships between them were mathematically established and experimentally verified. On this basis, the flow rates of the biomaterials solution dispensed were modelled and the needle moving speed of the dispensing system was determined and used in the scaffold fabrication.

Chapter 4 concerns with the cell density effects on the mechanical properties of cell-encapsulated alginate scaffolds. Ogden model was adopted to describe the mechanical properties of the scaffolds at varying cell densities and on this basis, simulations were performed to study the local stresses and strain energy on cells when cells are subjected to loadings.

Chapter 5 is about the development of cell damage laws that relates cell damage rate to forces and exposure time for cells (Schwann cells and 3T3 cells). The cell damage laws were developed and then applied to the dispensing-based scaffold fabrication process to predict the cell damage percentage in the process. The models were validated by comparing the experimental and simulations results.

Chapter 6 presents the development of a novel means to study cell damage in the scaffold biofabrication by employing computational fluid dynamic (CFD) method. It was illustrated the use of CFD is an effective means to investigate cell damage mechanism and thus to predict cell

damage in the scaffold biofabrication. The effectiveness was illustrated by both experiments and simulations.

Chapter 7 is about the influence of temperature on shear-induced cell damage. A cell damage law was established to quantitatively describe the relationship between the cell damage percent and temperature. This law was applied to predict cell damages in the scaffold fabrication process with varying temperatures.

Chapter 8 presents the conclusions drawn from this research, which is followed by suggestions and recommendations for possible future work.

1.4 Contributions of the Primary Investigator

It is noted that all papers presented in this dissertation are co-authored. However, it is the mutual understanding of all authors that Xiaoyu Tian, as the first author, is the primary investigator and that Xiaoyu Tian, as the second author of manuscript presented in Chapter 7, contributes to the research equally with the first author.

CHAPTER 2

BIO-RAPID-PROTOTYPING OF TISSUE ENGINEERING SCAFFOLDS AND THE PROCESS-INDUCED CELL DAMAGE*

* This chapter has been published as "Xiaoyu Tian, Minggan Li and Xiongbiao Chen. (2013). Bio-Rapid-Prototyping of Tissue Engineering Scaffolds and the Process-Induced Cell Damage. *Journal of Biomimetics, Biomaterials and Tissue Engineering*. 17:1-23". According to the Copyright Agreement, "the authors retain the right to include the journal article, in full or in part, in a thesis or dissertation".

2.1 Introduction

Tissue engineering has been developed to meet the tremendous need for the repair or replacement of damaged tissues and organs, by applying the principles of biology, material science and engineering to develop artificial tissue substitutes [8-11]. In tissue engineering, scaffolds mimic the extracellular matrix (ECM) of native tissue by providing nutrients, oxygen, and growth factors (proteins), encouraging cell proliferation, and supporting the tissue formation in its 3D structure [12]. Accordingly, tissue scaffolds play a vital role in tissue engineering and the fabrication of the tissue scaffold is of fundamental importance.

In tissue engineering, cells are either seeded onto prefabricated porous scaffolds or incorporated during scaffold fabrication process [13]. In the former strategy, the lack of vascularisation, difficulties in achieving high-density cell seeding throughout the scaffold, and the difficulties in incorporating multiple cell types and growth factors within the same scaffold limit the utility of this strategy [14]. To address these problems, in the later strategy cell-encapsulatedcell-encapsulated scaffolds were proposed to incorporate living cells in biomaterials during the scaffold fabrication process, which is referred to as biomanufacturing.

Biomanufacturing has emerged as a novel tissue scaffold fabrication strategy and since the cell-encapsulated scaffolds can mimic native tissues with respect to anatomical geometry [15], cell placement [16], and the microenvironment of the cells, it has attracted a great deal of attention in cell-capsulation technology and tissue engineering [17].

Various biomanufacturing techniques have been explored to fabricate cell-encapsulated tissue scaffolds and they can be classified into the categories of micromolding, photolithography, microprinting, and microfluidics. In micromolding, biomaterials are delivered into a template with designed patterns and subsequently polymerized to create structures of different shapes and sizes [18, 19]. In photolithographic processes, biomaterials are exposed to UV light through a mask. As the light reaches the photocurable biomaterials through the transparent regions of a mask it crosslinks the biomaterials [20]. In both microprinting and microfluidics, cells are mixed with biomaterial solutions and delivered through a fine nozzle or channel under a pressure. Since photolithography, microprinting, and microfluidics can fabricate scaffolds with both designed external shape and desired internal structures, they are referred to as bioRP in this chapter. In some of bioRP techniques, particularly in microprinting and microfluidics, cells flow with the biomaterial solutions and deform under fluid shear stresses, which may cause cell membrane rupture or cytoskeleton failure, leading to cell damage [7, 21].

To understand and represent cell damage under process-induced stresses, several theories and methods have been employed. To describe cell damage observed from experiments, some phenomenal models were proposed [21-23]. To better understand the mechanism of cell damage, strain energy theory was also introduced as a cell damage criterion for mechanical force induced cell damage [24].

This chapter presents an overview on current biomanufacturing techniques for tissue scaffold fabrication, with emphasis on bioRP techniques and their issues. This chapter also surveys the cell damage modeling methods for the understanding of the cell damage mechanism and the prediction of cell damage in the bioRP processes. Discussions in further improvements of current bioRP technologies are given and novel methods to study mechanical cell damage mechanism are also proposed.

2.2 Cell encapsulation bioRP techniques

This section focuses on photolithography, microprinting, and microfluidics techniques given the fact that the review of micromolding has been well documented in [20, 25].

2.2.1 Laser-assisted biofabriaction

Laser-assisted method uses the energy of photons to manipulate cells and/or biomaterials to achieve desired cell and biomaterial patterns, such as laser guided direct writing (LGDW) [26-29], laser-induced forward transfer (LIFT)[30-33], and photolithographic patterning and stereolithography [34].

LGDW uses the optical force to directly manipulate cells and biomolecules to form designed scaffold pattern. Schematic of LGDW is shown in Fig. 2.1, in which a laser beam is focused by a lens onto a target area. Due to the scattering of photons by the cell-media interface, cells in the laser beam path experience radiation forces in the laser travelling direction and then be trapped and deposited at designated position. The patterning resolution of this method is only limited by the size of cells (~10 μm in diameter)[27]. This method was first introduced to directly pattern living cells by Ashkin et al. [35, 36] and then was modified to deposit cells

through hollow fibers [26, 37]. The effect of wavelength on cell growth was also studied by Liang et al.[38]. This technique was applied in tissue engineering to pattern cells and biomaterials in an aqueous suspension to form two-dimensional patterns[39]. Three-dimensional (3D) cell patterns were also fabricated to mimic the liver sinusoid-like structures [27, 40]. Nonetheless, the optical force is not high enough to deposit heavy particles larger than 10 μm [35] to form scaffold directly. However, this can be overcome by combining other RP techniques with LGDW, in which the other RP techniques can be used to create hydrogel structure and LGDW deposits cells simultaneously onto it, building cell-encapsulated tissue scaffolds.

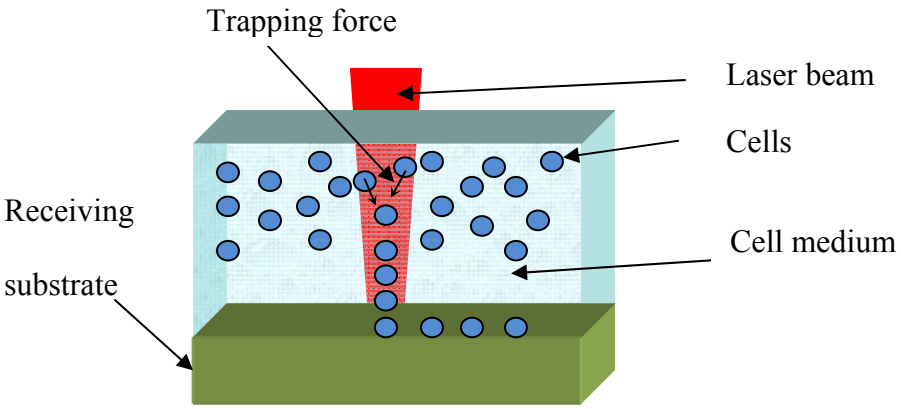

Fig 2. 1 Schematic of LGDW.

LIFT delivers cell-encapsulated hydrogel from a thin film coated onto the rear side of a transparent support substrate. The schematic of LIFT is shown in Fig. 2.2. The transfer is induced by focusing one or more laser pulses onto the support-film interface, where heating and phase change of the film propel material onto a receiving substrate [41]. Different from LGDW, LIFT utilizes the laser energy to heat the hyrogel film and the evaporation caused at the focusing spot drives the hydrogel to separate from the film. Due to this, not only can LIFT pattern various types of living cells [29, 42-45], but also deposit heavy particles, such as cell-encapsulated hydrogels, to form designed 3D structures [46-48]. Own to its high positioning accuracy, LIFT

has been recently combined with other solid RP to fabricate 3D cell-encapsulated tissue scaffolds, in which the solid RP fabricates the scaffold structure with designed microstructure and the LIFT technique precisely deposits living cells onto each fiber of the scaffolds[49]. The combination of the two techniques provides an effective way for the control over the microenvironment of artificial tissues.

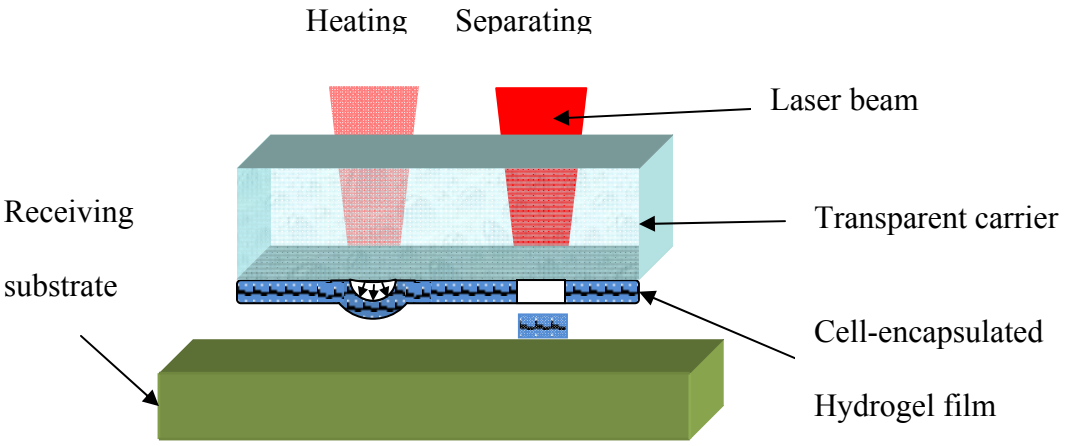

Fig 2. 2 Schematic of LIFT.

Photolithographic patterning techniques use ultraviolet (UV) light to cure photopolymerizable hydrogels with the help of patterned masks to produce topographically patterned hydrogel stamps and channels [50, 51]. Although photopatterning can construct layered patterns of cell-encapsulated hydrogels [52], the procedure is partially hand-operated and time-consuming and requires prefabricated masks for each layer of polymerization. Stereolithography can overcome these shortcomings by generating a spot of UV light to selectively polymerize the photosensitive hydrogel layer by layer, thus creating a hydrogel scaffold with seeded cells [53]. Laser micro-stereolithography [54] has a high resolution and been used for the fabrication of precise, spatially distributed microenvironments. Shown in Fig. 2.3 are the examples of 3D cellular scaffolds fabricated by means of stereolithography [55-57].

In addition, photolithergraphical patterning technique was also developed to combine with other fabrication methods such as capillary force lithography to produce multi-scale matrix structures[58].

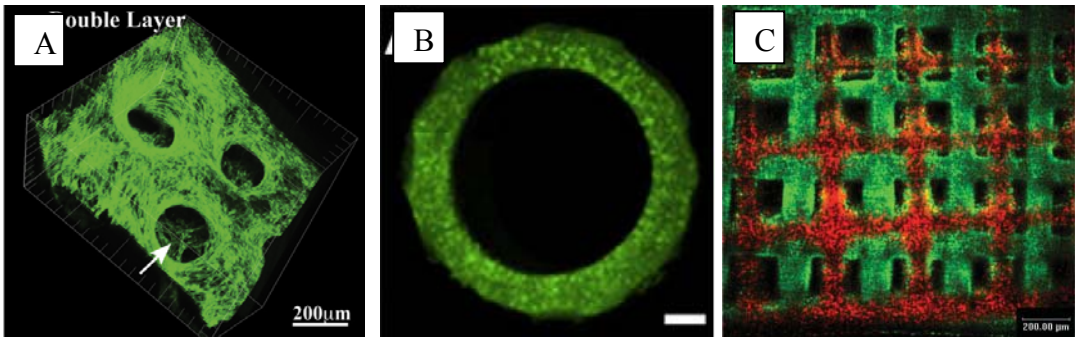

Fig 2. 3 ***3D tissue scaffold made by stereolithgraphy(A: human umbiliacal vein endothelial cells B: human stem cells hADSCs C: DMD-μSL cells)***

2.2.2 Microprinting

In microprinting, cell and biomaterial mixture is extruded through a fine nozzle by employing mechanical forces and deposited onto a designated location to form 3D scaffolds. To date, various microprinting techniques have been developed to fabricate cell-encapsulated tissue scaffolds. Table 2.1 lists the common microprinting techniques, along with the cells used and cell viability resulted in the fabrication processes.

Both inkjet printing and drop-on-demand printing use either pizeo-electric or thermal-dynamic driven method to force cell mixture out of a fine nozzle in either a small cell-encapsulated droplet or continuous strand. They are jetting-based techniques. The jetting mechanism in these techniques were reviewed in [59], with a comparison of their printing speeds, printing resolution, cell viability and cell throughput. Since these techniques can produce cell-

encapsulated droplet of small size, they can be used create cell-encapsulated tissue scaffolds with accurately-controlled shape and cell spatial distribution.

Table 2. 1 Microprinting techniques for tissue scaffold fabrication

Technique	Structure	Cell type	Cell viability	Reference
Inkjet printing	2D/3D	CHO, Motoneuron Primary feline H1 cardiomyocyte	>90% N/A	[32, 60-65]
BioAssembly Tool	3D	Fibroblasts Endothelial Hepatic cell	60% 86% 90%	[66-68]
RP deposition tool	3D	Hepatocytes	98%	[69]
Biodispensing tool	3D	Chondrocytes Hepatocytes	94% 95%	[69-74]
Direct cell writing	3D	HepG2	79-83%	[75]
Drop-on-demand printing	3D	Endothelial	N/A	[76, 77]
Bioprinting	3D	Endothelial	76-83%	[78]
Electro	3D	Jurkat	95-97%	[79]

-hydrodynamic jetting				
Hand injection	3D	Mesenchymal C3H10t1/2 Stem cells	N/A	[80-82]

CHO: Chinese hamster ovary cell, SMC: Smooth muscle cell, 2D: two dimensional

It is noted that bioassmebly tool, RP deposition tool, biodispensing, bioprinting, and direct cell writing techniques share the similar mechanism of driving cell-mixture. They use an air pressure or a plunge to extrude the cell mixture to flow through a fine nozzle and deliver it onto a designated substrate. They can be operated either in continuous manners by applying a continuous air pressure or plunge movement or in drop-on-demand manner by applying discrete air pressure or plunge movement [4]. Due to their ease in maintenance and control, these techniques have been widely applied in tissue scaffold fabrication with and without the presence of cells. By using multi-nozzle biodispensing, various scaffold structures were created and different cell types were simultaneously applied due the fabrication process [83]. It is noted that in the jetting techniques reviewed previously, the cells are driven by a high pressure and as such, cells suffer from the exposure of high stresses. In contrast, in the techniques reviewed in this section, speeds that cells travel at in the nozzle can be controlled and thus cell viability can be enhanced by using appropriate process condition.

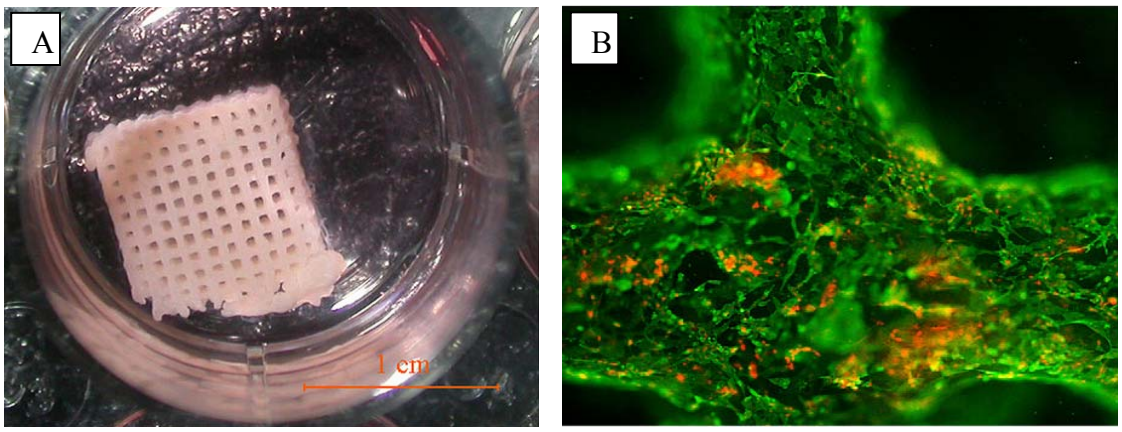

Fig 2. 4 Rapid prototyping of 3D cell-encapsulated scaffolds using bioprinting. (A: 3D structure of the scaffold, B: fluorescent cell image of bioprinted scaffolds[84]).

Electro-hydrodynamic jetting (EHDJ) is the modification of biodispensing by applying an electrical field between the nozzle and the substrate. The cell droplet velocity in EHDJ is typically below 0.1 m/s [79], which is far lower than that in ink-jetting, thereby improving the cell viability in the fabrication process. However, in EHDJ the high applied voltages and strong electric field gradients are typical required, which may alter the conformation of biomolecules and thus induce deleterious damage to cells [85]. Nonetheless, by using low electrical conductivity medium such as poly(dimethylsiloxane) [86], some experiments suggest that the EHDJ process has no significant effect on the cell viability and functions [86-88]. In addition, this technique was modified by using a coaxial needle, in which the high viscous biomaterials is forced through the outer layer of the needle while cell suspension through its inner layer. By using this method, a continuous cell-encapsulated thread can be formed to build cell-bearing 3D scaffolds [86, 87]. The electrospinning method typically produces nesting-like structure of polymer, in which the collection of flying fiber is a challenge. By adding designed patterns of electrodes on the receiving substrate, Li et al. illustrate the creation of oriented structure of fibers

(Fig. 2.5) [89], illustrating the feasibility to create cell encapsulated scaffolds with desired structures.

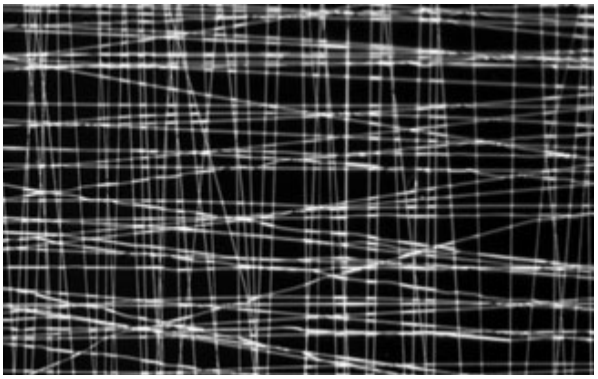

Fig 2. 5 Controlled orientation of electrospinning fibers[89].

Manual injection allows one to deposit cell-encapsulated hydrogel onto designated place. Although it can produce fine hydrogel strands, it is difficult to control the shape and accuracy. As such, it has been typically used in injectable hydrogel tissue engineering application [13].

Microprinting uses the rapid prototyping (RP) technique to create 3D cell-encapsulated tissue scaffolds. Not only can it fabricate scaffolds with designed external shape but also build desired internal channels to ensure nutrients supply and waste removal for tissue regeneration. With the multi-nozzle system such as 3D plotting device, microprinting can simultaneously encapsulate multi-phenotype cells as well as different growth factors into a scaffold. Moreover, by controlling the flow rate of each nozzle, desired cell concentration and growth factor gradients can be achieved, which is of importance to cell guidance, cell proliferation control and tissue formation.

2.2.3 Microfluidics

Microfluidics has emerged as a new endeavor for the cell-encapsulated tissue scaffold fabrication, in which the cell and biomaterial suspension is typically controlled in a laminar flow pattern. When two or more streams of laminar flow are joined into a single stream, the resultant streams flow parallel to each other and the mixing takes place by diffusion only between the interfaces (Fig.6). This ability to generate and sustain parallel streams of different solutions in microchannels provides a unique opportunity to pattern cells[90](Fig.2.7) and their environments [91].

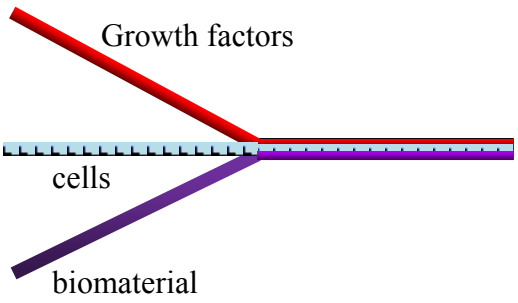

Fig 2. 6 Schematic of laminar flow streams jointing for synthesis of cell-encapsulated scaffolds.

To encapsulate multiphenotype cells into tissue scaffolds, cells suspension in one microchannel is mixed with a hydrogel solution in another microchannel. The two streams jointed together and were crosslinked at the channel exit to form cell-encapsulated constructs [92, 93]. Microfluidic device was used to pattern human endothelial cells on defined 3D structures [94] to improve cellular pattern integrity and to provide microscale control over cellular microenvironments. Microfluidics was also used to fabricate sub-mm-sized cell-encapsulated modules for tissue engineering [14] by cutting a continuous cell-containing fiber. A more

common method of using microfluidic systems to generate microparticles is the use of multiphase systems. In these approaches the viscous and surface tension forces are used to create homogeneous particles, which are crosslinked to form microscale hydrogels. A range of particle sizes and shapes can be created by generating the properly designed microfluidic channels. For example, by adjusting the dimensions of the microchannels, the flow rates and the droplet shapes, it is possible to create hydrogels in the form of spheres and rods [95].

Notably, microfluidics can be used to control the spatial properties of hydrogel. For example, one can create hydrogels with controlled gradients of signaling molecules or material properties embedded in the hydrogel [96]. These hydrogels can be used in various tissue-engineering applications where the concentration gradient is desired in the scaffolds. Microfluidics can also be merged with other techniques such as photolithography to fabricate cell-encapsulated modules [97]. Due to the laminar flow properties associated with microfluidics, modules fabricated by this method are uniform and it is easy to control their size and shape. Another advantage of microfluidics is the low shear stress in the flow stream. This will be particularly beneficial to preserve cell viability during the fabrication process. In most of the cell-encapsulated scaffolds fabricated by microfluidic devices, there are no significant losses of cell viability [14].

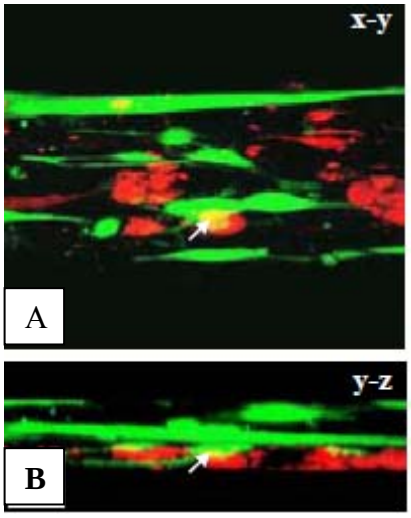

Fig 2. 7 Three-layer micro structure with different living cells shown as different colors (endothelial cells, smooth muscle cells and fibroblasts) (A: top view B: side view)[90].

2.2.4 Comparison of biofabrication techniques

A comparison of the three biofabircation technologies discussed above is summarized in Table 2.2. Generally, laser-assisted methods have high resolution and are suitable for the applications where precise cell displacement is required and/or the cell-cell and cell-ECM interaction is of particular interest. Notably, although LGDW and LIFT techniques can precisely manipulate cells, it is challenged to create 3D tissue scaffolds. Compared to laser-assisted methods, microprinting is more flexible and cost-effective and as such, has been widely used in 3D tissue model fabrication and cell encapsulation applications. With the use of multiple nozzles, microprinting can be applied to create 3D tissue scaffolds with varying distributions of multiple cells as well as controlled microstructure. Given the fact that microprinting utilizes strong mechanical forces to manipulate cells, cell viability is an issue as detailed later in this chapter. Microfluidic technique can be readily controlled to fabricate 3D tissue blocks with the desired

distributions of cells and growth factors. Also, by assembling such sub-millimeter tissue blocks, microfluidic technique provides a new means to fabricate 3D tissue/organ substitutes.

Table 2. 2 Comparison of different biofabrication techniques

Method	Laser-assisted biofabrication	Microprinting	Microfluidic
Material delivery mechanism	Optical force Laser heating	Pressure Piezoelectric impact Thermal impact	Pressure
3D structure formation	Gel support Layer support Selective Polymerization	Chemical or photo crosslinking	Chemical or photo crosslinking
Feature resolution	~1.3 [μm] – Stereolithgraphy ~10[μm] – LGDW ~100[μm] – LIFT and Photolithography patterning	~100[μm]	submillimeter
Operation	2.5[cell/min] – LGDW	0.1-150[mm/s]	Depends on

speed	50[μm/s] – Stereolithgraphy		flow rate
3D cell encapsulated	Yes	Yes	Yes
Process-induced stress on cells	Thermal, mechanical	Mechanical, thermal Electrical in EHDJ	Mechanical
Advantages	-Manipulating single cells -High resolution pattern -Photopolymerization	-Easy 3D formation -Multi-nozzle system -low cost	controlled growth factor gradient -High cell viability
Drawbacks	-not easy to make 3D structure -Photo and thermal effects on cell viability -Mask preparation and high cost -limited to photosensitive	-mechanical stress affects cell viability -Pattern resolution is limited -nozzle jam	-Limited to low viscosity materials -need assistant to form 3D structure

	materials		
Applications	-High resolution cell patterning -Cell-cell and cell-ECM interaction applications	-3D cell encapsulation -external shape controlled 3D scaffolds -Mimicry of ECM structure	-Multi-layered-strand 3D scaffold -Heterotypic cell-cell interactions -Tissue block -Tissue assembly

2.3 Process-Induced Cell Damage

In the bioRP processes discussed previously, cells are exposed to laser light in LGDW and LIFT, to mechanical forces in different printing process, or to high electrical field in EHDJ. If the radiation dose or mechanical force is small and exposure time is short, cells may survive the processes. If the dose or mechanical force is high and exposure time is long enough, the phenotypes of cells may be impaired or cell integrity may be broken, thus causing cell damage. Cell damage is an important concern in the bioRP process since damaged cell affects cell density, distribution and even the proliferation and differentiation. Thus it is desired to control and minimize cell damage.

From the biological perspective, cell damage may refer to the cell dysfunction resulting from some external stresses. DNA damage, membrane rupture and protein denaturation are often

considered as cell dysfunction. Since different processes may cause different effects on cells, in the following cell damage is presented in terms of its types, with emphasis on mechanical force-induced cell damage.

2.3.1 Laser-induced cell damage

When laser beam is focused to a very small focal volume, the high photon density can induce multiphoton absorption at the laser focus, even in transparent cells. Also, the high energy of photons can excite free electrons, which can in turn absorb photons and gain their energies. This recurring process can cause rapid growth in the number of free electrons, leading to the cascade ionization [98]. The high concentration of the free electrons in the focal volume can lead to plasma-mediated ablation of cells [99], thus causing photo-damage of cells.

Several mechanisms of laser-induced cell damage were proposed. When exposed to a laser pulse, a rapid transient heating ($\Delta T \approx 100°C$) was produced in the cells, which was thought to be a possible factor triggering dysfunction of sperm cells [100, 101]. Local heating of cells may occur in the bioRP process since cells are trapped in the laser beam for certain time courses in LGDW and exposed to laser radiation in droplet formation process in LIFT process. Two-photo absorption is another theory for laser-induced cell damage. Laser can produce cytotoxic oxygen radicals and singlet oxygen through charge transfer and energy transfer, causing cell damage by oxidative stress [102-104]. Laser can also introduce photochemical reaction in cells, producing chemical species toxic to cells [105, 106].

It has been illustrated that cell viability after laser exposure ranges from 39% to 79%, depending on the laser energy [107]. The damage process in the laser trapping process was well characterized by using a microscope [108]. Obviously, laser-induced cell damage is highly

dependent on the energy of the laser. The dependence of cell viability and proliferation on laser energy in LIFT process was systematically investigated [109, 110], which provide a very useful reference for development and application of LGDW and LIFT techniques. Although low energy light has no cytotoxic or genotoxic effects on cells [111], high energy lasers have the potential to harm cells or other small molecules in cells due to their photonic and thermal effects[112, 113]. Thus, the selection and control of the laser energy is critical in photolithography methods and long-term effect of laser irritation on cells is of interesting initiate for future research.

Notably, cells in the LGDW and LIFT process are not only exposed to laser radiation but also subjected to mechanical forces during the droplet formation and deposition process, which may also result in cell damage. It was found that although cell viability decreased from 95% to 78% as the laser energy increased from 258 to 1428 mJ/cm^2, the cell damage was mainly caused by the mechanical stress during the cell droplet formation and deposition process [114].

2.3.2 Electrical cell damage

Cell membrane consists primarily of a thin lipid bilayer, in which amphipathic phospholipids spontaneously arrange so that the hydrophobic tails are shielded from the surrounding polar fluid. The normal transmembrane potential difference of a cell is about 50-70 mV in magnitude, which is produced by the difference in ionic strength of the cell's intra- and extra-cellular fluids. Transmembrane potential above 200-300mV will cause membrane structure rearrangement or breakdown [85]. Since disruption of the plasma membrane causes rapidly metabolic exhaustion, membrane rearrangement or breakdown directly leads to cell damage. In addition, the current passing through the cells can alter the molecular and organelle structures, which also result in cell dysfunction or damage. Fig.2.8 (a) illustrates the cell membrane

alteration after exposed to a high electrical field and Fig.2.8(b) shows the cell membrane break down upon the application of a field pulse of 15kV/cm[115] .

In the cell-encapsulated EHDJ process, although cells are exposed to high voltage electrical field, the obtained fiber is very fine (in nanoscale) and is dried already at the receiving end. As a result, the fiber structure is nonconductive and electrical current will not be present in the fiber. Thus, transmembrane potential cannot be formed and cells are generally safe in this process.

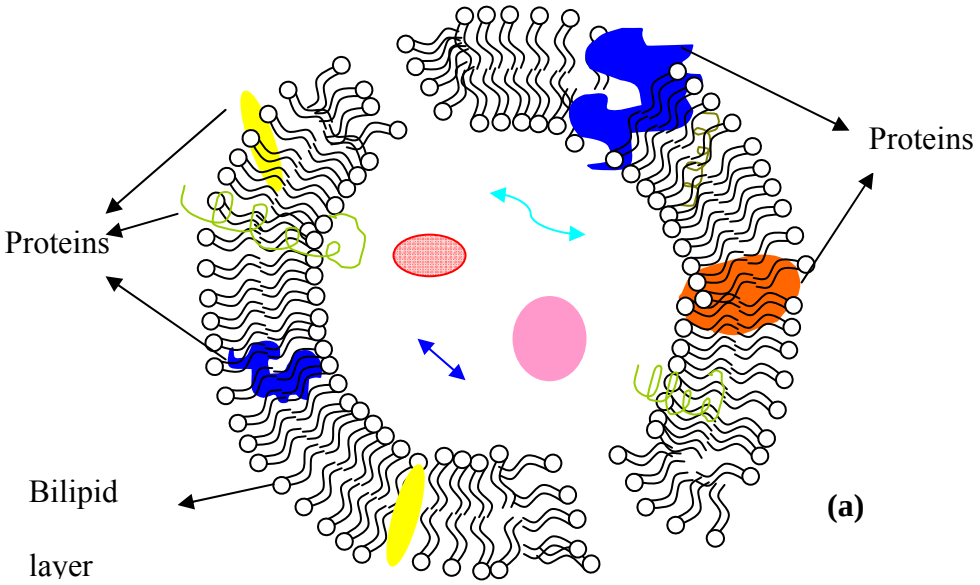

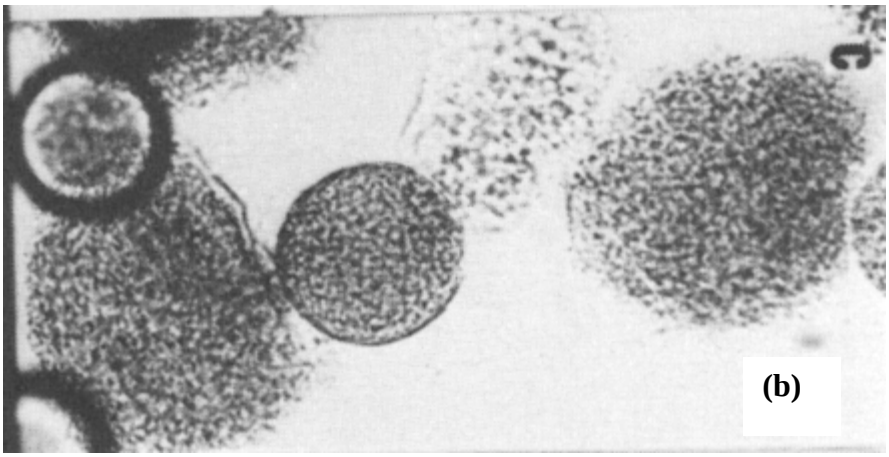

Fig 2. 8 Schematic of cell membrane alteration following high electrical field exposure (a) [85] and image of cell membrane break down upon the application of a field pulse of 15kV/cm(b)[115].

2.3.3 Mechanical force-induced cell damage

The mechanical cell damage is the structure failure of a cell caused by mechanical forces. Mechanical cell damage may include membrane rupture, failure of the cytoskeleton, or membrane backbone. The plasma membrane is a composite structure consisting of a two-dimensional bilipid layer and a variety of membrane associated proteins with a fibrous protein backbone of cortical cytoskeleton. The membrane proteins include ion channels, receptors, and signaling molecules. They can freely diffuse in the lipid bilayer or be linked to the cortical cytoskeleton, to the ECM, or to both. The mechanics of cell membrane has been studied in [116, 117], the mechanics of the cytoskeleton was reviewed in [118] and mechanics of a cell as a whole was investigated in [119]. In this section, from a different angle we focus on the cell deformation and damage, particularly occurring in the bioRP process.

Our previous study [21] illustrates that the hydrostatic pressure lower than 500 kPa has no significant influence on cell viability and that cell damage in a fluid flow is mainly caused by shear stress. When a shear stress is applied on cells, they will deform due to the weak elastic mechanical properties. However, cells can withstand large deformation due to its viscoelasticity

and can recover to its original structure upon the removal of stress [120]. As an example, Fig.2.9 shows the deformation of human red blood cells in shear flow under different shear stress [121].

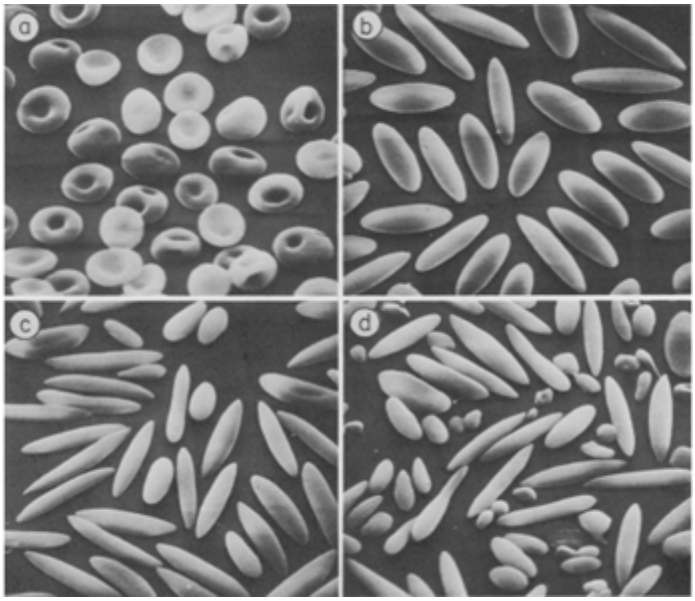

Fig 2. 9 Cell deformation under shear stress of (a) 100, (b)2000, (c) 3500, and (d)4500 dyn/cm2 [121].

In both microprinting and microfluidic techniques, cells suspended in biomaterial solution undergo mechanical forces, such as pressure and shear stress. The cohesion of the membrane is due to the separation of hydrophobic chains that form the core of the bilayer from the surrounding aqueous environment. Thus, within a physiological range, forces elicit adaptive responses acutely and chronically [7]. If the forces exceed certain thresholds and/or the forces are applied beyond a certain time period, cells will be harmed and even damaged. As listed in Table 2.1, cell viability varies in different bioRP techniques, depending on the operation parameters and cell types.

In the microprinting process, cells are deposited through a nozzle and the cell travel path in the nozzle is generally short (< 20mm). Thus the time period for cells exposed to shear stress is small, which benefits to the cell integrity. However, the shear rates of flow in this method are

normally high, which means the shear stresses are also high and may kill cells. For example, cell damage rates in biodispensing range from 30% to almost 60%, depending upon the pressures applied [122]. On the contrary, in microfluidics the microchannel is relatively long, resulting a long duration of cells exposed to force. Fortunately, the shear rates in microfluidics are relatively low and as such, the shear stress produced in the flow has a limited influence on the cell damage [94, 123].

2.4 Modeling and Analysis of Mechanical Cell Damage

Both cell printing and jetting have been widely used in manipulating various cells and rapidly-prototyping tissue scaffolds. Since cells are exposed to the mechanical forces or stresses in these processes, development of cell damage models for these processes has been desired to predict cell damage and optimize the process control.

In the microprinting and microfluidics bioRP process, if the stresses exceed certain thresholds and/or the stresses are applied for a certain time period, cell membrane may be harmed and even damaged. In the fabrication process, the mechanical forces are functions of process parameters, such as the pressure applied to the process and the nozzle or channel size, and thus cell damage during the process also depends on these parameters. It has been shown that pressure lower than 5Mpa has no noticeable effect on cells [21] and thus cell damage during this process mainly attributes to the shear stresses in the flow stream.

As different bioRP process parameters (such as the driven pressure and nozzle size) generate different forces and force durations on cells, cell damage laws that relate process-induced forces to cell damage are required to predict cell damage in different processes. Power law function and its modifications are commonly used to establish cell damage laws[124-127].

The basic power law model describes the relationship between shear force (τ) and cell damage percentage (*PCD*)[124, 125] , by

$$PCD = k\tau^a \tag{2.1}$$

This equation was modified to include the time-dependant effect (t) on cell damage in the form of[22]:

$$PCD = k\tau^a t^b \tag{2.2}$$

It is noticed that cells can mechanically adapt to small forces by deformation, thus can survive from certain levels of forces, which is referred to threshold force (τ_0). To include this effect, the above power law cell damage model can be generalized as [23]:

$$PCD = k(\tau - \tau_0)^a t^b \tag{2.3}$$

In the above Equations (2.1), (2.2) and (2.3), k, a, and b are the model parameters and for a given kind of cell, they are determined by experiments. The power law model and its modifications can be used to predict cell damage in certain ranges. Their shortage is that they are not applicable to the cases involving high stress since the percent of cell damage may exceed 100% due to the monotone increasing nature of the power law function used. For improvement, a bivariant normal distribution function was used as the cell damage law [21], which is given by

$$PCD = \int_t \int_\tau f(\tau, t) d\tau dt \tag{2.4}$$

where $f(\tau, t)$ is normal distribution probability density function. The above cell damage law has been successfully applied in the biodispensing process for cell damage prediction [21]. Given the fact the parameters involved in the above cell damage law are typically identified under low stress conditions by means of a rheometer, the model with the identified parameters may not be

applicable to the applications that involves high stresses. This is mainly due to the fact that cell damage occurs under high stresses much more quickly than that under low stresses [128].

Also, a strain energy density (SED) function was employed to characterize the effects of mechanical stress on cells [24, 129], in which cell deformation was treated as the principal trigger for cell damage and the cell damage criterion is defined as[129] :

$$\Gamma(W_{cell}) > \Gamma(W_{cr}) \Rightarrow cell\ \ damage \tag{2.5}$$

where W_{cell} and W_{cr} are respectively the strain energy density of cells and the critical strain energy density where cells start to die. Γ is probability function for cell damage. This method theoretically improved the current cell damage laws and has been applied in cell damage prediction in soft tissues and engineered tissue constructs. In the bioRP process, it is noticed that cells flow in the biomaterial solutions and cell-fluid interaction are involved. , which is a challenge and difficulty in solving the cell deformation under cell-fluid interaction. As a result, this method has not been applied on the cells in fluid flows for cell damage study.

In cell manipulation process, temperature typically needs to be controlled precisely as the process demands. For example, the process temperature was maintained at 10°C to prevent polymerization of the collagen [66], at 43°C to investigate the physiological properties of cells at high temperature [130], or simply at a room temperature[73]. To consider temperature effects on cell viability, a model was proposed to predict cell damage in the bioRP process[131] and it reads

$$PCD = \frac{1}{1+\tau^{-k}e^{-(aT+b)}} \tag{2.6}$$

where T is the process temperature. This model has been successfully applied to predict the damage rate of Schwann cells in the biodispensing process with the temperature ranging from 0 to 45°C.

2.5 Recommendations for Future Research

BioRP techniques are able to fabricate cell-encapsulated tissue scaffolds with designed external shape and internal microstructure. It holds the promise to simultaneously integrate the multiphenotype of cells, the ECM materials and growth factor together to create artificial tissue constructs that mimic the mechanical, chemical and biological properties of native tissue. Despite significant progress has been made in bioRP techniques in the past decades, several issues must be addressed by research before they becomes feasible and controllable means to fabricate cell-encapsulated scaffolds for various tissue engineering applications.

Strategic combination of various BioRP techniques for fabricating multiscale scaffolds is one of the issues to be addressed by further research. Native tissues are very complex, yet highly organized, structures composed of living cells and manifold ECM materials. Like the hierarchy system of human body, which consists of levels from skeleton, organ, to cell and subcellular organs, biomimetic scaffolds should also possess multiscale structures so that both cells proliferation in microscale and tissue regeneration in macroscale can be well supported and organized. Strategic combination of different techniques is an important research initiation to create such multiscale structures, which has recently begun to draw researchers' attention. For example, the combination of 3D plotting and electrospinning techniques [132] was able to fabricate hybrid scaffolds, in which the 3D plotter extruded the microscale PCL fiber and the

electrospinning made the nesting nanoscale fibers between the microscale fiber layers. It is noted that the EHDJ technique is able to spin cell-embedded nanofibers, thus potentially providing a means to replace the electrospinning to make cell-encapsulated hybrid scaffolds. Another interesting method to fabricate cell-encapsulated hybrid scaffolds is to strategically use different bioRP techniques, in which RP techniques are used to produce the skeletal structure of scaffolds by depositing cell-encapsulated fiber at microscale level while the laser-based methods such as LGDW and LIFT are used to manipulate single cells and/or molecules precisely, thus creating cell-encapsulated scaffolds of multiscale structures.

The capacity of simultaneously integrating and regulating cells and various growth factors in hydrogel fibers is of great importance in the creation of novel tissue scaffolds. Previous studies have illustrated this potential by using microfluidics, coaxial micro-nozzle printing and laser-based techniques. In the study[133], microfluidics was combined with microprinting to fabricate scaffolds with different encapsulation contents, including cells and other molecules. By taking advantage of the physical properties of different phases of fluids, biophysical scaffolds were fabricated without the assistant of other tools[134]. It is urged that further research should be pursued in this regard so as to create novel tissue scaffolds. For example, nerve guidance by means of certain growth factors can be realized by adding the growth factors to specific locations and orientations of fibers. Vascular networks can be formed with appropriate distributions of endothelial or stem cells and the growth factors. Concentration and gradient of cell and growth factors distribution will be possibly controlled by combining microfluidics, laser-based methods and microprinting techniques.

Although above described researches will be able to pattern cells and biomaterials in the scales similar to native tissue microstructures, recent study shows that cells can fuse to tissue by

chemical and physical (electrical, mechanical and thermal) cues, providing an alternative way to create functional tissue substitutes. Tissue self-assembly is one of the research topics, in which submillimeter tissue blocks are fabricated with self-assembly properties and then fuse into tissues according to cells' natural functions. Microfluidic can create micro-tissue blocks with designed shapes and controlled cells types and thus may have the advantage in tissue self-assembly study. For example, microfluidics has been used to synthesize microparticles with various 2D and 3D shapes and assembled to complex structures[135].

Cell viability is another critical issue in various bioPR techniques, leaving a lot to be desired regarding the understanding and prediction of cell damage mechanism as well as the process control for improved cell viability. In the cell-damage models reviewed previously, it is commonly assumed that the influence of cells, as particles, on the flow concerned is ignored. As such, the shear stresses are evaluated from single-phase fluid flow and the stress on cells is considered same as the one in the local fluid. Besides, the interaction of cells and fluids is ignored, which, however, is involved to affect cell activities and thus cell deformation and damage. Moreover, the stress distribution on cells in shear flow is usually not uniform and high percent of stress concentration may occur [136]. Therefore, in the development of models for cell viability, it is of desire to take into account the influence of cells on the flow as well as the interaction of cells and fluids. Computational fluid dynamics (CFD) has been shown promising to represent such knowledge or information as required in the model development. For example, the shear stress distribution on cell surface has been investigated by means of CFD[137, 138]. Meanwhile, it is also noted that in such studies, cells are usually treated with fixed and wavy boundaries, which is not true in the bioRP process due to the involvement of moving boundaries. For improvement, immersed boundary method (IBM)[139] was employed to handle such a

moving boundary problem [140-142]. This method allows for solving the fluid movement using Cartesian grid and the cell membrane movement by using Lagrange grid, thus greatly facilitating the application of CFD to such a moving boundary problem. These studies only focus on the representation of cell deformation during the flow, leaving cell damage to be desired. To address the cell damage issue, the use of strain energy accumulated on cells is emerging recently[139] . With the information obtained from CFD, such as by means of IBM, the distribution of strain energy over cells can be established and used as a criterion for cell damage. Further research is urged to be pursued along the direction in order to understand the cell damage mechanism as well as to predict the cell viability more accurately as compared to the existing models. The knowledge obtained will also allow one for better control over the bioPR process for improved cell viability.

2.6 Conclusions

BioRP techniques are promising to fabricate cell-encapsulated tissue scaffolds. This method allows for the fabrication of scaffolds with customized external shape and internal structure and has found wide applications in current tissue engineering. The combination of various bioRP techniques offers more advanced means for encapsulating cell and growth factor in tissue scaffolds. The development of bioRP techniques as well as their strategic combination for the fabrication of cell-encapsulatedcell-encapsulated scaffolds will be significantly advance tissue engineering towards the goal of producing functional substitutes for the damaged tissues and/or organs.

Cell damage is a critical issue in bioRP techniques. The mechanism of cell damage under different types of energies is still under investigation. Mechanical cell damage in the bioRP

techniques can be investigated by using the combination of CFD and solid mechanics along with the experimental studies. This would lead to the development of various models for the prediction of cell damage rate and cell distribution. As such, the bioRP techniques can be controlled and optimized by adjusting the process parameters to achieve desired cell distribution and preserve cell viability.

CHAPTER 3

CHARACTERIZATION OF THE FLOW BEHAVIOR OF ALGINATE/HYDROXYAPAPTITE MIXTURES FOR TISSUE SCAFFOLD FABRICATION*

* This chapter has been published as "Xiaoyu Tian, Minggan Li, Ning Cao, Jianwei Li and Xiongbiao Chen. (2009). Characterization of the flow behavior of alginate/hydroxyapatite mixtures for tissue scaffold fabrication. *Biofabrication*. 1(4):045005". According to the Copyright Agreement, "the authors retain the right to include the journal article, in full or in part, in a thesis or dissertation".

3.1 Introduction

In tissue engineering, scaffolds are three-dimensional constructs made from biomaterials and used to facilitate cell growth and transport of nutrients so as to produce artificial organ and tissue substitutes. As such, scaffolds are playing a vital role in tissue engineering. Nowadays, a number of biomaterials have been employed in tissue engineering for scaffold fabrication, including collagen, fibrin, gelatin, synthetic polypeptides, agarose, alginate, hyaluronate, chitosan, dextran, polylactic acid, polyglycolic acid, and some composite materials of hydrogels and inorganic compounds[25] . Among these, alginate/hydroxyapatite mixtures are often selected

due to their biocompatibility and suitable mechanical properties[143-146]. Alginate is a natural biomacromolecule isolated from seaweed and bacteria whose use in tissue engineering is limited due to its weak mechanical properties, lack of cellular interactions, and uncontrollable degradation [147]. Hydroxyapatite (HA) is a mineral found in teeth and bones within the human body whose use is also limited, mainly in the applications to hard tissue implants, due to its low strength and fracture toughness[148]. However, the composite of these two materials demonstrate improved mechanical properties due to the crosslinking effect of Ca^{2+} ions and, as such, they have been widely applied in biomedical engineering[145].

Both Material selection and fabrication technique are important in the fabrication of scaffolds that can support cell growth and tissue formation. To satisfy the scaffold requirements[149], a variety of fabrication methodologies has been employed and can be broadly classified into conventional and rapid prototyping (RP) techniques. Conventional techniques, such as solvent casting, particulate leaching, gas foaming, emulsion freeze drying, thermally induced phase separation, gravity and microsphere sintering, and electrospinning, lack the ability to precisely control scaffold microstructure[150]. Thus, rapid prototyping techniques have drawn recent attention[4] as they are not only capable of finely controlling the microstructure and macrostructure of scaffolds but also can create structures capable of increasing the mass transfer of oxygen and nutrients. In rapid prototyping, materials are usually deposited from the fine needle of a dispenser to form a three-dimensional (3D) structure in a layer-by-layer fashion. In this process, the flow behavior of biomaterials, featured by the relationship between shear stress and shear rate, is very important as it affects flow rate in the needle and, thus, the horizontal speed of the dispenser in order to construct a desired structure[151]. As such, in tissue scaffold fabrication, flow behavior plays an important role in determining the geometrical properties of

scaffolds including pore size, porosity, and pore interconnection [6]. If the flow behavior is not well chosen or controlled, numerous trial scaffold fabrications are likely, in which the designed pore size and porosity may or may not consistently be obtained, thus affecting future cell growth and tissue formation [152, 153].

Although the composite of alginate/HA has been widely used in tissue scaffold fabrication as well as other biomedical applications[143-145], very little research on the flow behavior of alginate/HA mixtures has been reported. In the state-of-the-art of the scaffold fabrication, the structure of the scaffolds has to be ensured by trial and error, which has proven to be costly and time consuming as well as on operator's experience. This chapter reports our recent investigation into the influence of the alginate and HA concentrations as well as temperature on the flow behavior of alginate/HA mixtures for the purpose of rational manipulation of the material in scaffold fabrication for tissue engineering.

3.2 Models for flow behavior characterization

Typically, pure alginate solutions or alginate solutions mixed with particles additives act as non-Newtonian fluids due to the high molecular weight of alginate[154, 155]. The relationship between the shear stress and shear rate (the ratio of shear stress to shear rate is defined as apparent viscosity) in non-Newtonian fluids is not constant, but a function of the shear rate, temperature, and concentration of materials in solution. No universally applicable equation describes the relationship of non-Newtonian fluids, but many empirical equations are available for the applications in food processing industries [156].

To model flow behavior of the alginate/HA mixtures, we employed the Herschel-Bulkley model to characterize the nonlinear relationship between shear rate and shear stress as follows:

$$\tau = \tau_0 + K\dot{\gamma}^n \tag{3.1}$$

where $\dot{\gamma}$ is shear rate, τ and τ_0 are shear stress and yield stress, respectively, K is a consistency index, and n is a flow behavior index. Flow behavior featured by the yield stress, consistency index is anticipated to vary with not only the concentration of alginate and HA, but also with temperature. To study the effect of these parameters on flow behavior, in this study the yield stress and consistency index are expressed as functions of alginate concentration C_1 (%), HA concentration C_2 (%), and temperature (°C), and are given by:

$$\tau_0 = Ae^{\frac{T_0}{T}} C_1^{g_1} C_2^{g_2} \tag{3.2}$$

$$K = Be^{\frac{T_1}{T}} C_1^{h_1} C_2^{h_2} \tag{3.3}$$

where T_0, T_1, A, B, g_1, g_2, h_1, and h_2 are constants that can be obtained experimentally. The flow behavior index, n, is often considered a temperature independent parameter[157]; in this study it is expressed as a function of alginate and HA concentration with:

$$n = DC_1^{j_1} C_2^{j_2} \tag{3.4}$$

where j_1 and j_2 are experimentally determined constants.

3.3 Materials and Methods

3.3.1 Materials and preparation

Alginate and HA (200 nm particle size) powders were purchased from Sigma Co., St. Louis, MO. Alginate/HA mixtures were prepared by weighing and mixing the powders together in varying proportions: A1-HA20 (1% alginate and 20% HA), A2-HA20, A3-HA20, A4-HA20, A5-HA20, A3-HA10, A3-HA30, A3-HA40, and A3-HA50. The alginate/HA mixtures were prepared by dissolving the mixed powder in tap water and stirring at room temperature until thoroughly mixed.

3.3.2 Apparatus and experimental procedures

An RVDV-III rheometer (Brookfield Engineering Labs Inc. MA, USA) with RP-52 spindle was used to determine fluid behavior parameters of the alginate/HA solutions. The cone and plate geometry (Fig.3.1) featured a conical vertex perpendicular to but not in contact with a flat plate, with a cone truncation of 49 μm. A sample of 0.5 mL is placed in the gap between the rotating cone and the stationary flat plate; and the cone is very obtuse (α less than 3°), ensuring the shear rate in the sample is constant for a given rotation speed of the cone. When the cone is rotated at a pre-set speed ω, the torque T applied to the cone is measured through the deformation of a spring connecting the motor and the cone. The shear stress in the sample is related to the measured torque T and the shear rate to the rotation speed. As such, the relationship between shear stress and shear rate can be established.

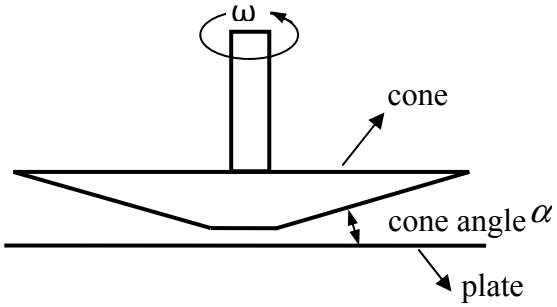

Fig 3. 1 Schematic of a cone and plate rheometer

In experiment 1, alginate concentration varied from 1 to 5% and HA concentration was held constant at 20%. In experiment 2, alginate concentration was held constant at 3%, and HA concentration varied from 10 to 50%. While experiments 1 and 2 were conducted at the room temperature, experiment 3 investigated the effect of temperature on flow behavior; concentrations of alginate (3%) and HA (20%) were kept at constant values and the temperature of the mixture varied from 20 to 60°C using a water bath. Data from these experiments are presented as plots of shear rate vs. shear stress (flow curves). Experiments to determine yield stresses were also performed in the cone and plate rheometer but at low shear rates ranging from 0.02 to 1.00s^{-1}. Yield stress data represent the mean from three replicates.

3.4 Experimental Results and Model Parameter Determination

3.4.1 Effect of alginate concentration on flow behavior

Flow behavior of the mixed solutions varies as alginate concentration increases from 1 to 5% percent (Fig.3.2 (a)). At low alginate concentrations, the flow curve is almost linear. At high alginate concentrations, the flow curve is non-linear, climbing steeply at low shear rates and smoothly at high shear rates. Notably, the flow curves meet the origin at low alginate

concentrations (no yield stress), but intercept the shear stress axis as alginate the concentration increases to 5% (presence of yield stress).

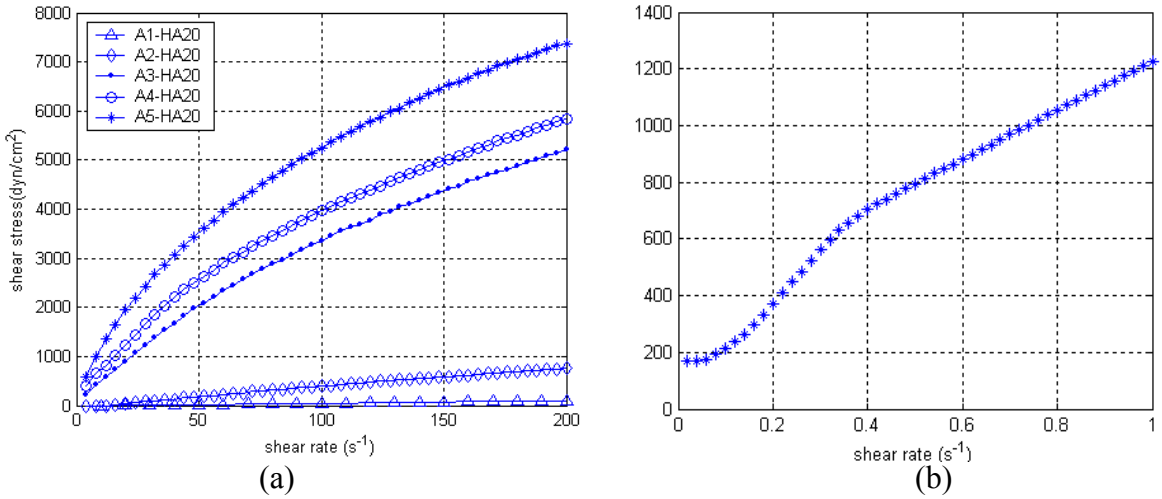

Fig 3. 2 Flow curves of alginate/HA mixtures obtained from: (a) tests with varying alginate concentration (b) yield tests.

For each mixture, the yield stress was determined from the yield stress test. Fig.3.2 (b), for example, shows the measured shear stresses at relatively low shear rates and then the yield stress is obtained by extrapolating it to zero shear rate. Fig. 3.3(a) shows the plot of yield stress vs. alginate concentration. It is demonstrated that the yield stress for the alginate solution with a concentrations less than 3% has a small value and, since then, increases rapidly. Accordingly, materials used in tissue scaffold fabrication should have high alginate concentrations enough to produce scaffold strands that can support their own weight. Otherwise, according to our previous study in[6], the strands will collapse and the intended scaffold microstructure cannot be achieved.

Consistency and flow behavior indices were identified from the flow curves in Fig.3.2 by using equation (3.1) (Fig.3.3 (b)). The consistency index K increases quickly with alginate concentration. An alginate concentration of 2% appears to be a critical value beyond which the

high molecular weight alginate chain has strong influence on the viscousness of the mixture. The increase of the consistency index means the increase of the resistance to flow, thereby reducing the flow rate in the tissue scaffold fabrication. In contrast, the flow behavior index decreases with alginate concentration (Fig.3.3(c)), indicating an increasing degree of nonlinear behavior.

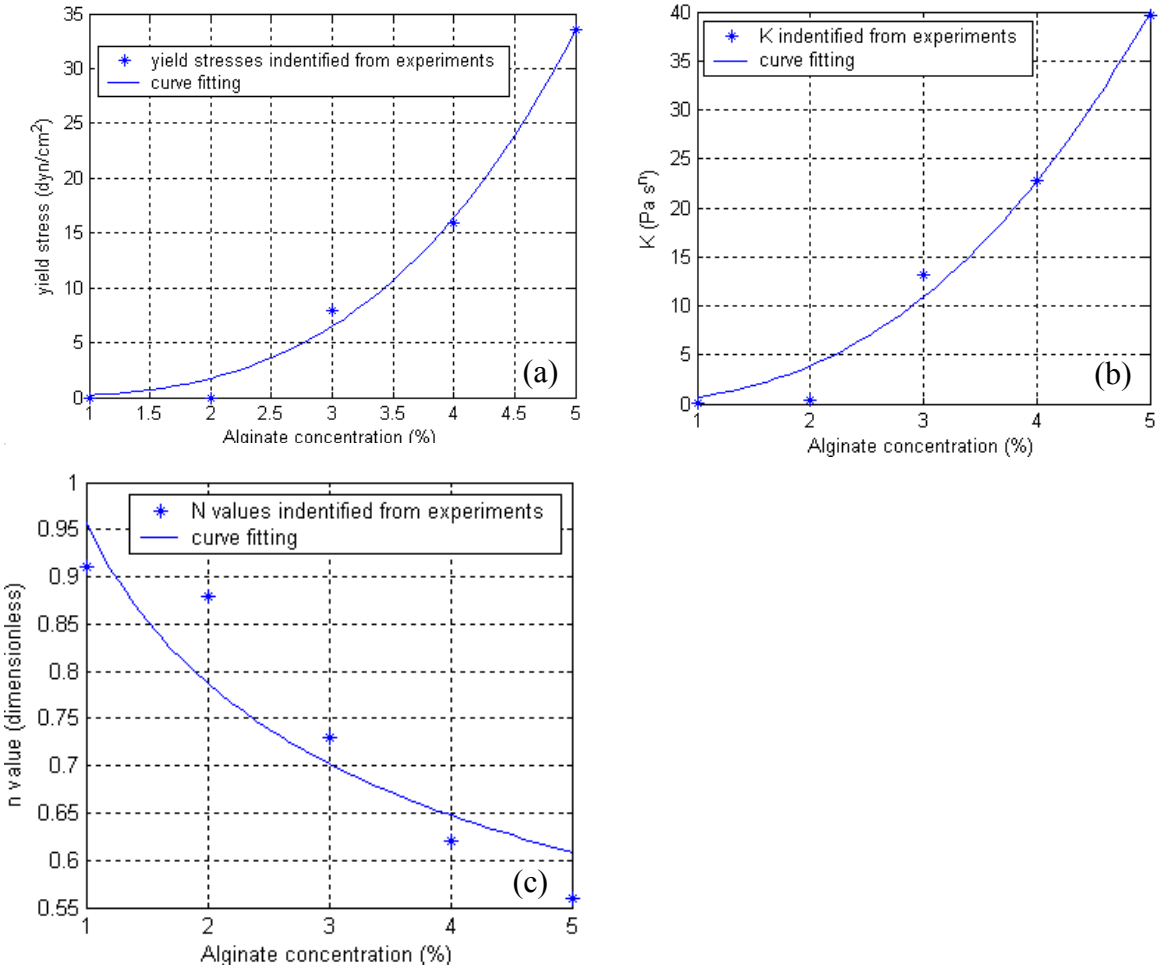

Fig 3. 3 Flow behavior parameters vs. alginate concentration: (a) yield stress, (b) consistency index, and (c) flow behavior index. (n=3)

3.4.2 *Effect of HA concentration on flow behavior*

The flow curves obtained when HA concentration was varied from 10 to 50% percent (Fig.3.4) also demonstrated the effect of concentration. Notably, the shape of the flow curves

varies with HA concentration and the intercept of the flow curves on the shear stress axis (yield stress) increases with HA concentration.

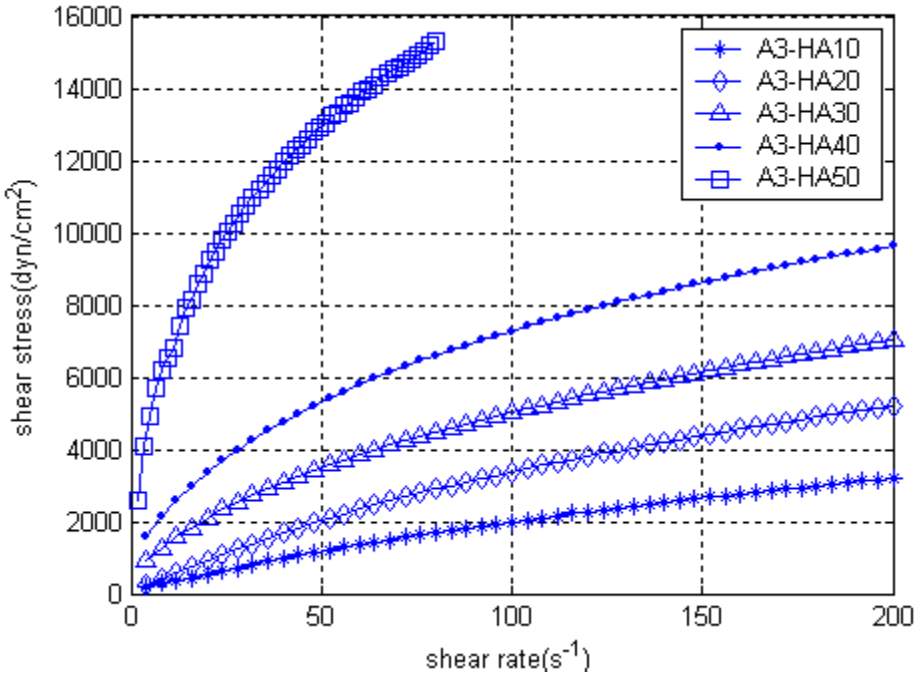

Fig 3. 4 Flow curves of alginate/HA mixtures with varying HA concentration.

Both yield stress (from yield stress tests) and consistency index (from equation (3.1)) increase exponentially with HA concentration (Fig. 3.5(a) and (b)); the flow behavior index decreases with HA concentration (Fig. 3.5(c)). For the purpose of scaffold fabrication, the yield stress results suggest high concentrations of HA can be used to increase the stiffness of the material to avoid the collapse of scaffold. However, as the HA concentration increases to 50%, the shear stress dramatically increases (Fig.3.4), indicating high HA concentration mixtures may give rise to difficulties during material manipulation.

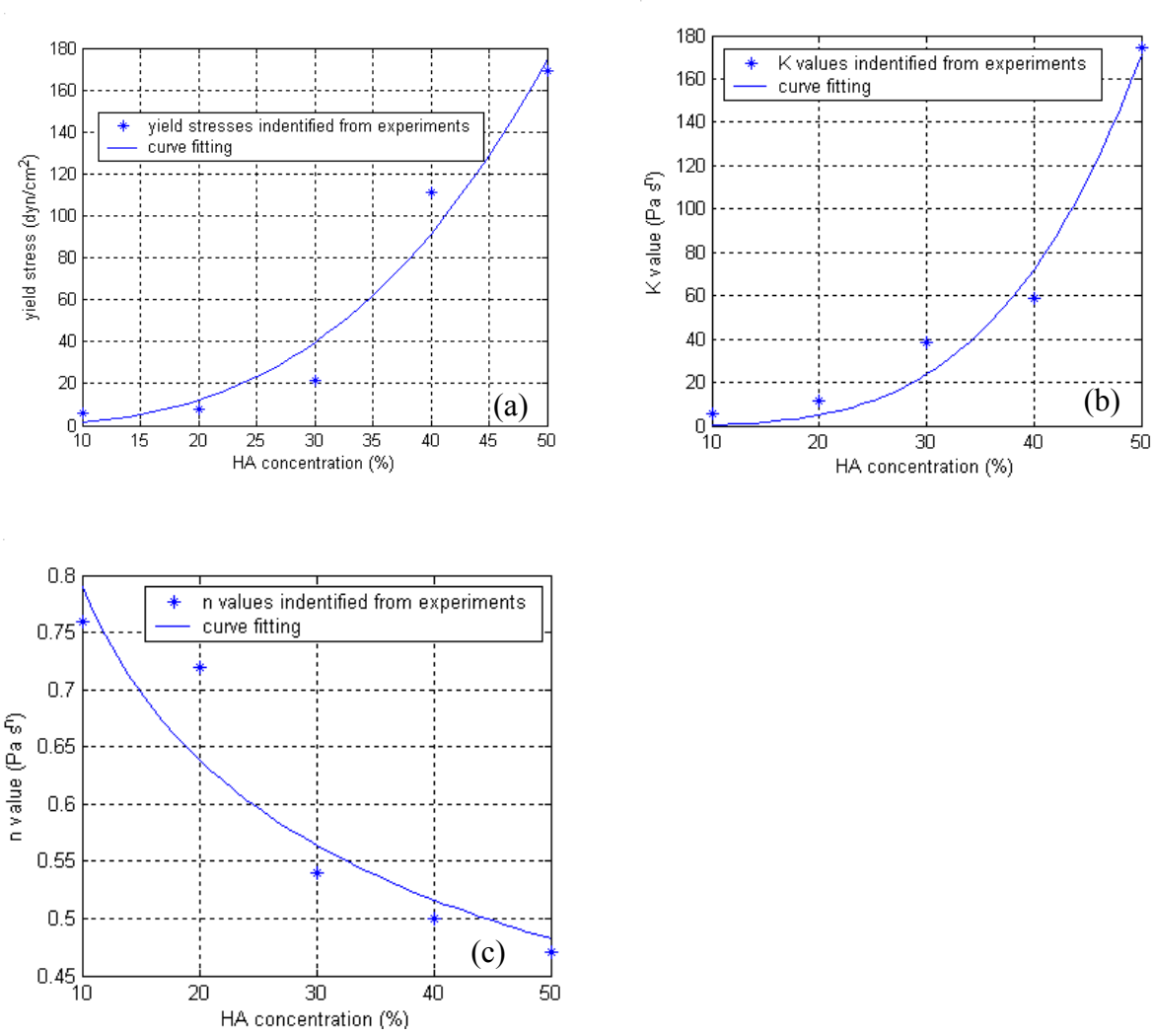

Fig 3. 5 Flow behavior parameters versus HA concentration: (a) yield stress, (b) consistency index, and (c) flow behavior index.

3.4.3 Effect of Temperature on flow behavior

Increasing the temperature of the alginate/HA mixtures results in a decrease in shear stress (Fig.3.6). Shear rate was fixed at $60s^{-1}$. Yield stresses values were determined at different temperatures and consistency indices were identified from flow curves using equation (3.1)

(Fig.3.7). Both yield stress and consistency index decrease with temperature. At high temperatures, the material possesses a lower yield stress and lower consistency index, which makes its manipulation easier. At low temperatures, the material has a high yield stress, indicating the material is more likely to support its own weight, thus facilitating the 3D structure formation in scaffold fabrication processes according to our previous study[6]. This property lends itself to many scaffold fabrication applications[158, 159] where the mixed material is heated to high temperatures for easy handling, then deposited at lower temperatures at which the material can support itself to form 3D microstructures.

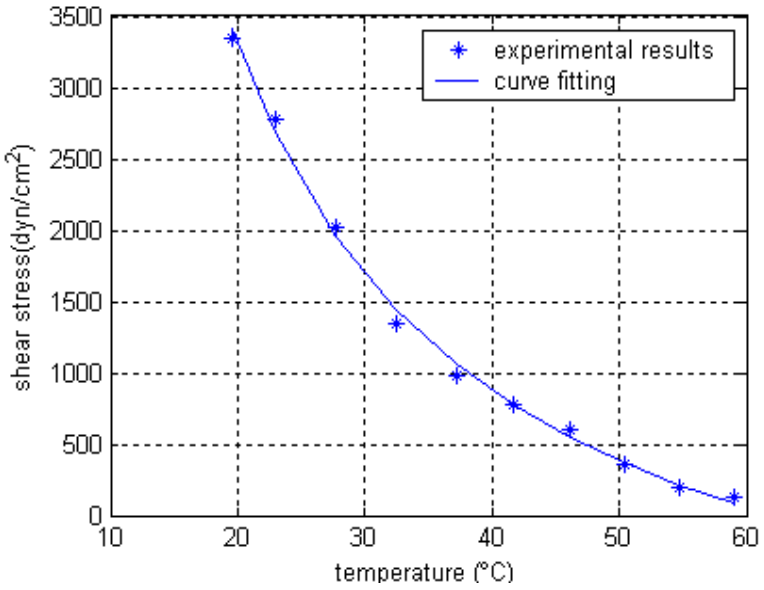

Fig 3. 6 Effect of temperature on shear stress for an alginate (3%)/HA (20%) mixture

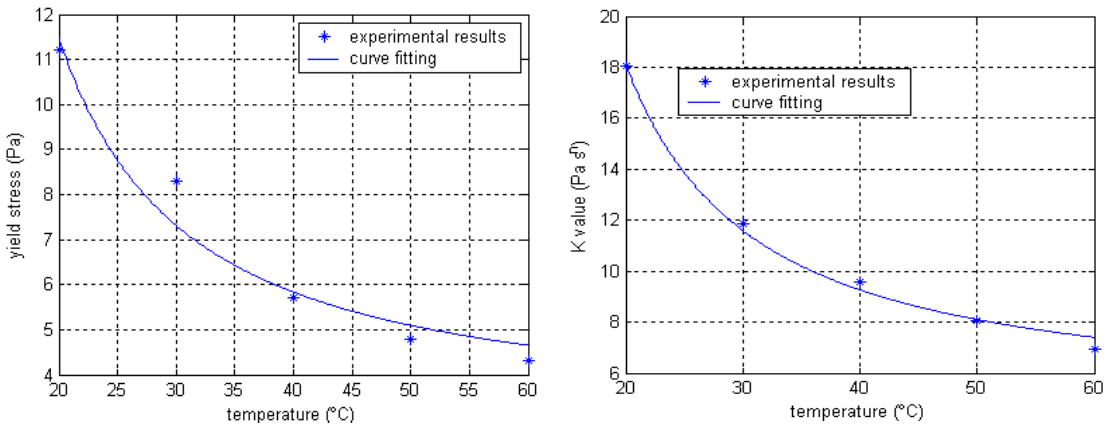

(a) (b)

Fig 3. 7 Effect of temperature on flow behavior for an alginate (3%)/HA (20%)

3.4.4 Integration and verification of flow behavior model

To quantify the effects of alginate/HA concentration and temperature on the flow behavior in an integrated form, data from the above experiments were used for regression by using equations (3.2) and (3.3). Values identified for equation parameters (Table3.1) were substituted parameters into equations(3.2) and (3.3) to generate a flow behavior model for the alginate/HA mixtures.

Table3. 1 Flow behavior parameters determined from experimental data

Parameter	A	T_0	g_1	g_2	B	T_1	h_1	h_2	D	j_1	j_2
Value	1.53×10^{-5}	27.1	3.21	2.91	1.9×10^{-6}	26.9	2.54	3.87	2.31	-0.28	-0.31

Two experiments were performed to validate the effectiveness of the developed model. The first employed A4-HA10 to verify the effect of alginate/HA concentration (Fig. 3.8(a)).

Equations (3.1-3.3) and the flow behavior parameters in Table 3.1 were used to predict the flow curves (Fig. 3.8). The second experiment employed A3-HA30 and a temperature of 45°C to verify the effect of temperature on flow behaviors (Fig.3.8 (b)). The close agreement of the experimental results and model predictions validates the utility of the model developed in this work for predicting flow behavior of alginate/HA mixtures. The model will facilitate the scaffold fabrication processes in many ways. It will aid in the selection of a material stiff enough so deposited strands can support their own weight as well as suitable temperatures for material deposition and 3D structure formation. The flow rate model [151] also allows estimation of the required flow rate for material deposition and therefore control of the deposition speed. The further illustration of the developed model as applied to the scaffold fabrication is presented in the following section.

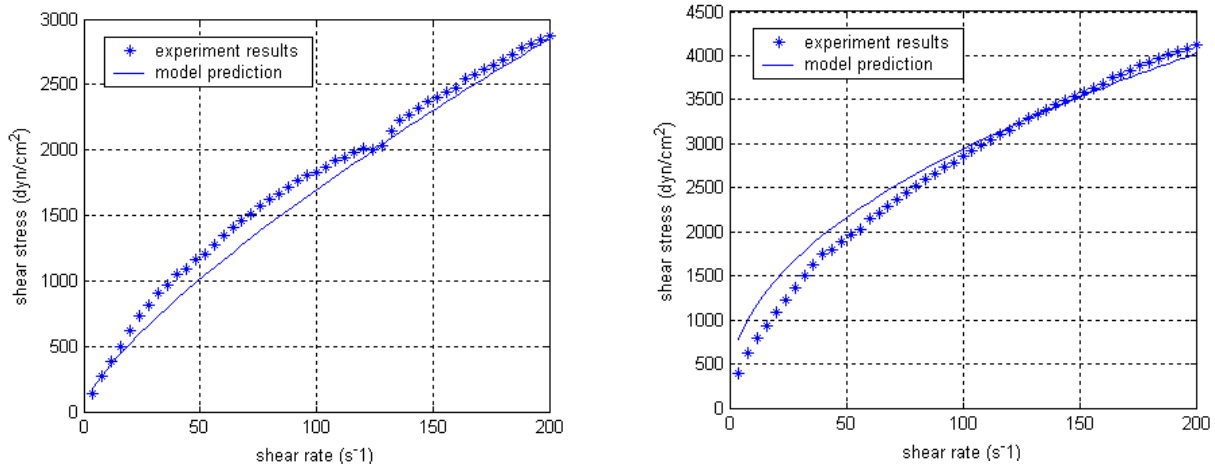

(a) (b)

Fig 3. 8 Experimental results vs. model prediction at (a) alginate concentration: 4%, HA concentration: 10%, and temperature: 25°C; (b) alginate concentration 3%, HA concentration 30%, and temperature: 45°C.

3.5 Applications to the Scaffold Fabrication

3.5.1 Flow rate prediction using flow behavior model

In the scaffold fabrication process, it is known that, to form continuous and uniform strands while avoiding strand break or stack, the horizontal moving speed of the needle (V) should be set as:

$$V = \frac{4Q}{\pi D^2} \tag{3.5}$$

where Q is the flow rate and D is needle inner diameter. Since the moving speed of the needle is determined by the flow rate, which is a function of process parameters. Therefore, modeling of the flow rate is of great importance in the fabrication process. In my previous work [4, 151], I developed a flow rate model and validated its effectiveness in the dispensing-based RP scaffold fabrication process. In this section, the flow rate model is adapted and used to predict the flow rate from the established flow behavior, and the predictions obtained are compared to the experimental results to illustrate the application of the developed flow behavior model to the fabrication process.

Three experiments of dispensing alginate/HA mixtures were carried out on the scaffold fabrication machine adapted from a commercial fluid dispensing system (C0720M, Asymtek), in which a needle with an internal diameter of 0.33mm and a length of 12 mm was used. In each of the experiments, the dispensing system was controlled to deliver the materials for 5 seconds under the pressures of 500 kPa. The average flow rates of 3 runs were measured by weighing the materials dispensed using an electronic balance with a resolution of 0.1 mg. In the first experiment, the HA concentration was fixed at 30% and the alginate concentration was changed from 2% to 5% (Fig. 3.9(a)). In the second experiment, the alginate concentration was

maintained at 5% and the HA concentration was varied from 20% to 50% for dispensing (Fig. 3.9(b)). In the third experiments to study the temperature effect on flow rate, the alginate and HA concentrations were maintained at 3% and 30%, respectively, and the temperature of the mixture was changed from room temperature (23 ^{o}C) to 50 ^{o}C (Fig. 3.10(c)). Based on the flow rate model reported in[4, 151] and the flow behavior model given in Eqns. (3.2)-(3.4), as well as the flow behavior parameters listed in table 3.1, simulations were performed in Matlab and the simulation results are shown in Fig. 3.9 along with the experimental results for comparison. The good agreement between the experimental and simulation results demonstrates the promising of the application of the established flow behavior to the determination of the flow rate in the dispensing-based fabrication process.

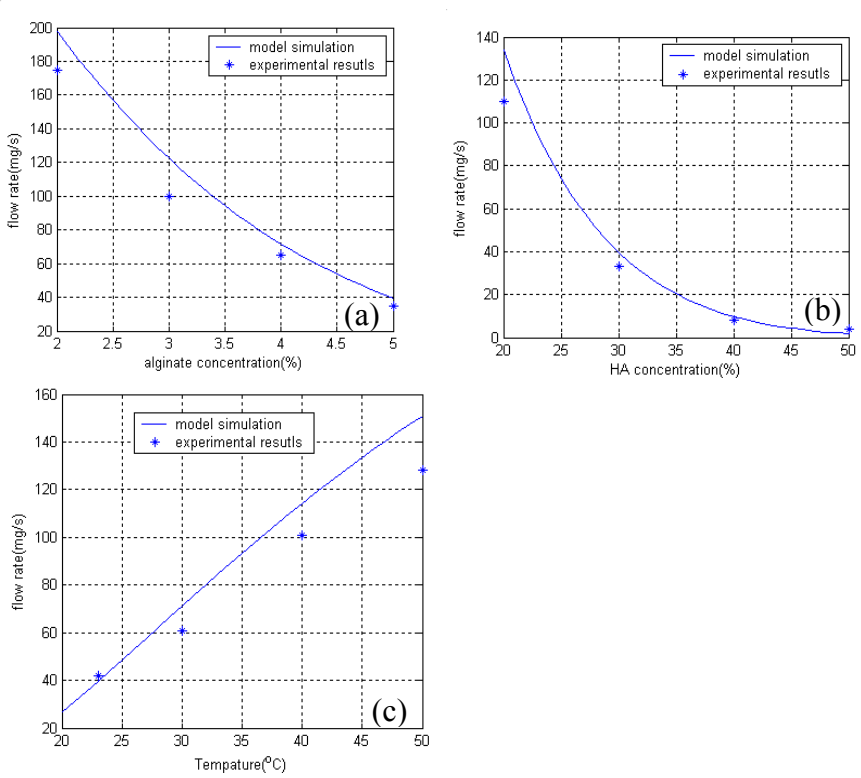

Fig 3. 9 Comparison of simulations to the experimental results under different conditions: (a) flow rate at different alginate concentrations, (b) flow rates under different HA concentrations, and (c) flow rates at different temperatures.

3.5.2 Scaffold Fabrication

In the scaffold fabrication, one can determine the needle moving speed from the flow rate by means of equation (3.5). Experiments for fabricating scaffolds by using so-determined moving speed was performed. Specifically, 7% of alginate was mixed with 50% of HA for 20 minutes and then loaded into a syringe for dispensing. A 0.33 mm needle was used and each layer was formed by horizontally moving the needle along a zigzag path. Based on the identified flow behavior and applied air pressure (500kPa), the flow rate was determined as 0.41mg/s, and he needle speed was established at 5mm/s by using equation (3.5). By means of these process parameters, the scaffolds were fabricated in a layer-by-layer fashion. Once one layer formed, the needle was lifted vertically 0.30 mm, dispensing another layer; and the process was repeated until 30 layers were obtained. The scaffolds fabricated were inspected under a microscope. Fig.3.10, for example, shows the interconnected microstructure of a scaffold.

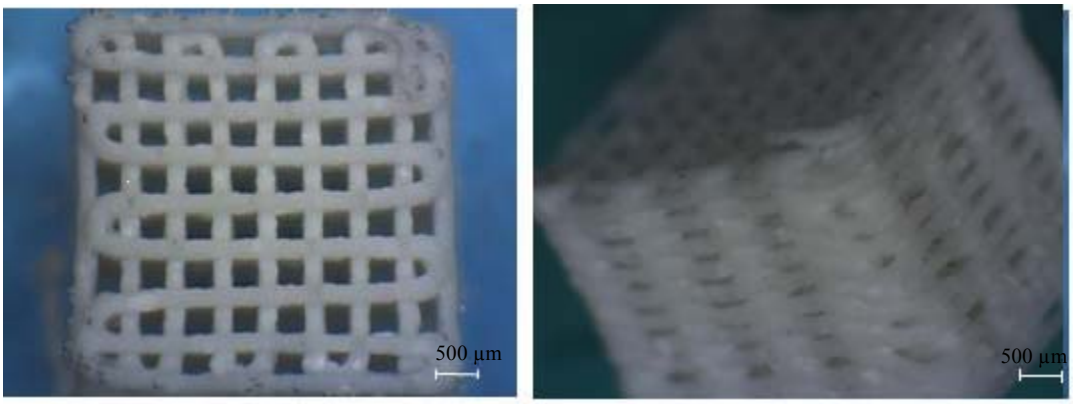

(a) (b)

Fig 3. 10 Scaffold fabricated (a) top view and (b) side view.

3.6 Conclusions

Examination of the flow behavior of alginate/HA mixtures in this study shows the flow behavior can be affected by alginate concentration, HA concentration, and temperature in exponential fashion. The effect of component concentration and temperature on the flow behavior was quantified through a model, and the effectiveness of this model was illustrated with experimental results. The resultant flow behavior model was then used to predict the flow rate in dispensing-based scaffold fabrication process; and the results obtained were validated by experiments. Furthermore, the needle moving speed was determined based on the developed models and used in the scaffold fabrication; and the scaffolds fabricated shows having the desired interconnected microstructure as designed. The illustrated ability to select the process parameters based on the developed models in the scaffold fabrication represents a significance improvement over the use of a trial and error process as previously reported in the literature.

CHAPTER 4

EFFECTS OF CELL DENSITY ON MECHANICAL PROPERTIES OF ALGINATE HYDROGEL TISSUE SCAFFOLDS*

* This chapter partly has been published as "Xiaoyu Tian, and Xiongbiao Chen. (2013). Effects of cell density on mechanical properties of alginate hydrogel tissue scaffold. *The 24th Canadian Congress of Applied Mechanics(CANCAM)*". According to the Copyright Agreement, "the authors retain the right to include the conference article, in full or in part, in a thesis or dissertation".

4.1 Introduction

Cell-encapsulated three-dimensional (3D) hydrogel scaffold mimics the microenvironment of native tissue. As such, it has been widely employed in various drug discovery and tissue engineering applications [160], including bone and cartilage regeneration [161], soft tissues of nerve [162], and brain repair [163]. Among various physical properties of hydrogel scaffolds, mechanical property is one of the critical aspects for successful application of hydrogel scaffolds in tissue engineering. The mechanical properties of scaffolds should match the ones of host tissues so that it can provide appropriate mechanical support to maintain the structure integrity [164]. It is also found that the mechanical properties can affect cell differentiation and tissue development and regeneration. Recent studies on mechanobiology have showed the significance of mechanical properties of scaffolds on cell function and tissue formation. Cells sense material elasticity as they touch and attach to their surroundings [165]. Many mature cells, such as fibroblasts, epithelial cells, neurons, and muscle cells, probe the stiffness of scaffolds, differentiate into dissimilar morphology and change their adhesive characteristics, depending on the scaffold stiffness [165, 166]. Therefore, fabrication of scaffolds

with desired mechanical properties is of great importance for tissue development and regeneration.

The density of cell encapsulated in scaffolds is a critical factor that affects the mechanical properties of hydrogel scaffolds. Cells are mechanically weak capsules, and when they are embedded into 3D hydrogel structures, the mechanical properties of the scaffold matrix change. The more cells are seeded, the softer the scaffolds matrix. The effects of cell density on mechanical properties of scaffolds have been observed in several studies in the literature. For example, the initial Young's modulus of agarose hydrogel scaffolds at chondrocyte density of 6×10^6 /mL is three times higher than those at cell density of 10×10^6 /mL [167]. Conor T. Buckley et al. examined the equilibrium modulus and 1Hz dynamic modulus of agarose scaffolds with cell density from 10, 40 to 60 million/mL and found that both of the moduli decrease with the increase of cell density [168]. These studies demonstrate that cell density should be carefully considered in scaffold design to obtain appropriate scaffold mechanical properties. They also provide a cue to improve cell differentiation and tissue formation. However, these researches only show some data points at certain conditions and cannot be used for rigorous design of mechanical property for scaffolds. More importantly, both cells and hydrogels exhibit non-linear hyperelastic properties [169] and thus Young's modulus is valid only in very small deformation range[170]. Thus a comprehensive understanding of the nonlinear mechanical properties of cell-encapsulated hydrogel scaffold and a mathematical model that can describe the mechanical property of scaffold for its entire deformation range is desired. This model will provide a basis for the precise design of the mechanical properties of scaffolds. A mathematical model is also a foundation to numerically evaluate the local deformation and strain energy on cells when

scaffolds are subject to loading, which then is used to predict mechanical cell injury or damage [169].

By using experimental and computational methods, this chapter modeled the hyperelasticity of cell-hydrogel scaffolds at different cell densities. A hyperelastic constitutive law was selected to describe the cell-hydrogel matrix. Based on the constitutive laws of the scaffolds, a two-level simulation was carried out to study the local strain energy on cells at different cell densities. The results obtained would allow one to design scaffolds with desired mechanical properties by varying cell density. Importantly, the local deformation and strain energy can be examined by using computational methods to evaluate cell mechanical injury when loading are applied on scaffolds.

4.2 Materials and methods

4.2.1 Cell Culture

Schwann cells, derived from Schwann cell line (ATCC, Rockville, MD), are cultured in Dulbecco's Modified Eagle's medium (DMEM) (Sigma, St, Louis, MO) supplemented with 10% fetal bovine serum (FBS) (Sigma, St, Louis, MO) and 1% antibiotic. Cells were incubated at 37℃ in a humidified atmosphere of 95% air and 5% CO2.

4.2.2 Alginate solution preparation

Low viscosity alginate powder (A2158-250G, Sigma, St. Louis, MO) was dissolved in deionized water to form 0.5% (w/v) solution and then it was filtered by a vacuum filtration system to obtain sterilized alginate solution. Next, the sterilized alginate solution was frozen entirely and freeze dried to get sterilized alginate floc. The alginate floc was dissolved in DMEM to form 6% (w/v) alginate-DMEM solution.

4.2.3 Cell-encapsulated scaffolds preparation

Cell solutions with different cell densities of 2×10^6, 6×10^6, 1×10^7, and 2×10^7 cells/ml were gently mixed in 6% alginate- DMEM solution with a pipet to form a 50% (v/v) cell mixture with a uniform cell distribution. Final cell density of 1×10^6, 3×10^6, 5×10^6, 1×10^7cells/ml were obtained. Then the cell mixture was extruded through a 0.8 cm inner diameter tube into 100 mMol $CaCl_2$ solution for initial alginate crosslink. After 2 minutes, the scaffold was transferred into 1.8 mMol $CaCl_2$ solution and incubated for 24 hours to achieve complete and uniform crosslink of alginate scaffolds. The diameter of the scaffold was carefully measured by a Vanier caliper and the diameter was 0.9 cm. All these procedures were carried on in a sterilized environment. Before mechanical tests, the scaffold was cut to obtain a cylindrical sample with 6.5 mm length. Five specimens were prepared for each test.

4.2.4 Cell viability and distribution before mechanical tests

Before mechanical tests, five 1 mm thick slices cut from a scaffold were tested by cell live assay in order to qualitatively evaluate cell viability and distribution of samples cut from the same scaffold. Cells were stained for viability using calcein AM. Cell viability and distribution were observed by a confocal microscope and live cells were counted three times respectively in a 3D space (507 μm × 507 μm × 114 μm) and live cell density was obtained by averaging fifteen data from five slices.

4.2.5 Mechanical properties tests

Uniaxial compressive tests were performed to measure the mechanical properties of scaffolds by using Bose Biodynamic 5010 system (Bose Corporation, USA) (Fig.4.1). A ramp

displacement signal generated by the WinTest digital control system at a constant rate of 5 cm/min was applied on specimens to obtain the stress-strain curve.

For dynamic tests, a sinusoidal displacement with a frequency varying from 0.5Hz to 100Hz and a fixed amplitude of 0.5 mm was applied to obtain the storage and loss modulus. Five specimens for each test were examined and average values were reported.

In both uniaxial compressive test and dynamic tests, to avoid the slip between the sample and the clamp surface and ensure uniform deformation in scaffold, metal pads with rough surface were taped onto the top and bottom surfaces of the clamp.

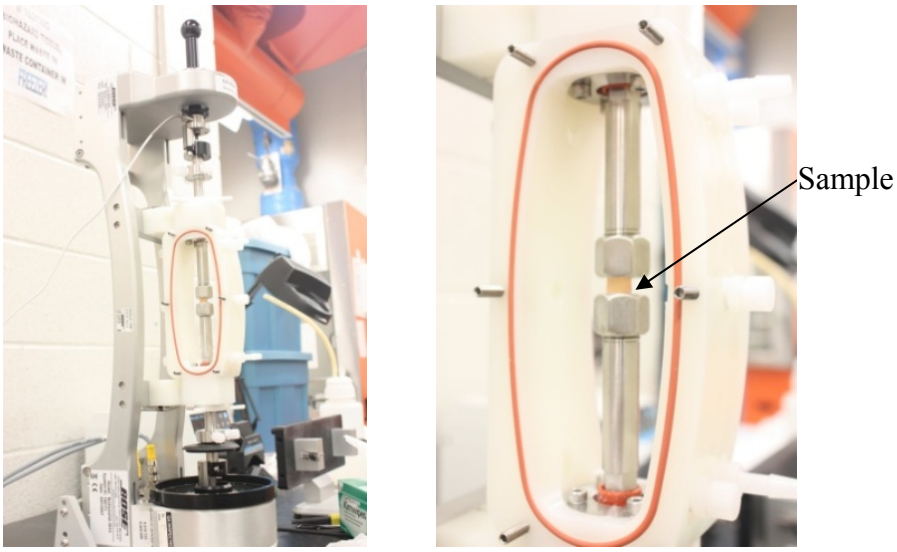

(a) (b)

Fig.4. 1 Bose biodynamic 5010 system: Experiment setup (a) Sample loading chamber (b)

4.2.6 Simulation of stress environment on cells

To study stress on cells under compression, a two-level 2D simulation was performed in Comsol 4.2a. Scaffold as a whole is first considered as homogeneous bulk material (macro level)

by using the bulk material model obtained in experiments. Then a small area (0.1mm×0.1mm) in the scaffold is considered (micro level), which consists of both alginate hydrogel and cell phases (Fig.4.2). At this level alginate has bulk material property (without cells) and cells are considered as neo-Hookean material with elastic modulus of 4,462 Pa. The boundary conditions are mapped from the first level simulation. Five models with different cell distributions were simulated to consider the effect of cell spatial heterogeneity. Five strain energy densities (SED) were obtained from each model and 25 values were averaged to obtain the final SED.

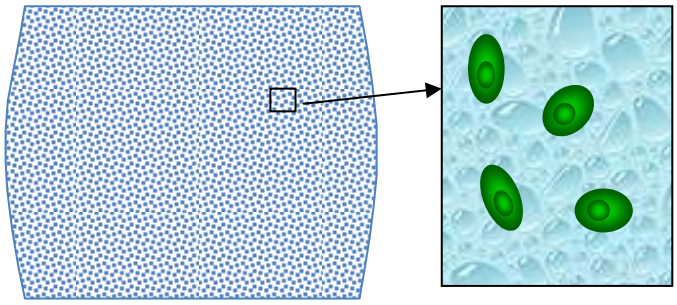

Fig.4. 2 Schematic of two-level simulation: Bulk simulation (a) Two-phase microscale simulation (b)

4.2.7 Statistics analysis

Statistics were performed using one way ANOVA test. All experimental data are reported as the mean and standard deviation of 5 samples per point.

4.3 Results

4.3.1 Cell viability and distribution before tests

From the fluorescent images, cell densities in scaffolds were examined, respectively, with values of 1×10^6, 3×10^6, 5×10^6, 1×10^7cells/ml before mechanical tests. Cells were also

observed being distributed evenly. Fig. 4.3 shows the 3D fluorescent images of cells in scaffolds with cell density of 1×10^7cells/ml from different angles.

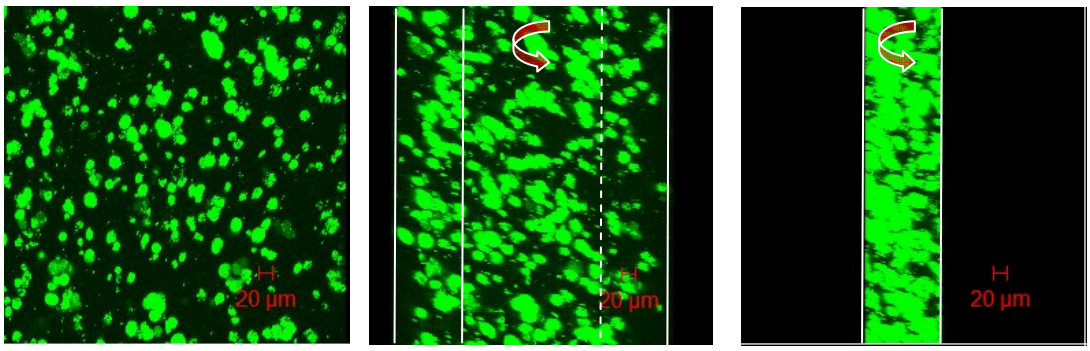

(a) (b) (c)

Fig.4. 3 3D image of cell viability at 1×10^7cells/ml before mechanical tests: front view (a) a 3D image at a rotating angle (b) side view(c)

4.3.2 Mechanical properties

The relationships between stress and strain at different cell densities were obtained from compression tests. The experimental results show that scaffolds with different cell density have different compression curves (Fig. 4.4). Pure alginate shows more linear relationship between stress and strain, while the stress-strain behavior of cell encapsulated alginate is highly non-linear. With the increase in cell density, it is observed that the curves become longer and that the nonlinearity of stress-strain curves becomes more profound. This indicates that low cell density hydrogels are stiffer and more brittle than the high cell density ones. At a high cell density, the mechanical property of cells causes the nonlinearity of scaffold mechanical properties.

Different nonlinear constitutive models were examined and adopted to fit the strain-stress curves to find a model to best describe the hyperelasticity of hydrogels with varying cell densities. By comparison among the Neo-Hookean, Mooney-Rivilin, and Ogden models, it was

found that third order Ogden model well fits the stress-strain curves at different cell densities and thus was selected as the constitutive law of cell-encapsulated alginate scaffolds (Fig. 4.5).

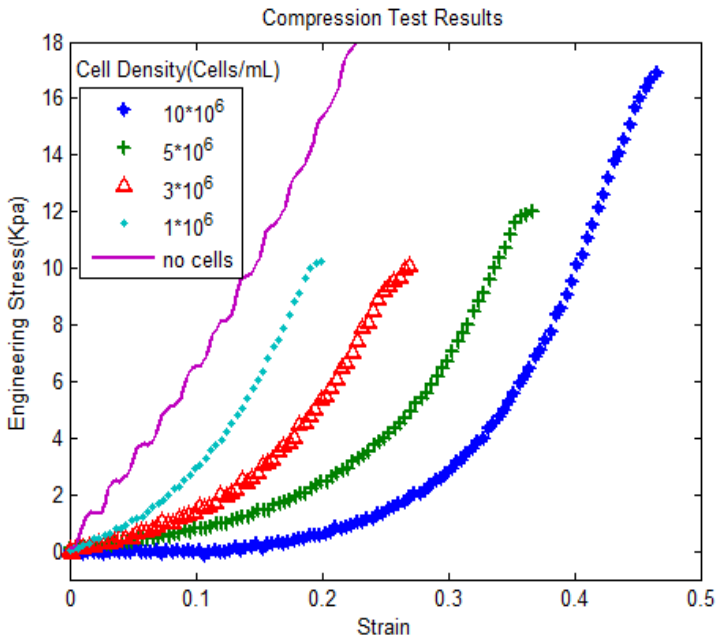

Fig.4. 4 Stress-strain curves of alginates with varying cell densities

In the Ogden model, the strain energy density (SED) is expressed in terms of principle stretches λ_j , j = 1, 2, and 3, as

$$W = \sum_n \frac{\mu_n}{\alpha_n}\left(\bar{\lambda}_1^{\alpha_n} + \bar{\lambda}_2^{\alpha_n} + \bar{\lambda}_3^{\alpha_n} - 3\right) \quad (4.1)$$

where μ_n and α_n (n=1,2,3) are material constants.

The values of these constants for alginate hydrogel scaffolds with different cell densities were identified by using data fitting using ANSYS 14.0 and are listed in Table 4.1. The model with identified constants can be used to quantitatively represent the stress and strain in the hydrogel scaffolds.

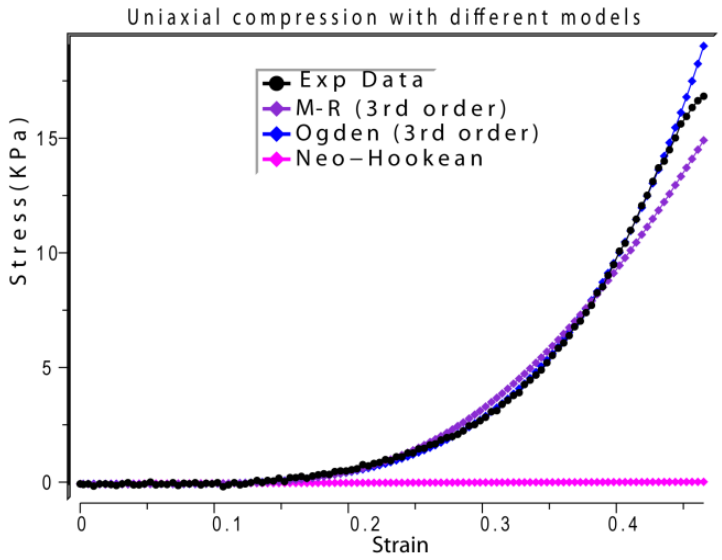

Fig.4. 5 Comparison of experimental results to curve fitting using different models at a cell density of 10×10^6 cells/ml

Table 4. 1 Values of Ogden model constants

Cell density (cells/ml)	μ_1	α_1	μ_2	α_2	μ_3	α_3
0×10^6	0.01	21.72	1.94	7.03	3.81	7.03
1×10^6	0.26	15.77	0.26	15.77	0.26	15.77
3×10^6	0.14	15.01	0.14	15.01	0.14	15.01
5×10^6	-952.7	1.51	132.5	3.44	2426	0.41
10×10^6	-67.28	7.64	31.41	8.44	36.95	6.73

Dynamic modulus were calculated and the storage modulus are always much higher than loss modulus, i.e., $E' \gg E^*$, at a frequency varying from 0.5Hz to 100Hz, which indicates alginate hydrogel scaffolds in the form of soft gel at the cell densities examined. The storage and loss moduli at 0.5 Hz is shown in Fig. 4.6. With the increase in cell density, storage modulus increases more rapidly than loss modulus, which indicates that the elastic part of viscoelasticity of scaffold increases with cell density. Experiments also indicated frequency has no obvious effects on dynamic modulus. Fig. 4.7, as an example, shows the storage modulus in different frequencies at a cell density of 1×10^6 cells/ml.

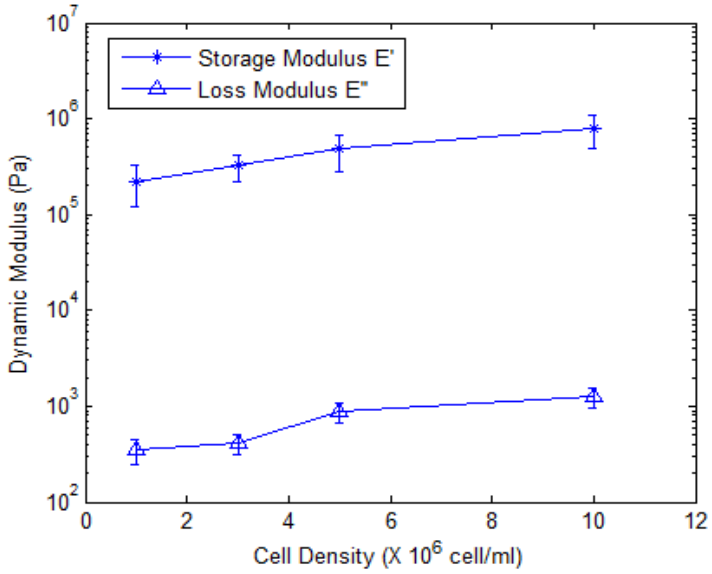

Fig.4. 6 Dynamic moduli verse cell densities at 0.5 Hz

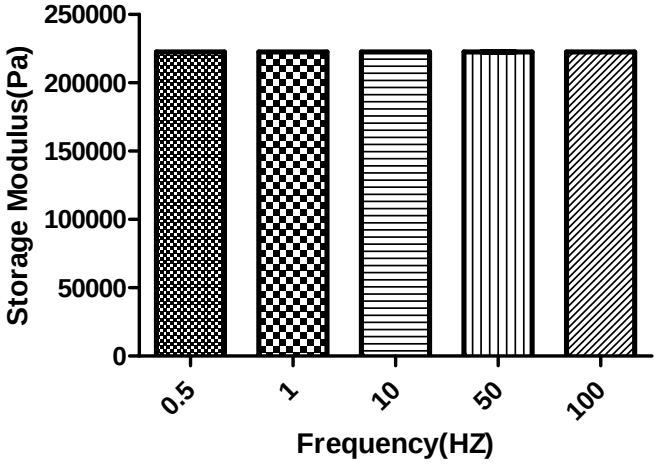

Fig.4. 7 Storage modulus with different frequency at

4.3.3 Simulation of stress on cells in the scaffolds

In the macro level simulation, Ogden models with their parameters (Table 4.1) were used and 2D simulations were performed at varying cell densities. Then a 0.1 mm × 0.1 mm area was picked from the bulk and the nodal displacements were mapped to the microscale ones.

Under the same compression conditions, maximum local SED on cells first increases from cell density of 1×10^6/mL to 3×10^6/mL and then decreases with the increase of cell density (Fig. 4.8). It decreases from 428 J/m3 at 3×10^6/mL to 393 J/m3 at 10×10^6/mL. This means cell density alters the mechanical properties of hydrogel and changes the stress environment on cells. The results show that generally the lower cell density scaffolds have higher stresses on cells and cells in low density scaffolds are more vulnerable at the same loading. The simulated results of relation between the hydrogel strain and SED on cells have a good agreement with experiments performed by Sun et al. [169]

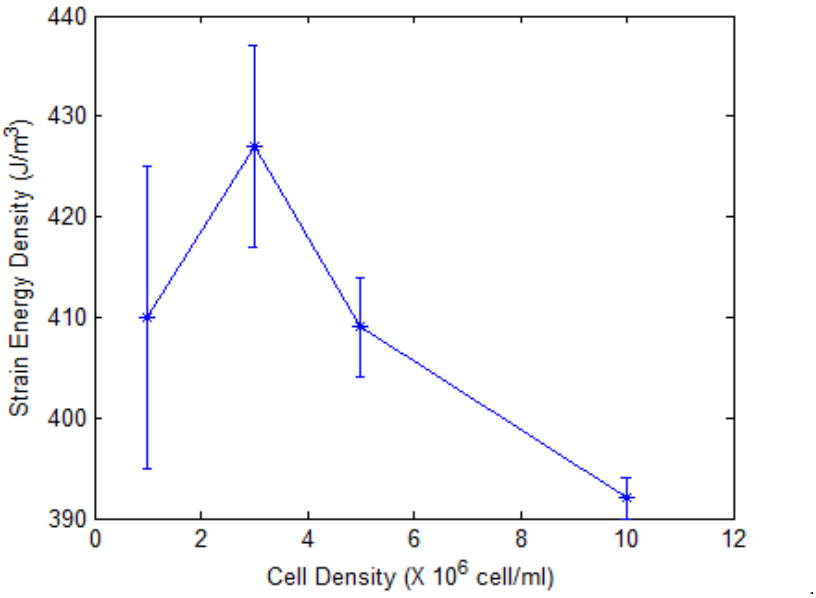

Fig.4. 8 Maximum SED on cells in scaffolds with different cell densities at compression of 10%

4.4 Conclusions

Cells are mechanically weak, and as they are encapsulated in to hydrogel scaffolds, the scaffold mechanical properties change. Different cell densities may lead to different mechanical properties of scaffolds. In this work, alginate hydrogel scaffolds with 3T3 fibroblasts encapsulated were fabricated through calcium ion crosslinking and the scaffold mechanical properties at different cell densities were studied through both experiments and simulations. Through experiments, the nonlinear constitutive laws for hydrogel scaffold mechanical properties were obtained and the dynamic modulus of hydrogel scaffolds at different cell densities were also examined. The experiments show that with the increase of cell density, the mechanical properties decrease, and Ogden model was chosen to best describe the hyperelasticity of scaffolds at different cell densities. Based on the model obtained from experiments, simulations were performed to examine the local stresses on cells under different loadings. The simulation results illustrate that cells experience varying stress environments at different cell densities and the stresses on cells decrease from 428 J/m3 at 3×10^6/mL to 393 J/m3 at 10×10^6/mL. The constitutive laws developed for hydrogels at different densities provide a foundation for quantitative study of the mechanical properties of cell-encapsulated hydrogel scaffolds, which is important not only for cell survival improvement but also for tissue regeneration promotion.

CHAPTER 5

MODELING OF SHEAR-INDUCED CELL DAMAGE AND ITS APPLICATION TO BIO-DISPENSING PROCESSES*

* This chapter partly has been published as "Xiaoyu Tian, Minggan Li and Xiongbiao Chen. (2008). Shear-induced cell damage and its application to bio-dispensing process". *The 16th Annual Conference of the CFD Society of Canada*. According to the Copyright Agreement, "the authors retain the right to include the conference article, in full or in part, in a thesis or dissertation".

5.1 Introduction

Various bio-fabrication methods have been developed in recent years, which employ mechanical means to manipulate cells to manufacture products with live cells[172]. Different cell manipulation techniques have been explored. In dispensing-based cell deposition technique [158, 173, 174] and rapid prototyping of hydrogel structures[66, 70, 175, 176], cells mixed with biomaterials are extruded from a fine nozzle to form a three dimensional (3D) constructs under an air pressure or a piston. In inkjet-based cell printing technique[177, 178], cells mixtures are jetted from a fine nozzle to form droplets and these droplets then form a 3D device under the control of a computer. Among these techniques, bio-dispensing is one of promising techniques, which is widely applied in 3D tissue scaffolds fabrication [175, 179], microfluidic devices[180, 181], and lab-on-a-chip devices [182, 183]. In these processes, cells are extruded from micro-needles and delivered to designated targets in a controllable manner. However, not all cells can survive and maintain their phenotype during these fabrication processes. During the fabrication process, cells are subjected to the pressure in the reservoir and/or the shear stress in the nozzle. Within a physiological range, the forces elicit adaptive responses acutely and chronically. If the

stresses exceed certain thresholds and/or are applied for a certain time period, cells will be harmed and even damaged. Some research has been done to study cell damage during the fabrication processes and cell damage rates under several process conditions have been reported [184]. However, these cell damage rates only valid at certain experimental conditions and may not apply to other process conditions. Thus a model used to predict the percentage of cell damage in the process by means of the process parameters is desirable.

It is noted that there are several definitions for cell damage from biological point of view [7], in our work cell membrane failure is considered as cell damage in this thesis as the mechanical force in bio-dispensing process directly applies on cell membrane. Also, cell membrane failure has been widely used for determination of cell damage in literature[7] .

As suggested in[185] that the short-term low hydrostatic pressure (< 5Mpa) has no effect on cell viability, the shear stress is the only consideration for possible cell damage in the dispensing process. Given this, the shear stress is assumed being the key factor causing cell damage in this thesis. Under this assumption, an experimental method is used to develop a cell damage law and then this cell damage law is applied to predict cell damage in the bio-dispensing process. The cell dispensing experiments were carried out to validate the model through a dispensing system. In these experiments, 3T3 cells and Schwann cells were chosen for preliminary study and admixed with sodium alginate solution for dispensing.

5.2 Materials and Methods

5.2.1 Chemical formulation

Medium viscosity sodium alginate powder (Sigma, St. Louis, MO) was dissolved in deionized water overnight to form 5% (w/v) solution.

5.2.2 Cell culture

3T3 cells, derived from 3T3 cell line (ATCC, Rockville, MD) and Schwann cells (ATCC, Rockville, MD), are grown in Dulbecco's Modified Eagle's medium (DMEM) (Sigma, St, Louis, MO) supplemented with 5% fetal bovine serum (FBS) (Sigma, St, Louis, MO) and 1% antibiotic. Cells were incubated at 37℃ in a humidified atmosphere of 95% air and 5% CO2. Before experiments, the cells were gently mixed in sodium alginate solution with a pipet to ensure a uniform cell distribution. 1 ml mixture solution was used each time for cell dispensing experiment.

5.2.3 Application of Shear Stress on Cells

Shear stress induced cell damage experiments were carried out by using a cone-and-plate geometry rheometer with a spindle of CP-52 (RVDV-III, Brookfield, MA). The schematic of the cone-and-plate part of the rheometer is shown in Fig. 3.1. The shear stress applied on the cells, throughout the medium in the rheometer, can be expressed as:

$$\tau = \frac{3T}{2\pi R^3} \tag{5.1}$$

where T is the torque applied on the spindle and R is the radius of the cone.

The experiments were all conducted in a room temperature of about 23℃. Cell mixture was carefully delivered into the container of the rheometer by using a pipet, with a sample volume of 0.5 ml. The rotational speed of the rheometer was controlled to apply varying shear stresses on the cells loaded to the rheometer. Percentage of cell damage (PCD) under shear was examined as a function of shear stress. To develop the cell damage law to relate PCD to shear

stress, the modified power-law model, which was used for the prediction of cell damage in literature [23, 125], was employed in this study, which is given by:

$$PCD_s(\tau) = C(\tau - \alpha)^a \tag{5.2}$$

where C, α and a are constants for a given kind of cells.

5.2.4 Cell-Dispensing System

A cell-dispensing machine adapted from a commercial fluid dispensing system (C0720M, Asymtek) was used in these experiments[6, 151]. The schematic of a typical dispenser is shown in Fig.5.1. It employs pressurized air to drive the solution in the syringe out the needle. P is the pressure of air applied to the syringe, P_e the pressure in the colloidal gel at the exit of the needle, D the internal diameter of the needle, and L the length of the needle. In the bio-dispensing process, the following assumptions are made: (1) the cell suspension is incompressible, implying its density is constant during the process; (2) the fluid flow in the needle is steady and fully-developed, at which the velocity profile does not change with time; (3) there is no slip between the cell suspension and the needle wall, (4) the pressure drop in the reservoir due to the fluid flow is negligible given the syringe diameter is much greater than the needle diameter; and (5) the minor losses due to entrance effects can be neglected given that the fact that the flow velocity in the needle is small. Under these assumptions, the pressure drop in the needle can be expressed as $\Delta P = P - P_e$ and under this pressure drop, the solution is driven out the needle.

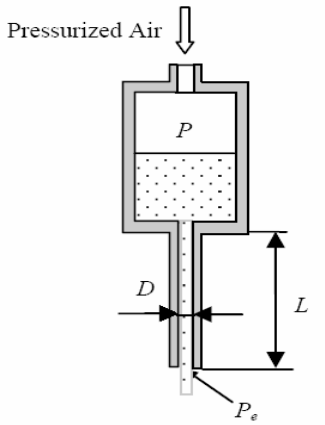

Fig.5. 1 Schematic of dispenser

The shear stress distribution along radial direction can be obtained [186]:

$$\tau_{rz} = \frac{-\Delta P}{2L} r \,. \tag{5.3}$$

whrere *r* is the radius. Suppose the cell density in the needle is denoted by *d*, the number of the total cells in the needle is $d\pi R^2 L$. In addition, from Equations (5.2) and (5.3), it can be seen that the *PCD* is a function of the radius *r*. Thus, the number of the damage cells in the dispensing process can be expressed by using the integration of $aL\int_0^R 2\pi r PCD_S(\tau_{rz})dr$, where *R* is the radius of the needle. Then the cell damage in dispensing process (PCD_d) can be obtained:

$$PCD_d = \frac{2\int_0^R rPCD_s(\tau_{rz})dr}{R^2} \tag{5.4}$$

where $PCD_s(\tau_{rz})$ is the cell damage law under shear stress (τ_{rz}) in the needle.

5.2.5 Cell Viability Assay

Niagara blue was used to stain the cells in the tested samples immediately after each dispensing process. The live/dead cells were manually counted under a light microscope (Leica, Microsystem, Bannockburn, IL) immediately following the each experiment.

5.3 Results

5.3.1 Cell Damage Law

To develop the shear-induced cell damage law, the percentages of cell damage under different shear stresses were measured and evaluated by experiments. In these experiments, cell mixtures were sheared in the rheometer for 5 minutes and each of them had a control group to compare the effect of shear stress on cell viability. Control groups were maintained in the same conditions as the tested ones except the shear stresses. After each experiment, live/dead cells are counted under microscope. A typical image under the microscope is shown in Fig. 5.2, in which black points indicate dead cells and white ones are live cells.

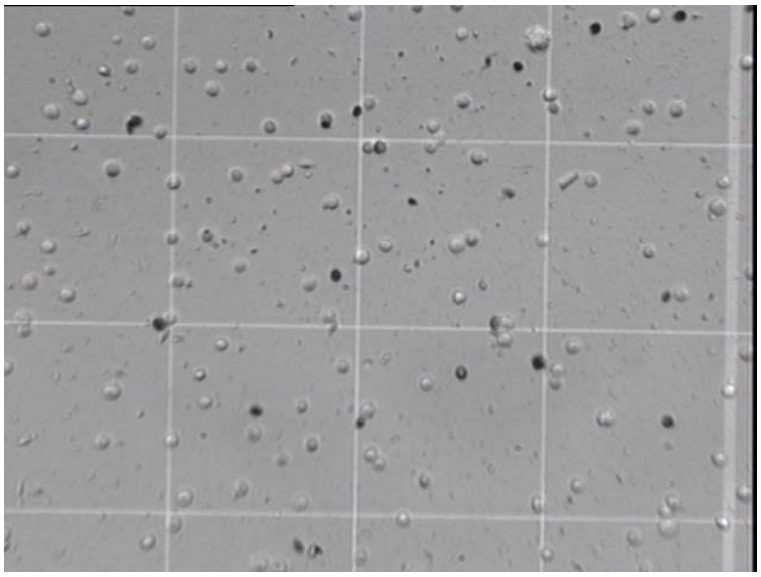

Fig.5. 2 live/dead cell under microscope

In the first experiment, the threshold shear stress for cell damage was obtained by trial and error. Different shear stress levels from 60 Pa to 120 Pa with increment of 20 Pa were applied, on the cell mixtures for both 3T3 and Schwann cells; and the number of the dead cells was counted. It was found that if the shear stress is less than 70Pa, there is no detectable cell

damage compared to the control groups for 3T3 cells and that if the shear stress is less than 80Pa, there is no detectable cell damage for Schwann cells. Thus, 70Pa and 80 Pa are considered as the threshold shear stress of 3T3 and Schwann cells, respectively, under which cells are not injured.

In the second experiment, six stress levels of 200, 400, 600, 800, 1000, and 1200 Pa, were applied for 3T3 and Schwann cells. After each experiment, both control and sheared samples were tested. The live and dead cells were counted under light microscope. Then the percentage of cell damage was calculated and the difference between the tested samples and the control groups were considered as the shear stress induced cell damage.

For each stress level, the experiment was repeated six times and the mean values of the percentage of cell damage were used to evaluate cell damage and the standard deviations were also calculated. The results are shown in Fig. 5.3. Fig.5.3 (a) is the cell damage rate of 3T3 cells under different shear stresses and Fig.5.3 (b) is the cell damage rate for Schwann cells. Asterisks are the mean values of the experimental values and the error bars are standard deviation of the experimental data.

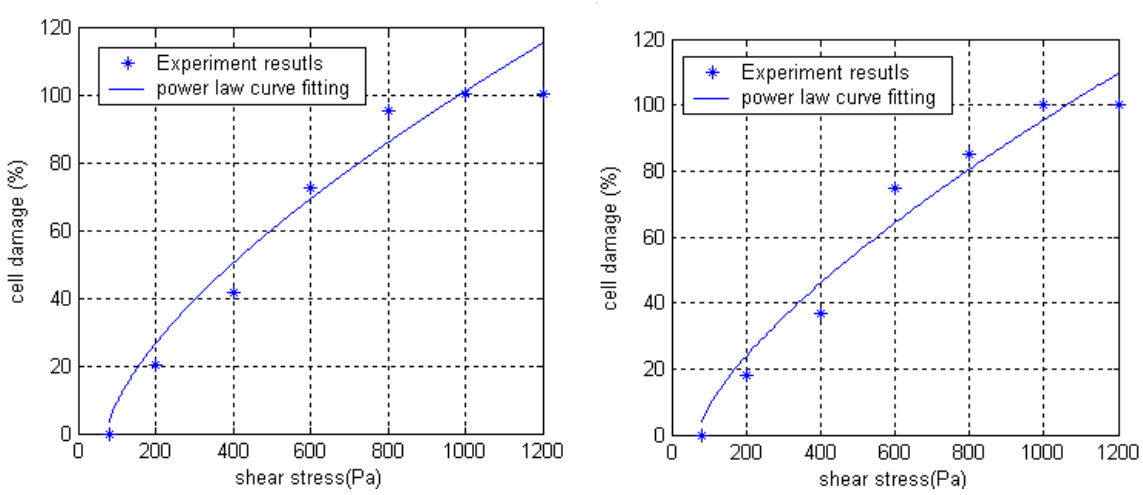

Fig. 5. 3 Cell damage under different shear stress: 3T3 cells(a) and Schwann cells(b)

The parameters in Equation (5.2) are obtained by fitting the cell damage data, which are shown as solid curve in Fig.4. The cell damage law for 3T3 cells is found to be:

$$PCD_S(\tau) = 0.768(\tau - 70.0)^{0.701}. \qquad (5.5.T)$$

and the cell damage law for Schwann cells is:

$$PCD_S(\tau) = 1.031(\tau - 80.0)^{0.665} \qquad (5.5.S)$$

The equation 5.5.T means the cell damage law for 3T3 cell and 5.5.S indicates the cell damage law for Schwann cells.

5.3.2 Cell Damage in Bio-dispensing Processes

Cell dispensing experiments were carried out to validate the cell damage law and the cell damage model for bio-dispensing processes in Equation (5.4). First, 3T3 cells mixed with alginate solution was extruded from a fine needle with the diameter of 150 μm under different pressure levels ranging from 1bar to 5 bar. The control groups consisted of collecting cell

mixture directly from the syringe without the needle under the passive effect of gravity. After each experiment, both control and dispensed samples were tested and the live and dead cells were counted under light microscope. The percentages of damaged cell were calculated and the difference between the tested samples and the controls were considered as the cell damage caused by the bio-dispensing processes. At each pressure level, the experiment was repeated six times and the mean values were reported as the cell damage results.

Percentage of cell damage in the dispensing process for 3T3 cells can be obtained by combining Equations (5.3), (5.4), and (5.5.T). It is worth to note that as cell suspension flow through a cylindrical tube, cells tend to move toward the axis of the tube, leaving a thin cell-rare layer near the wall[187, 188]. The thickness of this layer is about 10μm as measured in[188, 189]. To consider this effect, in this study the thickness of cell-rate layer (h) is subtracted from the needle radial and thus percent of cell damage can be expressed as:

$$PCD_d = \frac{2\int_0^{R-h} r \cdot 0.768(\frac{\Delta P}{2L} r - 70.0)^{0.701} dr}{R^2}. \tag{5.6}$$

Simulation based on Equation (5.6) under different pressure was performed in Matlab. Both experimental and simulation results are shown in Fig. 5.4.

Experiments for Schwann cells were also carried out. Schwann cells mixed with alginate solution was extruded from a fine needle with the diameter of 150 μm under the pressure of 1 bar to 5 bar and the same cell live/dead assay were used to evaluate cell damage in dispensing process. The similar cell damage rate in dispensing process also can be obtained by combining Equations (5.3), (5.4), and (5.5.S) and the simulation results are compared to the experimental ones in Fig. 5.4 (b).

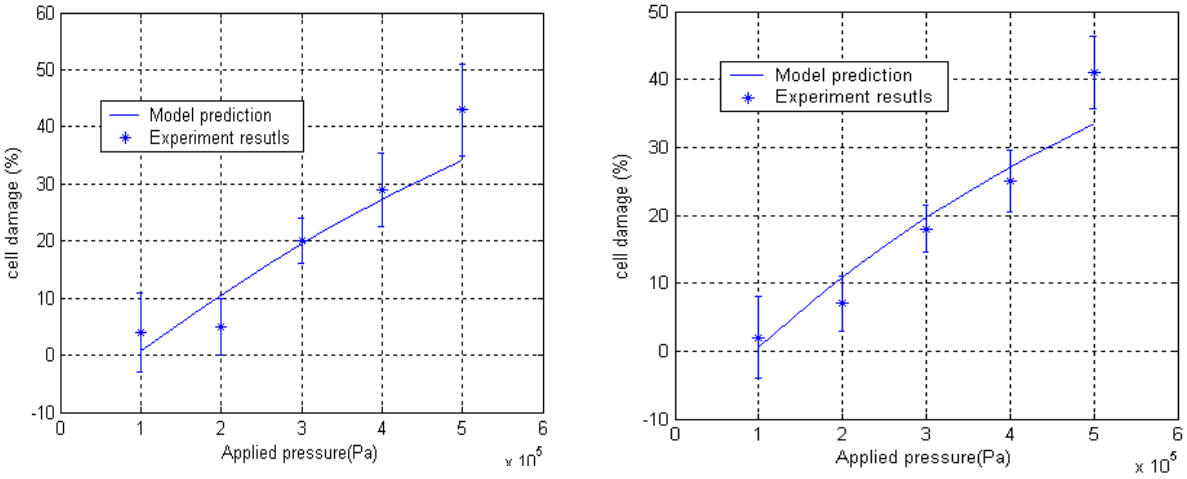

(a) (b)

Fig.5. 4 Percentage of cell damage in bio-dispensing process under different pressure. Percentage of cell damage for 3T3 cell damage (needle diameter =100microns, needle length = 12mm) (1); percentage of cell damage for Schwann cell (needle diameter=150microns, needle length = 20mm) (2)

Experimental data shows that percentage of cell damage increase with pressure applied in the syringe for both 3T3 and Schwann cell. For 3T3 cell, the percentage of cell damage increase from 3% at the pressure of 1 bar to 43% at the pressure of 5 bar. For Schwann cells, the percentage of cell damage increased to 41% at the pressure of 5 bar. The simulation results agreed with the experimental results, indicating the effectiveness of the cell damage model.

5.4 Discussion

In this research, the time effect of shear stress is not considered given that cells are extruded from a needle in a very short time course. This is also supported by our preliminary experiments, in which it is observed that there is no obvious change in the cell damage percentage when cells were sheared for 5 mins, 10 mins, and 30 mins, respectively. Therefore, it

may be reasonable to ignore the influence of the shear stress duration considering that cells are driven out of needles in a few seconds.

5.5 Conclusions

Cell damages for 3T3 and Schwann cells under different shear stresses levels were investigated in this chapter. Based on the measured cell damage percentages, a modified power law function was employed to develop the cell damage law. Then this cell damage law was applied into bio-dispensing processes; and the cell damages during bio-dispensing processes were investigated by developing the cell damage model. Experiments were carried out to study the effect of applied pressure on cell viability; and the results obtained showed the effectiveness of the cell damage model.

The method developed in this chapter will allows one to specify the influence of the process parameters on the cell damage percentage and, ultimately, to optimize the bio-dispensing process to minimize cell damage and achieve desired cell distribution for biological contractures and devices.

CHAPTER 6

COMPUTATIONAL FLUID DYNAMIC MODELING OF SHEAR-INDUCED CELL DAMAGE IN BIOFABRICATION PROCESS

6.1 Introduction

Biofabrication has emerged as a novel manufacturing technique, in which cells are mixed with biomaterial solutions and extruded from a fine needle to form constructs with a three-dimensional (3D) shape [69, 83, 177]. It has been widely used in tissue scaffold fabrication [179], lab-on-a-chip device [182], and drug deliver model [178]. In this extruding process, cells are exposed to the field of shear stress and deform under velocity gradient in the needle. Within a physiological range, cell deformations elicit adaptive responses acutely and chronically [7]. If the deformation exceeds a certain level, cell membrane will be over-stretched to the point the membrane cannot maintain its integrity, causing membrane rupture and cell damage.

Cell damage in fabrication process determines the cell viability in fabricated bio-products such as tissue scaffolds. Further, initial cell viability in cell-encapsulated bioproducts plays an important role in affecting biological and mechanical functions of products and their derivatives. For example, cell viability will affect cell propagation in tissue scaffolds, tissue growth speed as well as biological and mechanical properties of scaffolds. Hence, the investigation of cell damage in fabrication process is of importance and the models describe the relation between system parameters and cell damage can provide quantitative means and tactics to avoid process-induced cell damage.

Nowadays, some researches have been done regarding cell damage in flowing fluids but always hover over experiments and phenomenal models. Chang et al. [122] examined HepG2 cell damage percentage under different dispensing conditions including needle diameter and pressure. This study provides a straightforward experimental method to characterize cell damage in biofabrication process but at the same time shows the experimental method is not convenient and repeatable means to predict cell damage in fluids because if there is a change in system parameter, lots of experiments should be done. Further, some empirical models such as power law models , normal distribution models were proposed and develped to predict cell damage[21, 23, 190]. Model based on "damage accumulation" was developed to evaluate red blood cell damage in shear flow [190] and power-law function was employed to describe cell damage [23]. In our previous researches [21, 191], we quantitatively modelled cell damage percentage in biofabrication process based on a normal distribution cell damage law. Although these empirical models in some sense provide a mathematical tool to quantitatively predict cell damage, they lack of motivation to investigate cell damage process mechanism such as how cells are affected by the flowing solution and how cells deform, which directly leads to cells damage. To better understand cell deform and cell damage process, computational fluid dynamics (CFD) method was introduced. Tirella et al.[192] used CFD method to describe cell deformation, in which the cell mixture were considered as two phase flow and cells were modelled as fluid droplet. This research provides a numerical method to study cell-fluid interaction and cell deformation, however, cells are commonly considered as hyperelastic material and cannot deform like a fluid.

In this research, a new CFD-based cell damage law is developed to simulate the cell damage mechanism and predict cell damage in dispensing-based biofabrication process. Unlike previous methods, in this method, cells are considered as deformable capsules enclosed by a

hyperelastic membrane. Immersed boundary method (IBM)[193] is used to model cell-fluid interaction in the fine needle in cell dispensing process. Cell moving velocity is obtained by interpolating neighbouring fluid and as cell moves, it deforms. Strain energy density (SED) on cell membrane is calculated after each deformation and a critical SED is used as membrane fracture criteria to determine cell damage. Normal distribution function is employed as cell damage probability at a given SED. Cell damage percentage is calculated at the exit of the needle. Experiments were carried out to verify the model, in which Schwann cells encapsulated in 3% alginate solution were dispensed under different dispensing conditions.

6.2 Modeling cell damage in dispensing needle

Typical cell dispensing configuration is shown in Fig. 5.2, in which cell mixture is extruded out of the fine needle under a pressure. Fig. 6.1 shows the cell deformation in fluid flow in the needle.

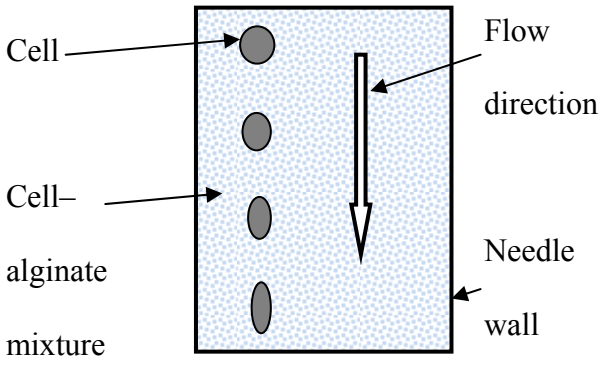

Fig.6. 1 Schematic of the cell deformation in needle

As cell mixture extruded from the needle, cells are moving from entrance to the exit of the fine needle with the mixture. Due to the high viscosity of the cell mixture, cells are gradually stretched by the shear stress of the solution in the flowing direction, as schematically shown in

Fig. 6.1. The challenge of modeling the cell damage process in the needle is that large deformation occurs on cells while they move along the needle. To solve this problem, immersed boundary method is used to model cell deformation in the flowing cell mixture. Generally, fluid domain is discretized into Lagrangian mesh and cell membrane is discretized into Eulerian points (Fig. 6.2). Cell moving velocity is interpolated from neighbouring points in fluid domain. As cell moves in the velocity gradient of fluid, cell deforms and produces elastic forces. This force is then spreading onto the neighbouring points of fluids. Strain energy density of cell membrane is calculated and is used to determine cell viability. These steps will be detailed in this section.

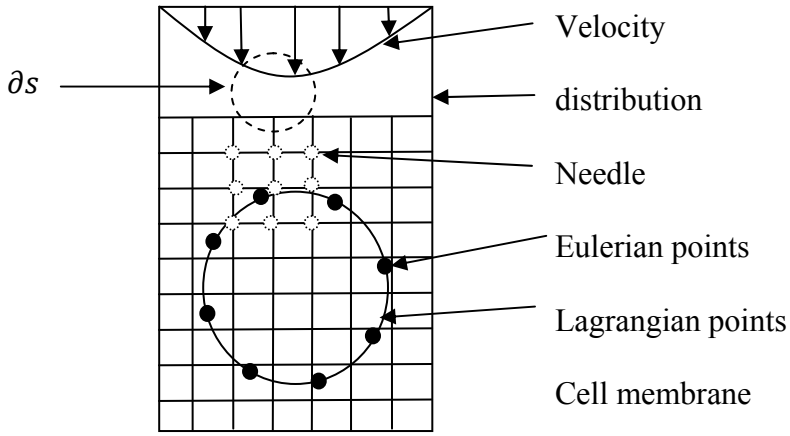

Fig.6. 2 Schematic of IBM method and domain

6.2.1 Fluid description

Cell mixture is a composite of cells and high molecular weight polymer. Due to large molecular chain, cell mixture often shows non-Newtonian flow behavior which is featured by a nonlinear relationship between the shear stress τ and velocity u as

$$\tau = m\nabla u^n \tag{6.1}$$

where m is the consistency index and n the flow behavior index.

The fluid motion in the needle is governed by Navier-Stokes equations:

$$\rho\left(\frac{\partial u}{\partial t} + u \cdot \nabla u\right) = -\nabla p + \nabla^2 u + f \tag{6.2}$$

$$\nabla \cdot u = 0 \tag{6.3}$$

where ρ is density, τ is shear stress of the fluid, f is external force exerted by the elastic cell membrane, p is pressure and u is velocity.

6.2.2 Cell description

Cells are considered as capsules with viscous fluid inside and infinitely thin membranes as shown in Fig.6.2. In this study, the fluid inside of the cell is assumed to have the same flow behavior as cell mixture. Cell membrane is characterized by a hyperelastic material which can be described by neo-Hookean law. The strain energy function is given by [194]

$$W = E_s h[{\epsilon_1}^2 + {\epsilon_2}^2 + (\epsilon_1 \epsilon_2)^{-2}] \tag{6.4}$$

where E_s is the shear modulus of elasticity of the membrane, h is the thickness of membrane and ϵ_1 and ϵ_2 are the principal stretch ratios. For a 2D membrane described as a closed curve, the tension in the membrane can be expressed as [194]

$$T = \frac{E_s h}{\epsilon^{3/2}}(\epsilon^3 - 1) \tag{6.5}$$

where $\epsilon = \epsilon_1$ is the stretch ratio along membrane curvature direction. For a discretized cell, T is the tension on a line segment along membrane from one Lagrangian grid to an adjacent one. The elastic force F at the Lagrangian grid is the resultant vector of the tensions in two adjacent segments, $F = T_i e_i - T_j e_j$, where i and j denote two adjacent line segments, and e_i and e_j are the

unit tangent vectors along them. Force F produced by the deformed membrane will be spreading onto the adjacent Eulerian grid and thus the cell interacts with fluid flow.

6.2.3 Cell and Fluid interaction

IBM has been applied to describe the force interactions between fluid flow and elastic structure[195, 196]. Briefly, a smooth version of Dirac delta function[193] in equation (6.6) is used to link fluid and structure, in which fluid is spatially discretized by Eulerian grid and structure is spatially discretized by Lagrangian grid as shown in Fig.6.2.

$$\delta(r) = \begin{cases} \frac{1}{4}\left(1 + cos\left(\frac{\pi r}{2}\right)\right), & |r| \leq 2 \\ 0 \quad , & otherwise \end{cases} \tag{6.6}$$

where $r = \frac{position\ coordinate}{grid\ unit\ size}$. At the grid point (black point) of the membrane, the velocity $(U(X,t))$ is expressed as the weighted combination of velocities $(u(x,t))$ of the fluid grid points (small circle) surrounding it as below

$$U(X,t) = \int_S u(x,t)\delta(x-X)dx \tag{6.7}$$

On the fluid grid, the force $f(x,t)$ is obtained by spreading the elastic forces $F(X,t)$ produced by cell membrane by using the same Dirac delta function:

$$f(x,t) = \int_{\partial s} F(X,t)\delta(x-X)dX \tag{6.8}$$

where $f(x,t)$ is a body force in governing equation (6.2), S is the affected fluid area and ∂s is the affected interface (Fig. 6.2).

6.2.4 Cell damage

In this study, strain energy density on cell membrane is calculated and used as the cell membrane rupture criteria. If the maximum stain energy density on a cell membrane is greater than a critical value, cell membrane breaks. An energy density value is assumed as critical strain energy (W_c) if:

$$if\ W_{cell\_max} > W_c \rightarrow cell\ damage \tag{6.9}$$

In practice, cells are individually different in terms of physical properties and thus they may not die at the same critical strain energy density. To describe the coherent physical variation of cells, the critical energy density is considered as a variable which obeys normal distribution. Thus the cell damage percentage corresponding to the strain energy of W_{cell_max} can be obtained by:

$$CDP = \int_0^{W_c} PDF(W_{cell\_max}) dW_{cell\_max} \tag{6.10}$$

where CDP is cell damage percent and PDF is the probability density function. This equation gives a quantitative relationship between critical strain energy and cell damage percentage. It will be used to calculate cell damage percentage at a given maximum SED.

In dispensing needle, it is assumed that cell density ρ_c is uniform throughout the cell mixture. In the unit height h at the exit of the needle, the cell damage in a concentric cylindrical annulus with inner radius $r - \frac{1}{2}\Delta r$ and outer radius $r + \frac{1}{2}\Delta r$ can be expressed as $2\pi r \Delta r h CDP(r)\rho_c$. Then the number of damaged cells at needle exit cross section is $\int_0^{R_n} 2\pi r h CDP(r)\rho_c dr$ and the number of the total cells at the same site is $\pi R^2 \rho_c h$. Thus, the cell damage in the dispensing process (CDP_n) can be obtained by

$$CDP_n = \frac{\int_0^{R_n} 2rCDP(r)dr}{{R_n}^2} \tag{6.11}$$

This is the total cell damage percent of cells at the exit of dispensing needles.

6.3 Experiments

6.3.1 Chemical Formulation

Low viscosity sodium alginate powder (Sigma, St. Louis, MO) was dissolved in deionized water to form 6% (w/v) solution.

6.3.2 Cell culture and Cell mixture

Schwann cells, derived from Schwann cell line (ATCC, Rockville, MD), are grown in Dulbecco's Modified Eagle's medium (DMEM) (Sigma, St, Louis, MO) supplemented with 10% fetal bovine serum (FBS) (Sigma, St, Louis, MO) and 1% antibiotic. Cells were incubated at 37℃ in a humidified atmosphere of 95% air and 5% CO2. Before experiments, cell cultures were gently mixed in the sodium alginate solution with a pipet at a ratio of 1:1 (v/v) to form a uniform cell suspension. All experiments were conducted at room temperature (~23℃).

6.3.3 Cell viability assay

Niagara blue was used to stain the cells in the tested samples immediately after each experiment. The live/dead cells were manually counted under a phase contrast microscope (Leica, Microsystem, Bannockburn, IL).

6.3.4 Physical parameters of fluid and cell

Flow behavior of cell mixtures was measured by a rheometer and parameters were identified by least square method using equation (6.1). 500mL cell mixture was scaled by a

weight scale (resolution: 0.1mg) to determine the density. Cell size was obtained by averaging ten cell diameters measured by the microscope. These values are listed in Table 6.1 and were used in simulation process.

Table 6. 1 Parameters in simulations

Fluid parameters	*values*	*Cell parameters*	*values*
m	2.65 $Pa \cdot s^n$	Cell radius	$5\mu m$
n	0.7	E_s	$10^4 dyn/cm^2$ [197]
ρ	$913 kg/m^3$	h	100Å [197]

6.3.5 Critical strain energy density distribution

In order to obtain critical strain energy density distribution PDF(W_c), both cell damage experiments and simulation were carried out. Cell damage experiments under uniform mechanical force were conducted by using a cone and plate rheometer with the spindle of CP-52 (RVDV-III, Brookfield, MA) to generate uniform shear stress. Different shear stresses of 80, 200, 400, 600, 800, 1000, 1200 Pa were applied to cell mixtures respectively. The control group was maintained still in tubes. Each of the experiments was repeated six times. The cell damage differences between shear induced groups and the control groups were considered as the results of shear flow. The experimental conditions were then used to calculate the maximum strain energy density on cells based on equations (6.1)-(6.11) in Matlab. Cell damage percents v.s. corresponding maximum SEDs are plotted in Fig. 6.3. Curve fitting was used to obtain critical strain energy density distribution (Fig. 6.3 solid curve). A normal distribution well fitted the data points and its density distribution is shown in Fig. 6.4. The distribution parameters obtained will be used in equation (6.10) for later cell damage simulation.

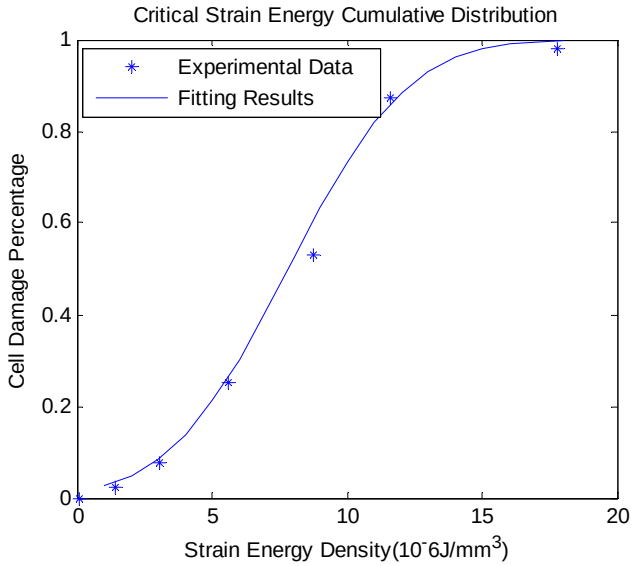

Fig.6. 3 Cell damage percentage v.s. maximum strain energy

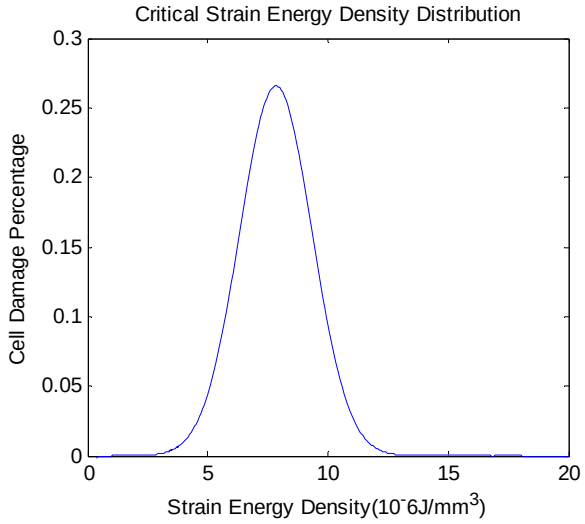

Fig.6. 4 Critical strain energy density distribution

6.3.6 Cell damage in dispensing process

To obtain cell damage in dispensing process, a commercial fluid dispensing system (C0720; Asymtek, Carlsbad, CA) was used. This system is designed to dispense the cell mixture out of the needle by air pressure, which is described in detail in[6]. In dispensing experiments, different air pressures (1, 2, 3, 4, 5 Bar) were used to extrude 2 mL cell mixture out of a needle

with length 20 mm and diameter 150 μm. The experiments were repeated six times for each pressure. Control group was maintained at the atmosphere pressure.

6.4 Simulation results and experimental validation

Simulation was performed using the same dispensing conditions asthose in experiments described in Section6.3.6. equ. (6.1) – (6.11) was used to code this model in Matlab. In the first simulation, three cells were placed at the needle entrance from near the needle center, in the middle and near the needle wall, respectively. Flow was steady and fully developed and cells are initially round in shape. Fig. 6.5 shows cell deformations as they flow in the needle. At the needle center, cells move faster, but smaller deformation. Fig. 6.6 shows the details of the deformed cells at different radial positions. Near the wall of the needle (Fig. 6.6a), cell shows larger deformation due to the high velocity gradients. Near the center of the needle (Fig. 6.6b), cells have very smaller deformation because of the low velocity gradients. For each cell, the local strain energies are different along the cell membrane illustrated by the coded colors. Red indicates high strain energy and blue means low strain energy. At different radial positions, cells suffer from different deformation and maximum strain energy. The greater the deformation, the higher the strain energy as expressed in equation (6.4). Near the needle wall, although the cell moves slower than the one at the center, its deformation is much higher and so is its strain energy.

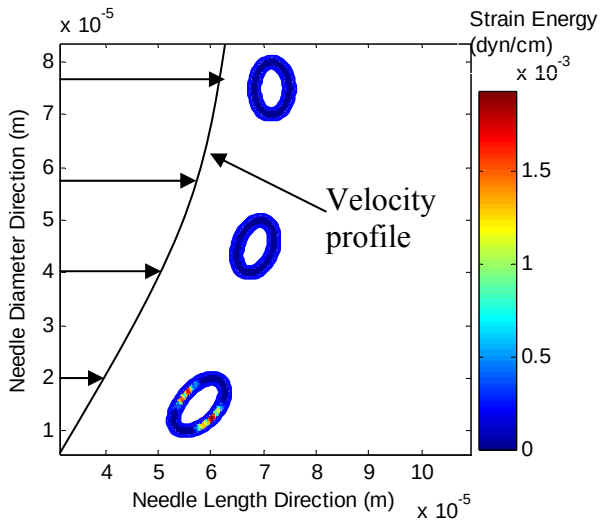

Fig.6. 5 Cells deformation at the different positions

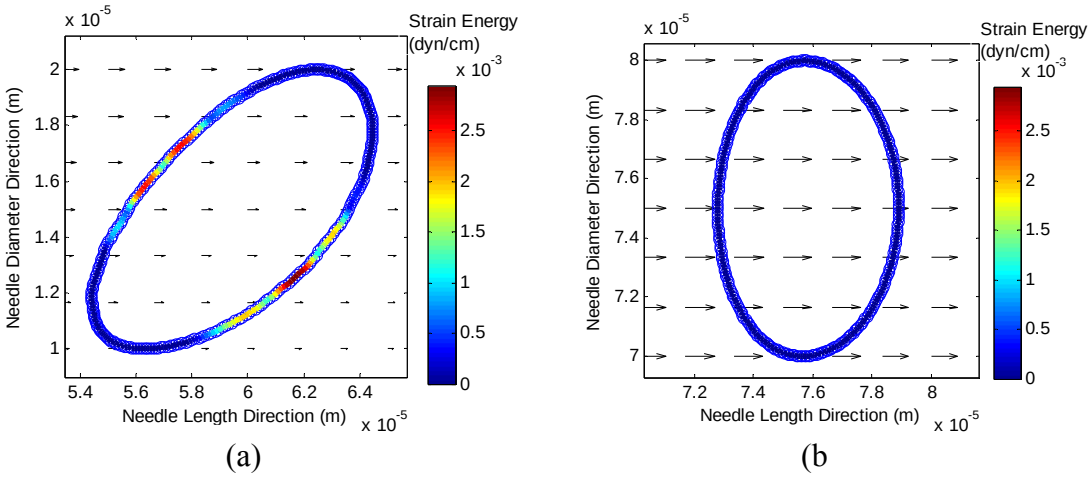

Fig.6. 6 Detailed cell deformation at near the needle wall (a) and at near the needle center (b)

The strain energy of a cell under deformation process was calculated to be 0.0012 to 6.234 dyn/cm, which shows good agreement with the strain energy of from 0.025 dyn/cm to 8 dyn/cm in literature [197]. The critical strain energy density is 7.8×10^{-6} J/mm3 is compared to previously published strain energy ($6 \sim 8 \times10^{-6}$ J/mm3) of cells under mechanical force.

From numerical simulation, the maximum strain energy density in dispensing process can be obtained. According to the known critical strain energy density in Section 6.3.5, the cell

damage percent at the exit of needle can then be calculated (Fig. 6.7, solid line). The simulation results are compared with experimental ones in Fig.6.7. It can be seen from the figure that with the increase of the pressure, cell damage percent increase quickly, from almost zero at 1 bar to 35% at 5 bar. This increased cell damage percent is cause by the higher velocity gradients in the dispensing needle at higher pressure. The velocity gradients stretch the cells when they move in the needle from the entrance to the exit. The close agreement of the simulation and experimental results shows the effectiveness of the method.

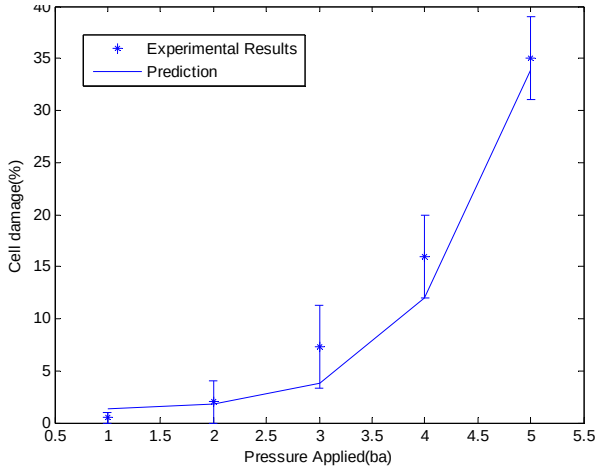

Fig.6. 7 Cell damages under different pressures in dispensing process

6.5 Conclusions

This research proposed a new method to model shear-induced cell damage in cell dispensing processes. IBM is used to model cell movement and large deformation in the flowing solution in dispensing needle. Cell membranes are considered as hyperelastic material and cell mixture is a non-Newtonian fluids. Strain energy density on cell membrane is used as cell damage criteria to determine cell viability. Both simulation and experiments were conducted and the agreement of both of the results shows the validation of this method. The CFD method

provides a novel technique to better understand cell damage progress in cell dispensing processes in various biofabrication applications.

It is worth to note that the modelling method used in this chapter is a general CFD method for cell damage study in cell mixture flow and should not be limited only to cell damage prediction in cell dispensing processes for biofabrication applications. It can be readily extended to study mechanical cell damage in various fluid based cell transportation processes such as cell printing, cell filtration and biomicrofluidics, where cell damage is essential for the final products.

CHAPTER 7

TEMPERATURE EFFECT ON THE SHEAR-INDUCED CELL DAMAGE IN BIOFABRICATION*

* This chapter has been published as "Minggan Li, Xiaoyu Tian and Xiongbiao Chen. (2010). Characterization of the flow behavior of alginate/hydroxyapatite mixtures for tissue scaffold fabrication. *Artificial Organs*. 35(7):741-746". The second author contributed to the research equally with the first author. According to the Copyright Agreement, "the authors retain the right to include the journal article, in full or in part, in a thesis or dissertation".

7.1 Introduction

Biofabrication methods have been dramatically advanced in recent years, by which living cells are incorporated into various bio-products such as cell-encapsulated tissue scaffolds [69] and lab-on-a-chip device [182]. Different biofabrication techniques have been explored, including inkjet cell printing [60], biodispensing cell deposition [173], and bio-assembly tools [66]. In these manufacturing processes, temperature typically needs to be controlled precisely as the process demands. For example, the process temperature was maintained at 10°C to prevent polymerization of the collagen [66], at 43°C to investigate the physiological properties of cells at high temperature [130], or simply at a room temperature [198].

During the fabrication processes, cells are subjected to mechanical forces and if the forces are relatively small, cells can survive the processes. If the forces are higher than certain level, cells may be damaged [7, 199]. Force induced cell damages were investigated experimentally [122] and quantitatively [21] in the literature. These studies show that the cell damage is mainly caused by shear stress and provide a cue to preserve cell viability in the biofabrication processes. Nevertheless, these studies were all performed at a room temperature,

and therefore the effect of temperature on process-induced cell damage remains unknown. Previous studies demonstrate that temperature can play an important role in cell properties. It affects the mechanical properties of both cell membrane [116] and cytoskeleton [200], leading to different vulnerability to the biofabrication processes. For example, at 2°C about 60% of the human fibroblasts remained viable using a pen delivery system [66]; at the room temperature 94% of Chinese Hamster Ovary (CHO) cells survived in an inkjet process [60]; at 37°C 98% of the prostate LNCaP and PC3 cells were alive once flowing through microchannels[201]; and at temperatures lower than 40.2°C about 90% of the CHO cells remained their viability in a cell perfusion process [202]. Previous studies also shown that within a range of 37 °C and 41.5°C, the CHO cell viability under the action of the same forces remained the same level, but became significant increasing once temperature reaches 45°C [130]. Thus, it is reasonable to assume that cell damage is associated with temperature, besides mechanical forces as reported in previous studies [21, 184].

This chapter presents the development of a cell damage law that quantitatively relates cell damage to temperature. The effectiveness of the developed cell damage law was also illustrated by applying it to the prediction of cell damage percents in the biofabrication process under different temperatures. Schwann cells were selected for use in this biofabrication process.

7.2 Materials and Methods

7.2.1 Chemical formulation

Sodium alginate powder (Sigma, St. Louis, MO) was dissolved in deionized water by a magnetic stirring bar overnight to form 7% (w/v) solution.

7.2.2 Cell culture and cell suspension

Schwann cells were selected in this study since they have been widely used in nerve tissue engineering. Schwann cells from Schwann cell line (ATCC, Manassas, VA) were grown in Dulbecco's Modified Eagle's medium(DMEM) (Sigma, St, Louis, MO) supplemented with 5% fetal bovine serum(FBS) (Sigma, St, Louis, MO) and 1% antibiotic. Cells were incubated at 37 °C in a humidified atmosphere of 95% air and 5% CO2 and cell medium was gently mixed in 7% sodium alginate solution with a pipette to ensure a uniform cell distribution according to the volume ratio of 1:3.

7.2.3 Cell damage under shear stress

A rheometer (RVDV-III, Brookfield) was used in this study to generate the uniform shear stress on the cell suspensions [203]. A water bath was connected to the rheometer for the control of cell suspension temperature. In each experiment, 0.5 mL of cell suspension was delivered to the rheometer by a pipette and maintained at the designed temperature for 5 minutes for thermal equilibrium. Each experiment under the identical conditions was repeated five times and the mean value and standard deviation of cell damage percents were obtained.

7.2.4 Mathematical model for cell damage law

Cell damage law is a mathematical function that relates the process parameters (e.g. temperature and mechanical forces) to the cell damage. Although different functions were proposed for the force-induced cell damage law, temperature effect was not considered in these models. Also, these cell damage laws generally take the form of power law function, which is not applicable to describe cell damage under a large range of stress. The reason is that as the

shear stress increase, the cell damage percents may exceed 100%, which is obviously not true. As such, cell damage laws which are able to overcome the above limitation are desirable. Our considerations to develop such laws include that (1) the cell damage percent be zero when there is no force apply on cells and be one hundred percent as force approaches to infinity; (2) the influence of temperature be well presented; (3) there be no cell recovery in the force-induced cell damage process, which is reasonable given the fact that the cell damage is examined immediately after fabrication process; and (4) the influence of the shearing duration be not involved by setting a short time period of shearing during the experiments.

With the above considerations, a mathematical model which involves the effects of both temperature and shear stress on cell damage is proposed as follows:

$$P_{law}(\tau, T) = \frac{1}{1 + \tau^{-a} e^{-(bT+c)}} \tag{7.1}$$

where P_{law} is the cell damage percent, τ is the shear stress the cells experience, T is the temperature, and a , b , c are the model parameters, which are to be identified experimentally.

7.2.5 Biofabrication system

The biofabrication system used in the present study was adapted from a commercial fluid dispensing system (C0720M, Asymtek) [6]. It employs air pressure to drive the suspension in the syringe out of a fine needle. Under the assumptions that the suspension flow is steady, incompressible, and fully-developed, the shear stress in the needle is given by [186]:

$$\tau_{rz} = \frac{-\Delta P}{2L} r \tag{7.2}$$

where ΔP is the pressure drop in the needle, r is the radial position of cells and L is the length of the needle. From the above equation, it is seen the shear stress varies along the radial direction. This suggests that the cell damage percentage is not constant across the cross-section of the needle, but a function of the radius. Thus, the total cell damage percent during the process can be established by integrating the cell damage percentage over the cross-section under the assumption that the cells are evenly distributed in the needle, i.e.,

$$PCD_d = \frac{2\int_0^{D/2} rP_{law}(\tau_{rz}, T)dr}{R^2} \tag{7.3}$$

where $P_{law}(\tau_{rz}, T)$ is the cell damage law under shear stress (τ_{rz}) and temperature T, as established by using equation (7.1), D is the diameter of the needle.

7.2.6 Cell viability assay

As cell membrane and intercellular skeleton are important to maintain and support cell integrity during cell deformations [204], in the present study the rupture of the cell membrane is considered as cell damage, which is consistent with the study reported in [7]. To test the cell membrane integrity, Niagara blue was used to stain the cells in the samples immediately after each experiment. The living/dead cells were manually counted under a light microscope (Leica, Microsystem, Bannockburn, IL) for the evaluation of cell damage percentage.

7.3 Experiments and Results

7.3.1 Development of shear-induced cell damage law

Cell damage experiments were performed on the rheometer as mentioned previously. Six temperatures (0°C, 15°C, 23°C, 37°C, 40°C and 45°C) were examined and at each temperature, different shear stresses of 200 Pa, 400 Pa, 600 Pa, 1000 Pa, and 1500 Pa were applied on cells respectively. Control groups were maintained at the same temperature as the experimental ones but without the application of shear stress. After each experiment, live/dead cells were countered using the cell viability assay. Cell damage percentages were then evaluated from the ratio of the number of dead cells to that of total cells. The difference between the experimental and the control group is considered as the cell damage caused by the shear stress and temperature.

The mean values of the cell damage percentages in each of the experiments are shown in Fig. 1. It can be seen that cell damage percentages increase with both the temperature and the shear stress. At each shear stress, cell damage percentage initially increases slowly and then faster once temperature reaches 15°C.

The experimental data obtained were used to identify the parameters in equation (7.1) based on the least square regression in MATLAB. The parameters obtained are shown in equation (7.4). Then this cell damage law was used to simulate cell damage under the same conditions as applied in the experiments and the results are shown in solid smooth curves in Fig. 1 for a comparison.

$$P_{law}(\tau, T) = \frac{1}{1 + \tau^{-3.6} e^{-(0.10838T - 26.177)}} \tag{7.4}$$

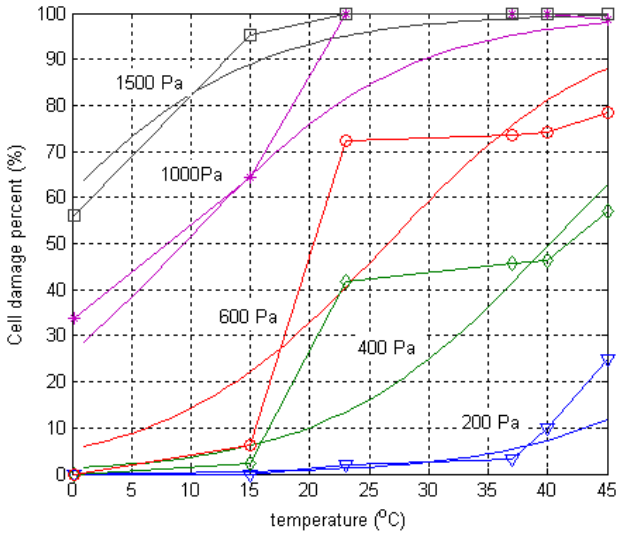

Fig.7. 1 Cell damage vs. temperature under different shear stresses (shearing time = 150s)

7.3.2 Validation of cell damage law

To validate the developed cell damage law, cell suspensions were sheared under different shear stresses (900 Pa and 1100 Pa) and cell damage percentages were examined as described previously. The shear stresses and the temperatures applied in the experiments were substituted into equation (7.4) and the corresponding cell damage percentages were calculated. Both the experimental and simulation results are shown in Fig.7.2 (a). The agreement between experimental results and simulation results indicates that the developed cell damage law is effective within the range of temperature and shear stresses examined in the present study.

7.3.3 Applications to the biofabrication process

The cell damage law was also applied to biofabrication process to predict the cell damage percentage. In these experiments, the cell suspensions were heated to the preset temperature for 5 minutes using the water bath; and then the cell suspensions were extruded from fine needles with a diameter of 0.2 mm and a length of 30 mm under an air pressure of 500 kPa. The control

groups were stored in the syringe without the needle and dropped into a container under the action of gravity. After each experiment, both control and dispensed samples were examined by the cell viability assay. The difference in the cell damage percentage between the dispensed and the control samples is considered as the cell damage caused by the dispensing process. At each temperature, experiments under the identical conditions were repeated five times and the mean value of cell damage percentage is shown as an asterisk in Fig. 7.2(b). Based on the developed model of equations (7.1) to (7.3), the simulation was performed and the results are shown in a solid curve in Fig. 7.2(b). Compared with the experimental data, simulation results also display the fluctuation up and down around experimental cell damage values. The agreement between the experimental results and simulation prediction indicates that the developed model can be used to quantitatively predict the cell damage in the biodispensing process.

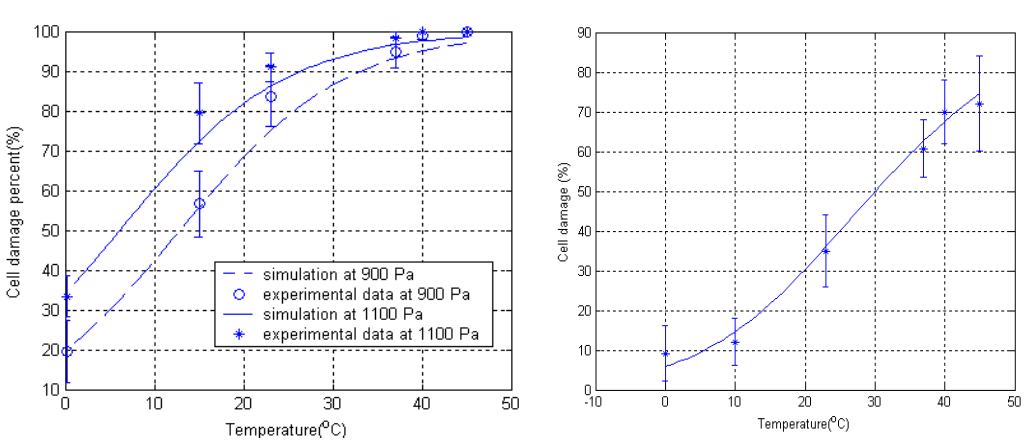

Fig.7. 2 Cell damage with temperatures (a) at the shear stress of 900 Pa and 1100 Pa (shearing time = 150s), and (b) in the biodispensing processes (needle diameter = 0.2mm, needle length = 30mm, pressure = 500kPa).

7.4 Discussions

It is noticed the identified parameters in equation (7.3) were obtained under the conditions of the shear stress ranging from 0 to 1500 Pa and temperature ranging from 0 to 45°C. The extended use of the equation (7.3) beyond the aforementioned ranges may be inapplicable. Cell-cell interaction in the cell suspension may also affect cell viability. If the cell density is high enough, cells may physically contact each other. As a result, stress concentration may occur, thus possibly changing cell properties and causing difference in cell damage. In this work, the cell density was fixed at around 1×10^6 /mL and cells were evenly dispersed in the cell suspension. As such, it is reasonable to neglect the cell-cell interaction. However, it is suggested that as the cell density increases, the effect of cell-cell interaction needs to be considered in establishing cell damage laws. Also, it should be noted that the applications of equation (7.3) to the biofabrication process as examined in this study were under the assumption that the fluid flow concerned in the process is steady, incompressible, and fully-developed. Readers should be aware of the possible error caused by the disagreement between this assumption and the conditions of the biofabrication process to which the cell damage law is applied. As of a general note, although the effectiveness of the developed method was illustrated in this study by using a special type of cells (i.e., Schwann cells) under certain conditions (i.e., the ranges of shear stress and temperature, and the cell density), the developed method can be readily extended and applied to the establishment of cell damage laws for other types of cells and the conditions beyond the ones examined in this study, as well as the applications to the biofabrication process by means of different cell-manipulation techniques such as cell printing.

In this study, the rupture of the cell membrane is considered as cell damage; and Niagara blue was used to stain these cells blue, while living cells with intact membranes remained

uncoloured. It is noted that injured cells may recover from membrane break, as reported in [205]. The recovery effect is not considered in this study and thus, the cell damage law developed is only applicable to the cell damage, which is examined immediately following the biofabrication process.

7.5 Conclusions

This chapter presents a method to study the effects of temperature on shear-induced cell damage and its applications in the biodispensing process. The relationship between cell damage and temperature was investigated experimentally by using Schwann cells; and a cell damage law was then developed to represent the effects of both shear stress and temperature. For validation, the cell damage law was applied to predict the percentages of Schwann cell damage occurring during the biofabrication process with varying temperatures. The agreement between the experimental and model simulation indicates the effectiveness of the method developed. The availability of the developed method and resultant models allow for effectively control and preserve cell viability in the biofabrication process.

CHAPTER 8

CONCLUSIONS AND FUTURE WORK

8.1 Conclusions

Cell-encapsulated scaffolds have been widely applied in tissue regeneration, drug delivery, biomedical testing. Dispensing-based bioRP technique not only shows a capability to fabricate desirable cell-encapsulated tissue scaffolds with biocompatible and biomimetic micro-environment such as designed mechanical properties, controllable porous structure and spatial control of cells and biomaterials distribution but also is potentially capable of be integrated to a all-in-one process to multi-batch manufacture tissue scaffolds. This research focuses on dispensing-based scaffold fabrication process, with the aim at investigating flow behavior of scaffold biomaterials, cell density and process-induced cell damage. The main conclusions of this research are summarized as follows:

1. Flow behavior of alginate/HA mixtures can be affected by alginate concentration, HA concentration and temperature in exponential fashion and their relationship can be quantitatively modelled. The relationship flow rate and flow behavior of materials can also be accurately modeled and on this basis, the system operation parameters such as pressure, needle moving speed, needle size can be determined according to flow behavior of scaffold biomaterials and temperature to fabricate scaffolds.

2. Cell density can affect the mechanical properties of cell-encapsulated hydrogel scaffolds. Compared with alginate scaffolds without cells, cell-encapsulated scaffolds exhibit hyperelasticity and viscoelasticity. For cell-encapsulated scaffolds, the less cell encapsulated, the more brittle and stiffer the scaffolds are. The elastic part of viscoelasticity of scaffold increases with cell density. Also, scaffolds with higher cell density exert less mechanical stresses on cells at the same strain, which provides a cue for cell-encapsulated scaffolds design for cell viability retain. Third order Ogden models can be used to represent the forced-induced hydrogel scaffolds deformation up to 45% strain.
3. A modified cell damage law considering a thin cell-rare layer near the wall can be used for predicting Schwann cell and 3T3 cell damage during the dispensing process. This work provides a simple method to predict cell damage in fabrication prOcess and a cue to control cell viability by adjusting manufacturing system parameters such as pressure, needle diameter and length.
4. A computational fluid dynamic cell damage model was successful developed to predict cell damage in dispensing system. Critical strain energy was introduced and used as a criterion of cell membrane fracture. A computational fluid dynamic model was developed to represent cell deformation during dispensing process and immerse boundary methods was applied to describe the interaction between cell membrane and fluid. This model not only effectively predicts cell damage during dispensing-based fabrication process but also provides a method to deeply investigate the force- induced cell failure mechanism.
5. Temperature effects on cell damage were investigated and a new cell damage model was developed to represent forced-induced cell damage under different operation temperature. This model was validated by a comparison between experiments and simulations. This

work also provides a cue to control temperature in scaffold fabrication process to obtain a desirable scaffold.

8.2 Contributions

In this research, both experimental and numerical studies for dispensing-based tissue scaffolds fabrication were carried out. The results obtained will facilitate the hydrogel scaffolds design and fabrication and improve the tissue regeneration in tissue engineering. The main contributions are summarized as follow:

1. Developed rheological models for alginate hydrogel and its mixture
2. Experimentally and numerically investigated the effects of cell density on the mechanical properties of hydrogel scaffold
3. Studied the shear-induced cell damage in biodispensing processes
4. Numerically investigated the cell-fluid interaction and cell damage mechanism
5. Developed models for effects of temperature on cell damage in biodispensing processes

8.3 Future work

Based on the work presented in this dissertation, a number of studies can be carried on to extend the current research.

1. Develop a 3D model for studying cell density effects on local strain energy under mechanical forces. In current research, a 2D model for uniaxial compression loading condition was developed. A 3D model will not only better represent the real environment of cells but also to simulate complex 3D space conditions such as scaffolds deformation under multiaxial loadings. To do so, 3D constitutive laws for both hydrogel and cells should be first established

and then 3D finite element analysis method can be used to investigate the cell density effects on mechanical properties of scaffolds.

2. Investigating cell density effects on cell viability under mechanical forces and developing models to represent the effects. This research indicated different cell density will affect the local strain energy on cells and the cell damage model also evaluated the cell membrane failure based on the critical strain energy. The proposed project can develop a model to evaluate cell density effects on cell viability with assistance of measuring cell viabilities after mechanical loading.

3. Optimizing the cell damage law. This research developed a CFD-based 2D framework to predict cell damage in fluidic condition. The model can be developed and optimized by considering following: 1) a 3D model development, 2) fluid is considered as a non-newtonian in Navier-stokes equations, and 3) a smoother fluid-structure interaction can take over IBM method

4. Development of cell damage law for different applications. The CFD-based cell damage law is a general method and can be used to describe cell damage process in different geometrical fluidic space such as taper-based dispensing process which is used in various applications. Also cell damage for difference cell types can be studied by using the mechanical properties of the corresponding cell membranes. This will help more tissue engineering applications since various types of cells are currently used in biofabrication processes.

5. In CFD-based cell damage model, one the currently assumption is that the viscosity inside and outside of cell membrane is the same. This may not true when different hydrogel solution is used in biofabrication processes. To improve the model, the viscosity of cell plasma and hydrogel solution should be taken into account in the model. Further, simulation of currently model starts from the entrance of a needle and cells are considered intact at the entrance.

However, the extensional flow from the syringe to the needle caused by the sudden geometrical change may harm cells in certain level. A better cell damage prediction model can be developed by calculating strain energy density on cells from the syringe instead of from the entrance of the needle.

The limitations of this work also should be noticed so that the following work can be carried out smoothly. First, the rheological behavior of alginate/HA mixture has a high yield stress so that it can hold its structure by itself. Thus the method used to fabrication scaffolds maybe not applicable to pure polymer solution. Second, for cell density effect s on mechanical properties of scaffolds, the cells are assumed to be uniformly distributed in scaffolds. This may not true in biofabrication process, especially when cells aggregate. A statistic method maybe needed to represent cell distribution in scaffolds. Third, cells in dispensing needles are assumed to be not contacted each other and thus no cell-cell interaction is considered in the CFD-based cell damage simulation. However, cell-cell interaction often happens in biofabrication process, it may be necessary to add cell-cell interaction if more precise cell damage prediction is expected.

LIST OF REFERENCE

[1] S. J. Hollister, "Porous scaffold design for tissue engineering," *Nat Mater*, vol. 4, pp. 518-24, 2005.

[2] J. Zeltinger, J. K. Sherwood, D. A. Graham, R. Mueller, and L. G. Griffith, "Effect of pore size and void fraction on cellular adhesion, proliferation, and matrix deposition," *Tissue Eng*, vol. 7, pp. 557-72, 2001.

[3] H. H. Lu and J. P. Spalazzi, "Biomimetic stratified scaffold design for ligament-to-bone interface tissue engineering," *Comb Chem High Throughput Screen*, vol. 12, pp. 589-97, 2009.

[4] M. G. Li, X. Y. Tian, and X. B. Chen, "A brief review of dispensing-based rapid prototyping techniques in tissue scaffold fabrication: role of modeling on scaffold properties prediction," *Biofabrication*, vol. 1, 2009.

[5] H. D. Ke, "Investigation into the dispensing-based fabrication process for tissue scaffolds," in *Department of mechanical engineering*, vol. Master of science. Saskatoon: University of saskatchewan, 2006.

[6] M. G. Li, X. Y. Tian, and X. B. Chen, "Modeling of Flow Rate, Pore Size, and Porosity for the Dispensing-Based Tissue Scaffolds Fabrication," *Journal of Manufacturing Science and Engineering-Transactions of the ASME*, vol. 131, 2009.

[7] K. A. Barbee, "Mechanical cell injury," *Ann N Y Acad Sci*, vol. 1066, pp. 67-84, 2005.

[8] R. Langer and J. P. Vacanti, "Tissue engineering," *Science*, vol. 260, pp. 920-6, 1993.

[9] L. E. Niklason and R. Langer, "Prospects for organ and tissue replacement," *Jama*, vol. 285, pp. 573-6, 2001.

[10] J. R. Fuchs, B. A. Nasseri, and J. P. Vacanti, "Tissue engineering: a 21st century solution to surgical reconstruction," *Ann Thorac Surg*, vol. 72, pp. 577-91, 2001.

[11] U. A. Stock and J. P. Vacanti, "Tissue engineering: current state and prospects," *Annu Rev Med*, vol. 52, pp. 443-51, 2001.

[12] M. J. Whitaker, R. A. Quirk, S. M. Howdle, and K. M. Shakesheff, "Growth factor release from tissue engineering scaffolds," *J Pharm Pharmacol*, vol. 53, pp. 1427-37, 2001.

[13] G. D. Nicodemus and S. J. Bryant, "Cell encapsulation in biodegradable hydrogels for tissue engineering applications," *Tissue Engineering Part B-Reviews*, vol. 14, pp. 149-165, 2008.

[14] A. P. Mcguigan and M. V. Sefton, "Design and fabrication of sub-mm-sized modules containing encapsulated cells for modular tissue engineering," *Tissue Engineering*, vol. 13, pp. 1069-1078, 2007.

[15] T. B. F. Woodfield, C. A. Van Blitterswijk, J. De Wijn, T. J. Sims, A. P. Hollander, and J. Riesle, "Polymer scaffolds fabricated with pore-size gradients as a model for studying the zonal organization within tissue-engineered cartilage constructs," *Tissue Engineering*, vol. 11, pp. 1297-1311, 2005.

[16] E. Alsberg, K. W. Anderson, A. Albeiruti, R. T. Franceschi, and D. J. Mooney, "Cell-interactive alginate hydrogels for bone tissue engineering," *Journal of Dental Research*, vol. 80, pp. 2025-2029, 2001.

[17] E. Bell, *Priciples of Tissue Engineering*, 2nd ed. San Diego: Academic Press, 2000.

[18] J. Fukuda, A. Khademhosseini, Y. Yeo, X. Y. Yang, J. Yeh, G. Eng, J. Blumling, C. F. Wang, D. S. Kohane, and R. Langer, "Micromolding of photocrosslinkable chitosan hydrogel for spheroid microarray and co-cultures," *Biomaterials*, vol. 27, pp. 5259-5267, 2006.

[19] J. Yeh, Y. B. Ling, J. M. Karp, J. Gantz, A. Chandawarkar, G. Eng, J. Blumling, R. Langer, and A. Khademhosseini, "Micromolding of shape-controlled, harvestable cell-laden hydrogels," *Biomaterials*, vol. 27, pp. 5391-5398, 2006.

[20] A. Khademhosseini and R. Langer, "Microengineered hydrogels for tissue engineering," *Biomaterials*, vol. 28, pp. 5087-5092, 2007.

[21] M. G. Li, X. Y. Tian, N. Zhu, D. J. Schreyer, and X. B. Chen, "Modeling Process-Induced Cell Damage in the Biodispensing Process," *Tissue Engineering Part C-Methods*, vol. 16, pp. 533-542, 2010.

[22] M. Grigioni, C. Daniele, U. Morbiducci, G. D'Avenio, G. Di Benedetto, and V. Barbaro, "The power-law mathematical model for blood damage prediction: Analytical developments and physical inconsistencies," *Artificial Organs*, vol. 28, pp. 467-475, 2004.

[23] M. Grigioni, U. Morbiducci, G. D'Avenio, G. Di Benedetto, and C. Del Gaudio, "A novel formulation for blood trauma prediction by a modified power-law mathematical model," *Biomechanics and Modeling in Mechanobiology*, vol. 4, pp. 249-260, 2005.

[24] R. G. M. Breuls, C. V. C. Bouten, C. W. J. Oomens, D. L. Bader, and F. P. T. Baaijens, "A theoretical analysis of damage evolution in skeletal muscle tissue with reference to pressure ulcer development," *Journal of Biomechanical Engineering-Transactions of the Asme*, vol. 125, pp. 902-909, 2003.

[25] N. E. Fedorovich, J. Alblas, J. R. de Wijn, W. E. Hennink, A. J. Verbout, and W. J. Dhert, "Hydrogels as extracellular matrices for skeletal tissue engineering: state-of-the-art and novel application in organ printing," *Tissue Eng*, vol. 13, pp. 1905-25, 2007.

[26] D. J. Odde and M. J. Renn, "Laser-guided direct writing of living cells," *Biotechnol Bioeng*, vol. 67, pp. 312-8, 2000.

[27] Y. Nahmias and D. J. Odde, "Micropatterning of living cells by laser-guided direct writing: application to fabrication of hepatic-endothelial sinusoid-like structures," *Nat Protoc*, vol. 1, pp. 2288-96, 2006.

[28] Y. Lin, G. Huang, Y. Huang, T. Tzeng, and D. Chrisey, "Effect of laser fluence in laser-assisted direct writing of human colon cancer cell," *Rapid Prototyping Journal*, vol. 16, pp. 202-208, 2010.

[29] R. K. Pirlo, D. M. Dean, D. R. Knapp, and B. Z. Gao, "Cell deposition system based on laser guidance," *Biotechnol J*, vol. 1, pp. 1007-13, 2006.

[30] J. A. Barron, P. Wu, H. D. Ladouceur, and B. R. Ringeisen, "Biological laser printing: A novel technique for creating heterogeneous 3-dimensional cell patterns," *Biomedical Microdevices*, vol. 6, pp. 139-147, 2004.

[31] C. Mezel, A. Souquet, L. Hallo, and F. Guillemot, "Bioprinting by laser-induced forward transfer for tissue engineering applications: jet formation modeling," *Biofabrication*, vol. 2, pp. 014103.

[32] I. Elloumi Hannachi, K. Itoga, Y. Kumashiro, J. Kobayashi, M. Yamato, and T. Okano, "Fabrication of transferable micropatterned-co-cultured cell sheets with microcontact printing," *Biomaterials*, vol. 30, pp. 5427-32, 2009.

[33] J. A. Barron, D. B. Krizman, and B. R. Ringeisen, "Laser printing of single cells: Statistical analysis, cell viability, and stress," *Annals of Biomedical Engineering*, vol. 33, pp. 121-130, 2005.

[34] B. Dhariwala, E. Hunt, and T. Boland, "Rapid prototyping of tissue-engineering constructs, using photopolymerizable hydrogels and stereolithography," *Tissue Engineering*, vol. 10, pp. 1316-1322, 2004.

[35] A. Ashkin, J. M. Dziedzic, and T. Yamane, "Optical Trapping and Manipulation of Single Cells Using Infrared-Laser Beams," *Nature*, vol. 330, pp. 769-771, 1987.

[36] A. Ashkin and J. M. Dziedzic, "Optical Trapping and Manipulation of Viruses and Bacteria," *Science*, vol. 235, pp. 1517-1520, 1987.

[37] D. J. Odde and M. J. Renn, "Laser-guided direct writing for applications in biotechnology," *Trends Biotechnol*, vol. 17, pp. 385-9, 1999.

[38] H. Liang, K. T. Vu, P. Krishnan, T. C. Trang, D. Shin, S. Kimel, and M. W. Berns, "Wavelength dependence of cell cloning efficiency after optical trapping," *Biophys J*, vol. 70, pp. 1529-33, 1996.

[39] R. K. Pirlo, Z. Ma, A. Sweeney, H. Liu, J. X. Yun, X. Peng, X. Yuan, G. X. Guo, and B. Z. Gao, "Laser-guided cell micropatterning system," *Rev Sci Instrum*, vol. 82, pp. 013708.

[40] Y. Nahmias, R. E. Schwartz, C. M. Verfaillie, and D. J. Odde, "Laser-guided direct writing for three-dimensional tissue engineering," *Biotechnology and Bioengineering*, vol. 92, pp. 129-36, 2005.

[41] C. Mezel, A. Souquet, L. Hallo, and F. Guillemot, "Bioprinting by laser-induced forward transfer for tissue engineering applications: jet formation modeling," *Biofabrication*, vol. 2, 2010.

[42] F. Guillemot, A. Souquet, S. Catros, B. Guillotin, J. Lopez, M. Faucon, B. Pippenger, R. Bareille, M. Remy, S. Bellance, P. Chabassier, J. C. Fricain, and J. Amedee, "High-throughput laser printing of cells and biomaterials for tissue engineering," *Acta Biomater*, vol. 6, pp. 2494-500.

[43] L. Koch, S. Kuhn, H. Sorg, M. Gruene, S. Schlie, R. Gaebel, B. Polchow, K. Reimers, S. Stoelting, N. Ma, P. M. Vogt, G. Steinhoff, and B. Chichkov, "Laser printing of skin cells and human stem cells," *Tissue Eng Part C Methods*, vol. 16, pp. 847-54.

[44] B. R. Ringeisen, H. Kim, J. A. Barron, D. B. Krizman, D. B. Chrisey, S. Jackman, R. Y. Auyeung, and B. J. Spargo, "Laser printing of pluripotent embryonal carcinoma cells," *Tissue Eng*, vol. 10, pp. 483-91, 2004.

[45] B. Guillotin, A. Souquet, S. Catros, M. Duocastella, B. Pippenger, S. Bellance, R. Bareille, M. Remy, L. Bordenave, J. Amedee, and F. Guillemot, "Laser assisted bioprinting of engineered tissue with high cell density and microscale organization," *Biomaterials*, vol. 31, pp. 7250-6.

[46] J. A. Barron, B. J. Spargo, and B. R. Ringeisen, "Biological laser printing of three dimensional cellular structures," *Applied Physics a-Materials Science & Processing*, vol. 79, pp. 1027-1030, 2004.

[47] M. Gruene, C. Unger, L. Koch, A. Deiwick, and B. Chichkov, "Dispensing pico to nanolitre of a natural hydrogel by laser-assisted bioprinting," *Biomedical Engineering Online*, vol. 10, pp. -, 2011.

[48] M. Gruene, M. Pflaum, C. Hess, S. Diamantouros, S. Schlie, A. Deiwick, L. Koch, M. Wilhelmi, S. Jockenhoevel, A. Haverich, and B. Chichkov, "Laser Printing of Three-Dimensional Multicellular Arrays for Studies of Cell-Cell and Cell-Environment Interactions," *Tissue Eng Part C Methods*.

[49] A. Ovsianikov, M. Gruene, M. Pflaum, L. Koch, F. Maiorana, M. Wilhelmi, A. Haverich, and B. Chichkov, "Laser printing of cells into 3D scaffolds," *Biofabrication*, vol. 2, pp. -, 2010.

[50] M. M. Stevens, M. Mayer, D. G. Anderson, D. B. Weibel, G. M. Whitesides, and R. Langer, "Direct patterning of mammalian cells onto porous tissue engineering substrates using agarose stamps," *Biomaterials*, vol. 26, pp. 7636-41, 2005.

[51] M. S. Hahn, L. J. Taite, J. J. Moon, M. C. Rowland, K. A. Ruffino, and J. L. West, "Photolithographic patterning of polyethylene glycol hydrogels," *Biomaterials*, vol. 27, pp. 2519-24, 2006.

[52] J. M. Karp, Y. Yeo, W. Geng, C. Cannizarro, K. Yan, D. S. Kohane, G. Vunjak-Novakovic, R. S. Langer, and M. Radisic, "A photolithographic method to create cellular micropatterns," *Biomaterials*, vol. 27, pp. 4755-64, 2006.

[53] K. Arcaute, B. K. Mann, and R. B. Wicker, "Stereolithography of three-dimensional bioactive poly(ethylene glycol) constructs with encapsulated cells," *Annals of Biomedical Engineering*, vol. 34, pp. 1429-1441, 2006.

[54] G. Mapili, Y. Lu, S. Chen, and K. Roy, "Laser-layered microfabrication of spatially patterned functionalized tissue-engineering scaffolds," *J Biomed Mater Res B Appl Biomater*, vol. 75, pp. 414-24, 2005.

[55] Y.-C. C. Robert Gauvin, Jin Woo Lee, Pranav Soman, Pinar Zorlutuna, Jason W. Nichol, Hjae Bae, Shaochen Chen, Ali Khademhosseini, "Microfabrication of complex porous tissue engineering scaffolds using 3D projection stereolithography," *Biomaterials*, vol. 33, pp. 3824-3834, 2012.

[56] H. Lin, D. Zhang, P. G. Alexander, G. Yang, J. Tan, A. W. Cheng, and R. S. Tuan, "Application of visible light-based projection stereolithography for live cell-scaffold fabrication with designed architecture," *Biomaterials*, vol. 34, pp. 331-9, 2013.

[57] Y. Lu, G. Mapili, G. Suhali, S. Chen, and K. Roy, "A digital micro-mirror device-based system for the microfabrication of complex, spatially patterned tissue engineering scaffolds," *J Biomed Mater Res A*, vol. 77, pp. 396-405, 2006.

[58] K. W. Kwon, J. C. Choi, K. Y. Suh, and J. Doh, "Multiscale fabrication of multiple proteins and topographical structures by combining capillary force lithography and microscope projection photolithography," *Langmuir*, vol. 27, pp. 7966.

[59] B. R. Ringeisen, C. M. Othon, J. A. Barron, D. Young, and B. J. Spargo, "Jet-based methods to print living cells," *Biotechnol J*, vol. 1, pp. 930-48, 2006.

[60] T. Xu, J. Jin, C. Gregory, J. J. Hickman, and T. Boland, "Inkjet printing of viable mammalian cells," *Biomaterials*, vol. 26, pp. 93-99, 2005.

[61] T. Xu, C. Baicu, M. Aho, M. Zile, and T. Boland, "Fabrication and characterization of bio-engineered cardiac pseudo tissues," *Biofabrication*, vol. 1, pp. -, 2009.

[62] S. Moon, S. K. Hasan, Y. S. Song, F. Xu, H. O. Keles, F. Manzur, S. Mikkilineni, J. W. Hong, J. Nagatomi, E. Haeggstrom, A. Khademhosseini, and U. Demirci, "Layer by layer three-dimensional tissue epitaxy by cell-laden hydrogel droplets," *Tissue Eng Part C Methods*, vol. 16, pp. 157-66.

[63] V. Mironov, R. P. Visconti, V. Kasyanov, G. Forgacs, C. J. Drake, and R. R. Markwald, "Organ printing: tissue spheroids as building blocks," *Biomaterials*, vol. 30, pp. 2164-2174, 2009.

[64] C. N. Jones, N. Tuleuova, J. Lee, E. Ramanculov, A. H. Reddi, M. A. Zern., and A. Revzin, "Cultivating liver cells on printed arrays of hepatocyte growth factor," *Biomaterials*, vol. 30, pp. 3733-3741, 2009.

[65] M. Nakamura, A. Kobayashi, F. Takagi, A. Watanabe, Y. Hiruma, K. Ohuchi, Y. Iwasaki, M. Horie, I. Morita, and S. Takatani, "Biocompatible inkjet printing technique for designed seeding of individual living cells," *Tissue Eng*, vol. 11, pp. 1658-66, 2005.

[66] C. M. Smith, A. L. Stone, R. L. Parkhill, R. L. Stewart, M. W. Simpkins, A. M. Kachurin, W. L. Warren, and S. K. Williams, "Three-dimensional bioassembly tool for generating viable tissue-engineered constructs," *Tissue Engineering*, vol. 10, pp. 1566-1576, 2004.

[67] H. X. Liu, Y. N. Yan, X. H. Wang, J. Cheng, F. Lin, Z. Xiong, and R. D. Wu, "Construct hepatic analog by cell-matrix controlled assembly technology," *Chinese Science Bulletin*, vol. 51, pp. 1830-1835, 2006.

[68] C. M. Smith, W. L. Warren, J. B. Hoying, and S. K. Williams, "Utilizing a three-dimensional bioassembly tool to fabricate spatially organized multicellular vascular constructs," *Faseb Journal*, vol. 19, pp. A160-a160, 2005.

[69] X. H. Wang, Y. N. Yan, Y. Q. Pan, Z. Xiong, H. X. Liu, B. Cheng, F. Liu, F. Lin, R. D. Wu, R. J. Zhang, and Q. P. Lu, "Generation of three-dimensional hepatocyte/gelatin structures with rapid prototyping system," *Tissue Engineering*, vol. 12, pp. 83-90, 2006.

[70] D. L. Cohen, E. Malone, H. Lipson, and L. J. Bonassar, "Direct freeform fabrication of seeded hydrogels in arbitrary geometries," *Tissue Engineering*, vol. 12, pp. 1325-1335, 2006.

[71] Y. N. Yan, X. H. Wang, Z. Xiong, H. X. Liu, F. Liu, F. Lin, R. D. Wu, R. J. Zhang, and Q. P. Lu, "Direct construction of a three-dimensional structure with cells and hydrogel," *Journal of Bioactive and Compatible Polymers*, vol. 20, pp. 259-269, 2005.

[72] Y. N. Yan, X. H. Wang, Y. Q. Pan, H. X. Liu, J. Cheng, Z. Xiong, F. Lin, R. D. Wu, R. J. Zhang, and Q. P. Lu, "Fabrication of viable tissue-engineered constructs with 3D cell-assembly technique," *Biomaterials*, vol. 26, pp. 5864-5871, 2005.

[73] K. Buyukhatipoglu, W. Jo, and A. M. Clyne, "The role of printing parameters and scaffold biopolymer properties in the efficacy of a new hybrid nano-bioprinting system," *Biofabrication*, vol. 1, pp. -, 2009.

[74] R. A. Barry, R. F. Shepherd, J. N. Hanson, R. G. Nuzzo, P. Wiltzius, and J. A. Lewis, "Direct-Write Assembly of 3D Hydrogel Scaffolds for Guided Cell Growth," *Advanced Materials*, vol. 21, pp. 2407-2410, 2009.

[75] R. Chang, Y. Nam, and W. Sun, "Direct cell writing of 3D microorgan for in vitro pharmacokinetic model," *Tissue Engineering Part C-Methods*, vol. 14, pp. 157-166, 2008.

[76] T. Boland, X. Tao, B. J. Damon, B. Manley, P. Kesari, S. Jalota, and S. Bhaduri, "Drop-on-demand printing of cells and materials for designer tissue constructs," *Materials Science & Engineering C-Biomimetic and Supramolecular Systems*, vol. 27, pp. 372-376, 2007.

[77] T. Boland, V. Mironov, A. Gutowska, E. A. Roth, and R. R. Markwald, "Cell and organ printing 2: Fusion of cell aggregates in three-dimensional gels," *Anatomical Record Part a-Discoveries in Molecular Cellular and Evolutionary Biology*, vol. 272A, pp. 497-502, 2003.

[78] S. Khalil and W. Sun, "Bioprinting endothelial cells with alginate for 3D tissue constructs," *J Biomech Eng*, vol. 131, pp. 111002, 2009.

[79] S. N. Jayasinghe, A. N. Qureshi, and P. A. M. Eagles, "Electrohydrodynamic jet processing: An advanced electric-field-driven jetting phenomenon for processing living cells," *Small*, vol. 2, pp. 216-219, 2006.

[80] L. Haines-Butterick, K. Rajagopal, M. Branco, D. Salick, R. Rughani, M. Pilarz, M. S. Lamm, D. J. Pochan, and J. P. Schneider, "Controlling hydrogelation kinetics by peptide design for three-dimensional encapsulation and injectable delivery of cells," *Proceedings of the National Academy of Sciences of the United States of America*, vol. 104, pp. 7791-7796, 2007.

[81] L. A. Haines-Butterick, K. Rajagopal, M. Lamm, D. J. Pochan, and J. P. Schnieder, "Controlling hydrogelation kinetics via peptide design for three-dimensional encapsulation and injectable delivery of cells," *Biopolymers*, vol. 88, pp. 518-518, 2007.

[82] C. D. Sims, P. E. M. Butler, Y. L. Cao, R. Casanova, M. A. Randolph, A. Black, C. A. Vacanti, and M. J. Yaremchuk, "Tissue engineered neocartilage using plasma derived

polymer substrates and chondrocytes," *Plastic and Reconstructive Surgery*, vol. 101, pp. 1580-1585, 1998.

[83] V. Mironov, T. Boland, T. Trusk, G. Forgacs, and R. R. Markwald, "Organ printing: computer-aided jet-based 3D tissue engineering," *Trends in Biotechnology*, vol. 21, pp. 157-161, 2003.

[84] M. Xu, X. Wang, Y. Yan, R. Yao, and Y. Ge, "An cell-assembly derived physiological 3D model of the metabolic syndrome, based on adipose-derived stromal cells and a gelatin/alginate/fibrinogen matrix," *Biomaterials*, vol. 31, pp. 3868-77.

[85] R. C. Lee, "Cell injury by electric forces," *Ann N Y Acad Sci*, vol. 1066, pp. 85-91, 2005.

[86] A. Townsend-Nicholson and S. N. Jayasinghe, "Cell electrospinning: a unique biotechnique for encapsulating living organisms for generating active biological microthreads/scaffolds," *Biomacromolecules*, vol. 7, pp. 3364-9, 2006.

[87] E. Ward, E. Chan, K. Gustafsson, and S. N. Jayasinghe, "Combining bio-electrospraying with gene therapy: a novel biotechnique for the delivery of genetic material via living cells," *Analyst*, vol. 135, pp. 1042-9.

[88] J. T. Seil and T. J. Webster, "Spray deposition of live cells throughout the electrospinning process produces nanofibrous three-dimensional tissue scaffolds," *Int J Nanomedicine*, vol. 6, pp. 1095-9.

[89] D. Li and Y. N. Xia, "Electrospinning of nanofibers: Reinventing the wheel?," *Advanced Materials*, vol. 16, pp. 1151-1170, 2004.

[90] W. Tan and T. A. Desai, "Layer-by-layer microfluidics for biomimetic three-dimensional structures," *Biomaterials*, vol. 25, pp. 1355-1364, 2004.

[91] H. Andersson and A. van den Berg, "Microfabrication and microfluidics for tissue engineering: state of the art and future opportunities," *Lab on a Chip*, vol. 4, pp. 98-103, 2004.

[92] W. G. Koh, L. J. Itle, and M. V. Pishko, "Molding of hydrogel multiphenotype cell microstructures to create microarrays," *Analytical Chemistry*, vol. 75, pp. 5783-5789, 2003.

[93] J. Su, Y. Z. Zheng, and H. K. Wu, "Generation of alginate microfibers with a roller-assisted microfluidic system," *Lab on a Chip*, vol. 9, pp. 996-1001, 2009.

[94] W. Tan and T. A. Desai, "Microfluidic patterning of cells in extracellular matrix biopolymers: Effects of channel size, cell type, and matrix composition on pattern integrity," *Tissue Engineering*, vol. 9, pp. 255-267, 2003.

[95] S. Xu, Z. Nie, M. Seo, P. Lewis, E. Kumacheva, H. A. Stone, P. Garstecki, D. B. Weibel, I. Gitlin, and G. M. Whitesides, "Generation of monodisperse particles by using microfluidics: Control over size, shape, and composition (vol 44, pg 724, 2005)," *Angewandte Chemie-International Edition*, vol. 44, pp. 3799-3799, 2005.

[96] J. A. Burdick and K. S. Anseth, "Photoencapsulation of osteoblasts in injectable RGD-modified PEG hydrogels for bone tissue engineering," *Biomaterials*, vol. 23, pp. 4315-4323, 2002.

[97] D. A. Bruzewicz, A. P. McGuigan, and G. M. Whitesides, "Fabrication of a modular tissue construct in a microfluidic chip," *Lab on a Chip*, vol. 8, pp. 663-671, 2008.

[98] A. Vogel and V. Venugopalan, "Mechanisms of pulsed laser ablation of biological tissues," *Chem Rev*, vol. 103, pp. 577-644, 2003.

[99] A. Heisterkamp, I. Z. Maxwell, E. Mazur, J. M. Underwood, J. A. Nickerson, S. Kumar, and D. E. Ingber, "Pulse energy dependence of subcellular dissection by femtosecond laser pulses," *Opt Express*, vol. 13, pp. 3690-6, 2005.

[100] Y. Liu, G. J. Sonek, M. W. Berns, and B. J. Tromberg, "Physiological monitoring of optically trapped cells: assessing the effects of confinement by 1064-nm laser tweezers using microfluorometry," *Biophysical Journal*, vol. 71, pp. 2158-67, 1996.

[101] Y. Liu, D. K. Cheng, G. J. Sonek, M. W. Berns, C. F. Chapman, and B. J. Tromberg, "Evidence for localized cell heating induced by infrared optical tweezers," *Biophysical Journal*, vol. 68, pp. 2137-44, 1995.

[102] K. Konig, H. Liang, M. W. Berns, and B. J. Tromberg, "Cell damage by near-IR microbeams," *Nature*, vol. 377, pp. 20-1, 1995.

[103] M. W. Berns, "A possible two-photon effect in vitro using a focused laser beam," *Biophysical Journal*, vol. 16, pp. 973-977, 1976.

[104] K. Konig, H. Liang, M. W. Berns, and B. J. Tromberg, "Cell damage in near-infrared multimode optical traps as a result of multiphoton absorption," *Optics Letters*, vol. 21, pp. 1090-1092, 1996.

[105] P. P. Calmettes and M. W. Berns, "Laser-Induced Multiphoton Processes in Living Cells," *Proceedings of the National Academy of Sciences of the United States of America-Biological Sciences*, vol. 80, pp. 7197-7199, 1983.

[106] K. Svoboda and S. M. Block, "Biological Applications of Optical Forces," *Annual Review of Biophysics and Biomolecular Structure*, vol. 23, pp. 247-285, 1994.

[107] M. B. Zeigler and D. T. Chiu, "Laser Selection Significantly Affects Cell Viability Following Single-Cell Nanosurgery," *Photochemistry and Photobiology*, vol. 85, pp. 1218-1224, 2009.

[108] K. C. Neuman, E. H. Chadd, G. F. Liou, K. Bergman, and S. M. Block, "Characterization of photodamage to Escherichia coli in optical traps," *Biophysical Journal*, vol. 77, pp. 2856-2863, 1999.

[109] S. Catros, B. Guillotin, M. Bacakova, J. C. Fricain, and F. Guillemot, "Effect of laser energy, substrate film thickness and bioink viscosity on viability of endothelial cells printed by Laser-Assisted Bioprinting," *Applied Surface Science*, vol. 257, pp. 5142-5147, 2011.

[110] B. Hopp, T. Smausz, N. Kresz, N. Barna, Z. Bor, L. Kolozsvari, D. B. Chrisey, A. Szabo, and A. Nogradi, "Survival and proliferative ability of various living cell types after laser-induced forward transfer," *Tissue Engineering*, vol. 11, pp. 1817-1823, 2005.

[111] J. Kujawa, I. B. Zavodnik, A. Lapshina, M. Labieniec, and M. Bryszewska, "Cell survival, DNA, and protein damage in B14 cells under low-intensity near-infrared (810 nm) laser irradiation," *Photomed Laser Surg*, vol. 22, pp. 504-8, 2004.

[112] A. G. Doukas, D. J. McAuliffe, and T. J. Flotte, "Biological effects of laser-induced shock waves: structural and functional cell damage in vitro," *Ultrasound Med Biol*, vol. 19, pp. 137-46, 1993.

[113] R. Lubart, Y. Wollman, H. Friedmann, S. Rochkind, and I. Laulicht, "Effects of visible and near-infrared lasers on cell cultures," *J Photochem Photobiol B*, vol. 12, pp. 305-10, 1992.

[114] Y. F. Lin, G. H. Huang, Y. Huang, T. R. J. Tzeng, and D. Chrisey, "Effect of laser fluence in laser-assisted direct writing of human colon cancer cell," *Rapid Prototyping Journal*, vol. 16, pp. 202-208, 2010.

[115] U. Zimmermann, "Electric field-mediated fusion and related electrical phenomena," *Biochimica et biophysica acta*, vol. 694, pp. 227, 1982.

[116] E. A. Evans, R. Skalak, and R. M. Hochmuth, "Mechanics and Thermodynamics of Biomembranes .1.," *Crc Critical Reviews in Bioengineering*, vol. 3, pp. 181-330, 1979.

[117] E. A. Evans and R. Skalak, "Mechanics and Thermodynamics of Biomembranes .2.," *Crc Critical Reviews in Bioengineering*, vol. 3, pp. 331-418, 1979.

[118] D. A. Fletcher and D. Mullins, "Cell mechanics and the cytoskeleton," *Nature*, vol. 463, pp. 485-492, 2010.

[119] P. A. Janmey and C. A. McCulloch, "Cell mechanics: Integrating cell responses to mechanical stimuli," *Annual Review of Biomedical Engineering*, vol. 9, pp. 1-34, 2007.

[120] T. W. Secomb, "Red-Blood-Cell Mechanics and Capillary Blood Rheology," *Cell Biophysics*, vol. 18, pp. 231-251, 1991.

[121] S. P. Sutera and M. H. Mehrjardi, "Deformation and Fragmentation of Human Red Blood-Cells in Turbulent Shear-Flow," *Biophysical Journal*, vol. 15, pp. 1-10, 1975.

[122] R. Chang and W. Sun, "Effects of dispensing pressure and nozzle diameter on cell survival from solid freeform fabrication-based direct cell writing," *Tissue Engineering Part A*, vol. 14, pp. 41-48, 2008.

[123] T. Braschler, R. Johann, M. Heule, L. Metref, and P. Renaud, "Gentle cell trapping and release on a microfluidic chip by in situ alginate hydrogel formation," *Lab on a Chip*, vol. 5, pp. 553-559, 2005.

[124] P. L. Blackshear Jr, F. D. Dorman, and J. H. Steinbach, "Some mechanical effects that influence hemolysis," *Transactions-American Society for Artificial Internal Organs*, vol. 11, pp. 112, 1965.

[125] M. Giersiepen, L. Wurzinger, R. Opitz, and H. Reul, "Estimation of shear stress-related blood damage in heart valve prostheses--in vitro comparison of 25 aortic valves," *The International journal of artificial organs*, vol. 13, pp. 300, 1990.

[126] R. Paul, J. Apel, S. Klaus, F. Schgner, P. Schwindke, and H. Reul, "Shear stress related blood damage in laminar couette flow," *Artificial organs*, vol. 27, pp. 517-529, 2003.

[127] B. Vickroy, K. Lorenz, and W. Kelly, "Modeling Shear Damage to Suspended CHO Cells during Crossflow Filtration," *Biotechnology progress*, vol. 23, pp. 194-199, 2007.

[128] L. Leverett, J. Hellums, C. Alfrey, and E. Lynch, "Red blood cell damage by shear stress," *Biophysical journal*, vol. 12, pp. 257-273, 1972.

[129] K. Chang Yan, K. Nair, and W. Sun, "Three dimensional multi-scale modelling and analysis of cell damage in cell-encapsulated alginate constructs," *Journal of biomechanics*, vol. 43, pp. 1031-1038, 2010.

[130] F. Dunn, "Cellular Inactivation by Heat and Shear," *Radiation and Environmental Biophysics*, vol. 24, pp. 131-139, 1985.

[131] M. Li, X. Tian, and X. Chen, "Temperature effect on the shear-induced cell damage in biofabrication," *Artificial organs*, vol. 35, pp. 741, 2011.

[132] G. Kim, J. Son, S. Park, and W. Kim, "Hybrid Process for Fabricating 3D Hierarchical Scaffolds Combining Rapid Prototyping and Electrospinning," *Macromolecular Rapid Communications*, vol. 29, pp. 1577-1581, 2008.

[133] M. Hu, R. Deng, K. M. Schumacher, M. Kurisawa, H. Ye, K. Purnamawati, and J. Y. Ying, "Hydrodynamic spinning of hydrogel fibers," *Biomaterials*, vol. 31, pp. 863-9, 2010.

[134] L. Moroni, J. A. A. Hendriks, R. Schotel, J. R. De Wijn, and C. A. Van Blitterswijk, "Design of biphasic polymeric 3-dimensional fiber deposited scaffolds for cartilage tissue engineering applications," *Tissue Engineering*, vol. 13, pp. 361-371, 2007.

[135] D. Dendukuri and P. S. Doyle, "The Synthesis and Assembly of Polymeric Microparticles Using Microfluidics," *Advanced Materials*, vol. 21, pp. 4071-4086, 2009.

[136] K. A. Barbee, T. Mundel, R. Lal, and D. P. F., "Subcellular distribution of shear stress at the surface of flow-aligned and nonaligned endothelial monolayer," *Am. J. Physiol*, vol. 268, pp. H1765-H1772, 1995.

[137] R. L. Satcher, Jr., S. R. Bussolari, M. A. Gimbrone, Jr., and C. F. Dewey, Jr., "The distribution of fluid forces on model arterial endothelium using computational fluid dynamics," *J Biomech Eng*, vol. 114, pp. 309-16, 1992.

[138] A. I. Barakat and P. F. Davies, "Mechanisms of shear stress transmission and transduction in endothelial cells," *Chest*, vol. 114, pp. 58S-63S, 1998.

[139] C. S. Peskin, "The immersed boundary method," *Acta numerica*, vol. 11, pp. 479-517, 2002.

[140] S. Jadhav, C. D. Eggleton, and K. Konstantopoulos, "A 3-D computational model predicts that cell deformation affects selectin-mediated leukocyte rolling," *Biophys J*, vol. 88, pp. 96-104, 2005.

[141] D. C. Bottino, "Modeling viscoelastic networks and cell deforamation in the context of the immersed boundary method," *Journal of Computational Physics*, vol. 147, pp. 86-113, 1998.

[142] C. D. Eggleton and A. S. Popel, "Large deformation of red blood cell ghosts in a simple shear flow," *Physics of Fluids*, vol. 10, 1998.

[143] H. R. Lin and Y. J. Yeh, "Porous alginate/hydroxyapatite composite scaffolds for bone tissue engineering: Preparation, characterization, and in vitro studies," *Journal of Biomedical Materials Research Part B-Applied Biomaterials*, vol. 71B, pp. 52-65, 2004.

[144] P. Parhi, A. Ramanan, and A. R. Ray, "Preparation and characterization of alginate and hydroxyapatite-based biocomposite," *Journal of Applied Polymer Science*, vol. 102, pp. 5162-5165, 2006.

[145] A. Tampieri, M. Sandri, E. Landi, G. Celotti, N. Roveri, M. Mattioli-Belmonte, L. Virgili, F. Gabbanelli, and G. Biagini, "HA/alginate hybrid composites prepared through bio-inspired nucleation," *Acta Biomaterialia*, vol. 1, pp. 343-351, 2005.

[146] S. J. Shieh and J. P. Vacanti, "State-of-the-art tissue engineering: From tissue engineering to organ building," *Surgery*, vol. 137, pp. 1-7, 2005.

[147] R. P. L. Anthony Atala, *Methods of tissue engineering*. New York: Academic Press, 2002.

[148] C. d. P. de Groot, P. Smitt, and A. Driessen, "Mechanical failure of artificial teeth made of dense calcium hydroxyapatite," presented at Proc. 11 th International Conf. on Science of Ceramics 1981.

[149] D. W. Hutmacher, "Scaffolds in tissue engineering bone and cartilage," *Biomaterials*, vol. 21, pp. 2529-43, 2000.

[150] L. S. N. Cato T. Laurencin, *Nanotechnology and Tissue Engineering: The Scaffold*. Boca Raton: CRC press Taylor& Francis Group, 2008.

[151] X. B. Chen, M. G. Li, and H. Ke, "Modeling of the flow rate in the dispensing-based process for fabricating tissue scaffolds," *Journal of Manufacturing Science and Engineering-Transactions of the Asme*, vol. 130, pp. -, 2008.

[152] T. K. Sampath and A. H. Reddi, "Importance of Geometry of the Extracellular-Matrix in Endochondral Bone Differentiation," *Journal of Cell Biology*, vol. 98, pp. 2192-2197, 1984.

[153] A. G. Mikos, G. Sarakinos, M. D. Lyman, D. E. Ingber, J. P. Vacanti, and R. Langer, "Prevascularization of Porous Biodegradable Polymers," *Biotechnology and Bioengineering*, vol. 42, pp. 716-723, 1993.

[154] S. Khalil, "Deposition and structural formation of 3D alginate tissue scaffolds ", vol. PhD. Philadelphia,PA: Drexel University 2005.

[155] T. Mikolajczyk, D. Wolowska-Czapnik, and M. Bogun, "Precursor alginate fibres containing nano-particles of SiO2," *Fibres & Textiles in Eastern Europe*, vol. 12, pp. 19-23, 2004.

[156] S. Holdsworth, " Rheological models used for the prediction of the flow properties of food products," *Trans. Inst. Chem. Eng*, vol. 71, pp. 139-179, 1993.

[157] X. B. Chen, G. Schoenau, and W. J. Zhan, "Modeling of time-pressure fluid dispensing processes," *IEEE Transactions on Electronics Packaging Manufacturing*, vol. 23, pp. 300-305, 2000.

[158] S. Khalil, J. Nam, and W. Sun, "Multi-nozzle deposition for construction of 3D biopolymer tissue scaffolds," *Rapid Prototyping Journal*, vol. 11, pp. 9-17, 2005.

[159] S. Khalil and W. Sun, "Biopolymer deposition for freeform fabrication of hydrogel tissue constructs," *Material Science and Engineering: C*, vol. 27, pp. 469-478, 2007.

[160] K. M. Yamada and E. Cukierman, "Modeling tissue morphogenesis and cancer in 3D," *Cell*, vol. 130, pp. 601-610, 2007.

[161] H. Park, J. S. Temenoff, Y. Tabata, A. I. Caplan, and A. G. Mikos, "Injectable biodegradable hydrogel composites for rabbit marrow mesenchymal stem cell and growth factor delivery for cartilage tissue engineering," *Biomaterials*, vol. 28, pp. 3217-3227, 2007.

[162] J. Park, E. Lim, S. Back, H. Na, Y. Park, and K. Sun, "Nerve regeneration following spinal cord injury using matrix metalloproteinase-sensitive, hyaluronic acid-based biomimetic hydrogel scaffold containing brain-derived neurotrophic factor," *Journal of Biomedical Materials Research Part A*, vol. 93A, pp. 1091-1099, 2010.

[163] F. Z. Cui, W. M. Tian, S. P. Hou, Q. Y. Xu, and I. S. Lee, "Hyaluronic acid hydrogel immobilized with RGD peptides for brain tissue engineering," *Journal of Materials Science-Materials in Medicine*, vol. 17, pp. 1393-1401, 2006.

[164] B. P. Chan and K. W. Leong, "Scaffolding in tissue engineering: general approaches and tissue-specific considerations," *European Spine Journal*, vol. 17, pp. S467-S479, 2008.

[165] D. E. Discher, P. Janmey, and Y. L. Wang, "Tissue cells feel and respond to the stiffness of their substrate," *Science*, vol. 310, pp. 1139-1143, 2005.

[166] A. J. Engler, M. A. Griffin, S. Sen, C. G. Bonnetnann, H. L. Sweeney, and D. E. Discher, "Myotubes differentiate optimally on substrates with tissue-like stiffness: pathological implications for soft or stiff microenvironments," *Journal of Cell Biology*, vol. 166, pp. 877-887, 2004.

[167] R. L. Mauck, C. C. B. Wang, E. S. Oswald, G. A. Ateshian, and C. T. Hung, "The role of cell seeding density and nutrient supply for articular cartilage tissue engineering with deformational loading," *Osteoarthritis and Cartilage*, vol. 11, pp. 879-890, 2003.

[168] C. T. Buckley, S. D. Thorpe, F. J. O'Brien, A. J. Robinson, and D. J. Kelly, "The effect of concentration, thermal history and cell seeding density on the initial mechanical properties of agarose hydrogels," *Journal of the Mechanical Behavior of Biomedical Materials*, vol. 2, pp. 512-521, 2009.

[169] K. C. Yan, K. Nair, and W. Sun, "Three dimensional multi-scale modelling and analysis of cell damage in cell-encapsulated alginate constructs," *Journal of Biomechanics*, vol. 43, pp. 1031-1038, 2010.

[170] K. W. Ng, L. E. Kugler, S. B. Doty, G. A. Ateshian, and C. T. Hung, "Scaffold degradation elevates the Collagen content and dynamic compressive modulus in engineered articular cartilage," *Osteoarthritis and Cartilage*, vol. 17, pp. 220-227, 2009.

[171] C. V. C. Bouten, M. M. Knight, D. A. Lee, and D. L. Bader, "Compressive deformation and damage of muscle cell subpopulations in a model system," *Annals of Biomedical Engineering*, vol. 29, pp. 153-163, 2001.

[172] T. H. Park and M. L. Shuler, "Integration of cell culture and microfabrication technology," *Biotechnology Progress*, vol. 19, pp. 243-253, 2003.

[173] R. Landers and R. Mulhaupt, "Desktop manufacturing of complex objects, prototypes and biomedical scaffolds by means of computer-assisted design combined with computer-

guided 3D plotting of polymers and reactive oligomers," *Macromolecular Materials and Engineering*, vol. 282, pp. 17-21, 2000.

[174] G. Vozzi and A. Ahluwalia, "Microfabrication for tissue engineering: rethinking the cells-on-a scaffold approach," *Journal of Materials Chemistry*, vol. 17, pp. 1248-1254, 2007.

[175] X. Wang, Y. Yan, Y. Pan, Z. Xiong, H. Liu, J. Cheng, F. Liu, F. Lin, R. Wu, R. Zhang, and Q. Lu, "Generation of three-dimensional hepatocyte/gelatin structures with rapid prototyping system," *Tissue Eng*, vol. 12, pp. 83-90, 2006.

[176] R. E. Saunders, J. E. Gough, and B. Derby, "Delivery of human fibroblast cells by piezoelectric drop-on-demand inkjet printing," *Biomaterials*, vol. 29, pp. 193-203, 2008.

[177] D. Varghese, M. Deshpande, T. Xu, P. Kesari, S. Ohri, and T. Boland, "Advances in tissue engineering: Cell printing," *Journal of Thoracic and Cardiovascular Surgery*, vol. 129, pp. 470-472, 2005.

[178] J. D. Kretlow, L. Klouda, and A. G. Mikos, "Injectable matrices and scaffolds for drug delivery in tissue engineering," *Advanced Drug Delivery Reviews*, vol. 59, pp. 263-273, 2007.

[179] W. Xu, X. H. Wang, Y. N. Yan, W. Zheng, Z. Xiong, F. Lin, R. D. Wu, and R. J. Zhang, "Rapid prototyping three-dimensional cell/gelatin/fibrinogen constructs for medical regeneration," *Journal of Bioactive and Compatible Polymers*, vol. 22, pp. 363-377, 2007.

[180] C. K. Fredrickson and Z. H. Fan, "Macro-to-micro interfaces for microfluidic devices," *Lab on a Chip*, vol. 4, pp. 526-533, 2004.

[181] A. R. Wheeler, W. R. Throndset, R. J. Whelan, A. M. Leach, R. N. Zare, Y. H. Liao, K. Farrell, I. D. Manger, and A. Daridon, "Microfluidic device for single-cell analysis," *Analytical Chemistry*, vol. 75, pp. 3581-3586, 2003.

[182] V. Srinivasan, V. K. Pamula, and R. B. Fair, "Droplet-based microfluidic lab-on-a-chip for glucose detection," *Analytica Chimica Acta*, vol. 507, pp. 145-150, 2004.

[183] J. G. Shackman, G. M. Dahlgren, J. L. Peters, and R. T. Kennedy, "Perfusion and chemical monitoring of living cells on a microfluidic chip," *Lab on a Chip*, vol. 5, pp. 56-63, 2005.

[184] R. Chang, J. Nam, and W. Sun, "Effects of dispensing pressure and nozzle diameter on cell survival from solid freeform fabrication-based direct cell writing," *Tissue Eng Part A*, vol. 14, pp. 41-8, 2008.

[185] J. J. Parkkinen, M. J. Lammi, R. Inkinen, M. Jortikka, M. Tammi, I. Virtanen, and H. J. Helminen, "Influence of short-term hydrostatic pressure on organization of stress fibers in cultured chondrocytes," *J Orthop Res*, vol. 13, pp. 495-502, 1995.

[186] J. F. R. Chhabra R. P. , *Non-Newtonian flow in the process industries*. Oxford: Butterworth-Heinemann, 1999.

[187] P. R.H., *Orientation and distribution of erythrocytes in blood flowing through medium-sized arteries*. New York: Pergamon press, 1969.

[188] P. L. Blackshear, Jr., R. J. Forstrom, F. D. Dorman, and G. O. Voss, "Effect of flow on cells near walls," *Fed Proc*, vol. 30, pp. 1600-11, 1971.

[189] G. Bugliarello and J. Sevilla, "Velocity distribution and other characteristics of steady and pulsatile blood flow in fine glass tubes," *Biorheology*, vol. 7, pp. 85-107, 1970.

[190] K. K. Yeleswarapu, J. F. Antaki, M. V. Kameneva, and K. R. Rajagopal, "A Mathematical-Model for Shear-Induced Hemolysis," *Artificial Organs*, vol. 19, pp. 576-582, 1995.

[191] M. G. Li, X. Y. Tian, D. J. Schreyer, and X. B. Chen, "Effect of needle geometry on flow rate and cell damage in the dispensing-based biofabrication process," *Biotechnology Progress*, vol. 27, pp. 1777-1784, 2011.

[192] A. Tirella, F. Vozzi, G. Vozzi, and A. Ahluwalia, "PAM2 (Piston Assisted Microsyringe): A New Rapid Prototyping Technique for Biofabrication of Cell Incorporated Scaffolds," *Tissue Engineering Part C-Methods*, vol. 17, pp. 229-237, 2011.

[193] C. S. Peskin and D. M. Mcqueen, "Modeling Prosthetic Heart-Valves for Numerical-Analysis of Blood-Flow in the Heart," *Journal of Computational Physics*, vol. 37, pp. 113-132, 1980.

[194] D. Barthes-Biesel, A. Diaz, and E. Dhenin, "Effect of constitutive laws for two-dimensional membranes on flow-induced capsule deformation," *Journal of Fluid Mechanics*, vol. 460, pp. 211-222, 2002.

[195] M. C. Lai and C. S. Peskin, "An immersed boundary method with formal second-order accuracy and reduced numerical viscosity," *Journal of Computational Physics*, vol. 160, pp. 705-719, 2000.

[196] P. Bagchi, P. C. Johnson, and A. S. Popel, "Computational fluid dynamic simulation of aggregation of deformable cells in a shear flow," *Journal of Biomechanical Engineering-Transactions of the ASME*, vol. 127, pp. 1070-1080, 2005.

[197] R. Skalak, A. Tozeren, R. P. Zarda, and S. Chien, "Strain Energy Function of Red Blood-Cell Membranes," *Biophysical Journal*, vol. 13, pp. 245-280, 1973.

[198] K. Buyukhatipoglu, W. Jo, W. Sun, and A. M. Clyne, "The role of printing parameters and scaffold biopolymer properties in the efficacy of a new hybrid nano-bioprinting system," *Biofabrication*, vol. 1, 2009.

[199] K. A. Barbee, "Mechanical cell injury," *Cell Injury: Mechanisms, Responses, and Repair*, vol. 1066, pp. 67-84, 2005.

[200] J. Xu, Y. Tseng, and D. Wirtz, "Strain hardening of actin filament networks. Regulation by the dynamic cross-linking protein alpha-actinin," *J Biol Chem*, vol. 275, pp. 35886-92, 2000.

[201] O. C. Farokhzad, A. Khademhosseini, S. Y. Yon, A. Hermann, J. J. Cheng, C. Chin, A. Kiselyuk, B. Teply, G. Eng, and R. Langer, "Microfluidic system for studying nanoparticles and microparticles the interaction of with cells," *Analytical Chemistry*, vol. 77, pp. 5453-5459, 2005.

[202] H. Drouin, J. B. Ritter, V. M. Gorenflo, B. D. Bowen, and J. M. Piret, "Cell separator operation within temperature ranges to minimize effects on Chinese hamster ovary cell perfusion culture," *Biotechnology Progress*, vol. 23, pp. 1473-1484, 2007.

[203] X. Y. Tian, M. G. Li, N. Cao, J. W. Li, and X. B. Chen, "Characterization of the flow behaviour of alginate/hydroxyapatite mixtures for tissue scaffold fabrication," *Biofabrication*, vol. 1, 2009.

[204] K. S. Ko and C. A. McCulloch, "Partners in protection: interdependence of cytoskeleton and plasma membrane in adaptations to applied forces," *J Membr Biol*, vol. 174, pp. 85-95, 2000.

[205] R. A. Steinhardt, "The mechanisms of cell membrane repair - A tutorial guide to key experiments," *Cell Injury: Mechanisms, Responses, and Repair*, vol. 1066, pp. 152-165, 2005.